STUDY OF SMART CONDUITS MADE OF SHAPE-MEMORY POLYMERS FOR PERIPHERAL NERVE REGENERATION

CHEN Cheng

M.Phil

The Hong Kong Polytechnic University

2017

THE HONG KONG POLYTECHNIC UNIVERSITY

INSTITUTE OF TEXTILES AND CLOTHING

Study of Smart Conduits Made of Shape-Memory Polymers for Peripheral Nerve Regeneration

By CHEN Cheng

A thesis submitted in partial fulfillment of the requirements for the degree of Master of Philosophy

April 2016

Certificate of Originality

I hereby declare that this thesis is my own work and that, to the best of my knowledge and belief, it reproduces no material previously published or written, nor material that has been accepted for the award of any other degree or diploma, except where due acknowledgement has been made in the text.

_____(Signed)

CHEN Cheng (Name of Student)

ABSTRACT

Shape-memory polymers (SMPs) are defined by their capacity to recover an initial shape from temporary deformations upon external stimulation. They have gained increasing attention over the recent decade in biomedical applications. Reported medical devices based on SMPs range from general surgical to intravascular applications and filling materials to drug delivery systems. However, there have been few reports on applications of SMPs to nerve regeneration. Yet, peripheral nerve repair and regeneration have been a unique clinical challenge for surgeons. Herein, we propose a novel kind of smart nerve conduit fabricated from SMPs that can achieve peripheral nerve regeneration by automatic lengthening. The design concept, preparation process, structure characterization, function evaluation, mechanism analysis for the SMPs and SNCs were presented in this thesis.

Briefly, a series of macromers with different (rac-lactide) to glycolide weight ratios were synthesized and the characteristics of the synthesized networks were studied. Cyclic thermo-mechanical measurements indicated the robustness of molecular structure for shape memory function. Body-water responsive shape-memory behavior was evaluated by angle recovery measurements. The shape recovery time of the polymer could be adjusted by the selection of comonomer ratio and then the overall gradual-recovery function of a device could be realized by suitable combination of different copolymers. Thus a tri-segment smart nerve conduit was fabricated from this

polymer system by electrospinning, shown to gradually recover in an in vitro experiment under stimulated physiological conditions, that is, body-liuid environmemnt (36°C water). In vitro culture and qualitative immunocytochemistry of Schwann cells assessed the biocompatibility of poly(rac-lactide-co-glycolide) networks. In vivo experiments in rabbit animal model were conducted to ensure the SNC has the required mechanical characteristics to perform adequately under practical conditions.

PUBLICATIONS

Research journal paper:

Cheng Chen, Jinlian Hu*, Huahua Huang, Yong Zhu, and Tingwu Qin, “Design of a smart nerve conduit based on shape-memory polymer,” *Advanced Materials Technologies*, admt.201600015R1

Patent:

胡金莲，陈诚，“矫形器，用于该矫形器的形状记忆高分子材料的制造方法，”2016101022670, China, 2016.

ACKNOWLEDGEMENTS

I would like to express my sincerest thanks to my supervisor, Prof. Jinlian Hu, for giving me the opportunity to pursue my MPhil degree. Without her patient and substantial help, it would be impossible for me to accomplish my study. Prof. Hu's profound academic attainments and professional integrity continuously inspired and encouraged me during my MPhil study. This period of study in PolyU would be the best memory in my life.

I am very grateful to Mr Jianping Han, for his suggestion and guidance in my research life. In addition, I would like to thank my colleagues: Dr Cuili Zhang, Dr Jing Lv, Ms Ruiqi Xie, Ms Susanna Li, Dr Lin Tan, Dr Huafu Zhao, Mr Tenghao Li and other friends whose name can not be listed here because of the limited space. Their help and support are greatly appreciated.

Finally, the endeavor made in this MPhil study is also accompanied with love, patience and care from my family. I wish to dedicate this thesis to my girlfriend Qian Wu for her love and continuous encouragement. It was their support and encouragement that make me to accomplish my study.

LIST OF CONTENTS

LIST OF FIGURES

LIST OF TABLES

LIST OF SYMBOLS AND ABBREVIATIONS

Symbol	Definitions
2D FFT	Two-dimensional fast fourier transform
FDA	Food and Drug Administration
MT	Martensitic transformation
PNR	Peripheral nerve regenetation
SMA	Shape-memory alloy
SMP	Shape-memory polymer
SME	Shape-memory effect
PNS	Peripheral nervous system
CNS	Central nervous system
ECM	Extracellular matrix
LCE	Liquid-crystal elastomer
FTIR	Fourier Infrared Spectra
GPC	Gel Permeation Chromatography
WCA	Water Contact angle
XRD	X-Ray Diffraction
SEM	Scanning Electron Microscope
DSC	Differential Scanning Calorimetry
UV	Ultraviolet

T_g	Glass transition temperature
T_m	Melting temperature
T_{trans}	Transition temperature
T_{high}	Higher temperature
T_{low}	Lower temperature
R_r	Strain recovery ratio
R_f	Strain fixity ratio
S	Entropy
K	Boltzmann’s constant
Ω	Number of configurations
BSC	Bovine serum albumin
DMEM	Dulbecco modified eagle medium
FBS	Fetal bovine serum
DMF	Dimethylformamide
THF	Tetrahydrofuran
LA	*rac*-lactide
GA	Glycolide
MEG	Ethylene glycol
DBTO	Dibutyltin oxide
DCM	Dichloromethane
DEGMA	Diethylene glycol dimethacrylate
EA	Ethyl acetate

PE	Polyethylene
MDI	4,4-diphenylmethane diisocyanate
PCL	Poly(ε-caprolactone)
PEG	Poly(ethylene glycol)
PGA	Poly(glycolic acid)
PLA	Poly(lactic acid)
PLGA	Poly(lactic-*co*-glycolic acid)
PLLA	Poly(L-lactide acid)
PMMA	Polymethylmethacrylate
POSS	Polyhedral oligosilsesquioxane
PHB	Poly(3-hydroxybutyrate)
PVAc	Poly(vinyl acetate)
PVDF	Poly(vinylidene fluoride)
PS	Polystyrene
STBS	Styrene-*trans*-butadiene-styrene
TPB	Poly(*trans*-butadiene)
TIP	*trans*-polyisoprene
FITC	Fluorescein isothiocyanate
F-actin	Filamentous actin
DAPI	4',6-Diamidino-2-phenylindole
RGDS	Arg-Gly-Asp-Ser
BMP-2	Morphogenetic factor 2

HE	Hematoxylin and eosin
SC	Schwann cell
MSC	Marrow stromal cell

CHAPTER 1 INTRODUCTION

1.1 Research background

Shape-memory materials including shape-memory alloys (SMAs) and shape-memory polymers (SMPs) are a type of smart material, which can memorize the permanent shape and be programmed to a temporary shape, and then spontaneously recover to its original shape upon external stimulus such as heating, lighting, and pH value change[1-3]. Currently, the most widely commercial applied shape-memory materials are SMAs[4]. Its shape-memory effect (SME) stems from two stable crystal structures: austenitic phase and martensitic phase. Normally, the austenitic phase is cubic, while the martensitic phase possesses a lower symmetry. The transition between these two phases is called martensitic transformation (MT). When the temperature is decreased below the transition temperature, MT starts by a shear-like mechanism, as the martensitic phase has a lower symmetry, many variants can be formed from the austenitic phase. When the temperature is increased over the transition temperature, the asymmetric martensitic phase becomes unstable, and recovers to the austenitic phase in original orientation, as shown in figure 1.1. Chang and Read first observed this SME on Au-Cd alloy in 1951[4]. However, the discovery of SME on nickel-titanium alloy in 1963 led to enormous interest towards commercial fields because of the combination merits of an adjustable transition temperature, biocompatibility, and a so-called two way SME. Despite the above-mentioned advantages, SMAs have also possessed some disadvantages that limit their further

application, such as limited recoverable strains, intrinsically high stiffness, high cost, and demanding processing condition. Such drawbacks have provided research motivation for the development of novel alternative shape-memory materials, especially polymeric materials.

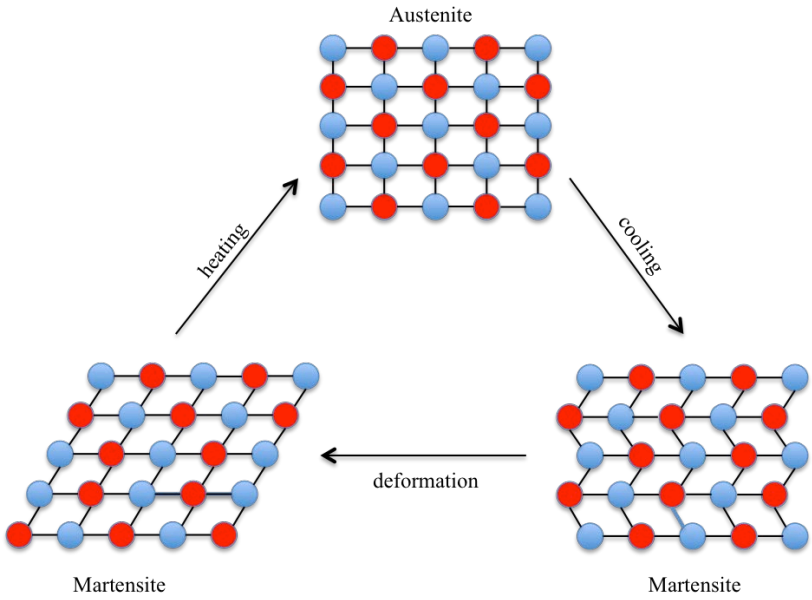

Figure 1.1 Microscopic diagram of the shape memory effect in SMA

Polymeric materials possess shape-memory function inherently, although the mechanisms differ significantly from those of SMAs. In metal alloys, pseudoplastic fixing is possibly achieved through the martensitic de-twinning mechanism, while recovery process is triggered by martensitic-austenite phase transition. In contrast, SMPs possess temporary shape fixing and original shape recovering ability through a mechanism being derived from the intrinsic elasticity of polymeric networks. Polymers, whether covalently or physically cross-linked, are elastic to large strains above either glass transition temperature or melting temperature. For $T > T_{trans}$, polymer networks exhibit superelasticity wherein the polymer chain segments

between cross-link points can be deformed freely and are prone to being entangled randomly, maintaining a maximum entropy. From a macroscopic viewpoint, the SME in polymers can be depicted as follows. First, deformations under increased temperature caused by external force can be fixed during cooling process. Thus, the load applied on the material can be stored as dormant strain energy because the recovery force is prohibited by vitrification, crystallization, or other means. The temporary fixed shape is stable, and upon subsequent heating above T_{trans}, the stored strain energy would be released. Then the deformed polymer can return to its original shape, whether chemically or physically cross-linked. The programming and recovering process in thermal-induced SME is illustrated in figure 1.2, which involves two common types of deformation, namely elongating and bending. The vitrification or crystallization of the rubber segment controls the locking of the polymer chains and therefore allows determining a temporary secondary shape. Based on the shape-memory mechanism described above, the features of a polymer with excellent SME include: 1) a narrow temperature transition gap that can be used to fix the temporary shape at low temperature and trigger shape recovery at high temperature; 2) superelasticity above the transition temperature that leads the shape recovery; and 3) complete fixing of the temporary shape by immobilizing the polymeric chains without creep.

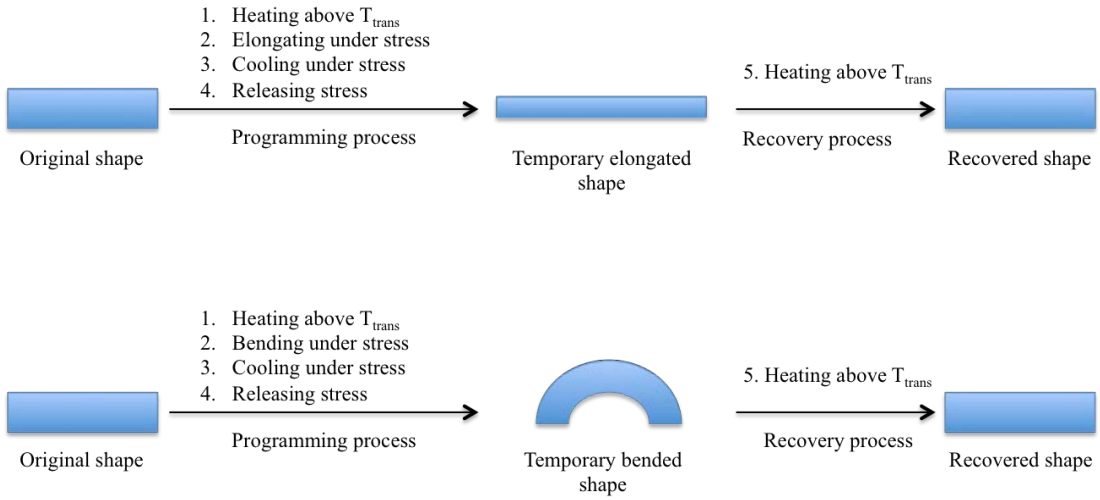

Figure 1.2 Macroscopic diagram of the shape memory effect of SMP

Recently, SMPs were developed widely in not only academic area, but industrial application field as well, which is due to the low cost, convenient processing ability, excellent shape recoverability and wide range of shape recovery temperature. In particular, in the field of biomedical materials, shape-memory function around human body temperature together with biocompatibility offer tremendous application potential for applying in minimally invasive surgery[5-8]. Through a small incision, degradable implant made from SMPs can be inserted into in a compacted shape. When the implant is placed at the correct position, it obtains its original shape after heating to body temperature. After a defined time period, the implant is degraded and can be absorbed. In this case a second surgery to remove the implant is not necessary. A number of biomaterial-based medical devices with shape memory function have been studied and developed. For example, a laser-actuated SMP microgripper device for minimally invasive delivery of endovascular device was illustrated in figure 1.3[9].

In this application, solutions of thermoplastic PU and polythiol were first solution cast over a cleaved optical fiber to form the SMP gripper, after which PU/polythiol solutions were UV cured. Pellet tipped nitinol was then axially crimped into the gripper and actuation was achieved using laser irradiation, which results in release of embolic device.

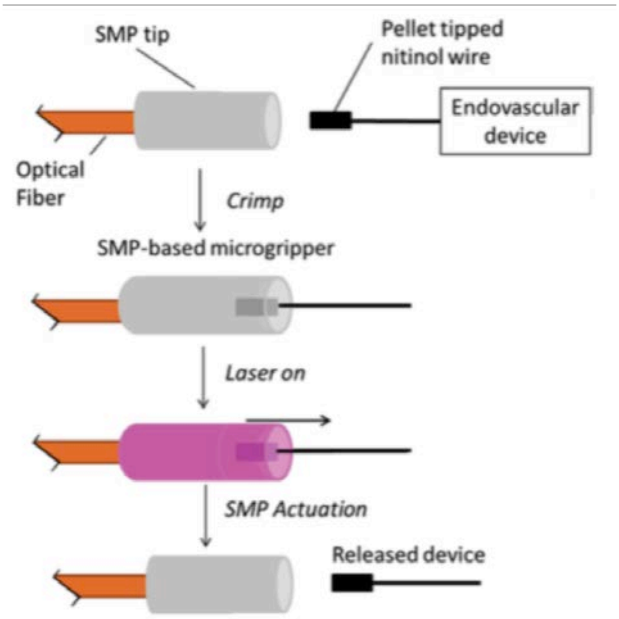

Figure 1.3 Schematic diagram for laser actuated SMP microgripper

1.2 Statement of problems

Thousands of peripheral nerve injuries occur throughout the world because of traffic accidents, natural disasters and other types of trauma[10]. The repair of such peripheral nerve injuries has been a challenging clinical problem for surgeons. In patients with minimal gap, direct nerve repair is normally operated. This method requires demanding surgery conditions including an injury area with good blood supply and soft-tissue coverage. The proper alignment of nerve stumps is also critical

to promote nerve recovery. Although with the abovementioned limitations, tensionless suture repair remains the preferred treatment option for nerve regeneration. If this is not available because of either gap formation or poor quality of tissue for repair, alternative methods should be utilized. Nerve gaps (> 2.5 cm) at the site of injury will commonly utilize nerve autograft technology, which is still considered as “the golden standard” for PNR. In this method, sensory donor nerves are most often used, with the sural nerve being the most commonly harvested. In all types, the graft is left 10% to 20% longer than the gap for ensuring a tension-free suture. Yet nerve autografts have several inherent drawbacks, such as the limited sources of suitable donor nerves and the need to regenerate axons to cross at two coaptation sites. Thus, the use of synthesized nerve tubes has been widely studied as a new type of treatment for PNR. It is commonly accepted that physical guidance of axons is a vital component of nerve repair. Current research is focused on developing prominent conduits that can be used to physically guide nerve regeneration. These “nerve guidance conduits” serve to direct axons sprouting from the proximal nerve end, introducing an environment for the diffusion of growth factors secreted by the injured nerve ends. However, up to now, none of these artificial conduits have shown to be as effective as conventional nerve autografts. Another potential method is to use a manual nerve-lengthening device. In this method, the repair of a nerve defect is induced by direct end-to-end neurorrhaphy after simultaneous gradual lengthening of both proximal and distal nerve stumps at the rate of 1 mm/day, as shown in figure 1.4[11]. This method has shown satisfactory results in animal tests. However, it is

extremely troublesome in practical application. For instance, it requires many additional and complex equipment and the lengthening operation is manually performed on a daily basis under sodium pentobarbital – induced anesthesia. In addition, to prevent infection, attachments such as an external fixator need to be sterilized and gauze is changed frequently. Thus alternative techniques need to be explored deeply for peripheral nerve regeneration.

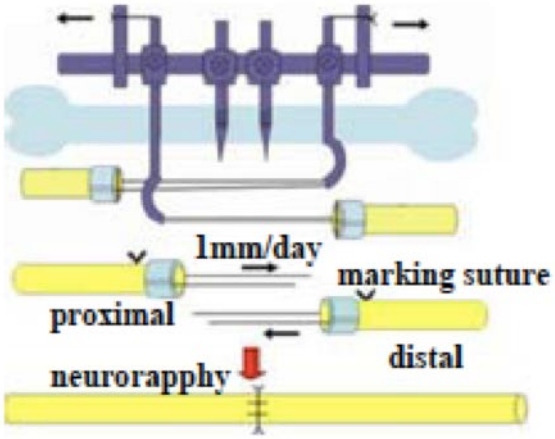

Figure 1.4 Manual nerve-lengthening method for nerve repair

According to the research progress about the peripheral nerve regeneration (PNR), this study will introduce a novel nerve conduit with shape-memory function and gain a systematic understanding of this smart nerve conduit to achieve PNR by automatic lengthening. To realize this goal, the key issues or problems addressed are:

1) How to obtain SMPs to meet the special requirements for PNR, such as a defined recovery time and a shape recovery condition of about 37°C in body fluid?
2) How to fabricate SNCs with optimal properties to provide adequate mechanical support and realize SMEs for PNR by automatic lengthening?
3) How to control the shape memory effect, and in particular, the shape recovery

rate of an SNC under *in vitro* and *in vivo* conditions, respectively?

4) How to achieve the peripheral nerve repair performance of SNCs under automatic lengthening with rabbit models?

1.3 Objectives

The objectives of this research are listed as follows:

1) To design and synthesize SMPs with body water triggered shape recovery function for PNR application
2) To fabricate SNCs by textile technology
3) To study the SMEs of SNCs under *in vitro* and *in vivo* conditions
4) To investigate the biological properties of SNCs
5) To evaluate the nerve repair efficacy of SNCs in animal models with nerve injury treatment

1.4 Significance

This will be the first study to introduce gradual-recovery shape-memory function into artificial nerve conduits, which can facilitate the lengthening of nerve stumps in an automatic and controlled manner. In addition, this biodegradable SNC can avoid second surgery after implantation, thus significantly reducing patients' suffering. Moreover, it will be the first attempt to exploit SMPs in a PNR application based on our thorough understanding of shape-memory mechanisms and familiarity with various polymeric materials, which will lead to a breakthrough in the biomedical field.

The long-term impact

1) A water-triggered SME with gradual-recovery function will result in a new generation of smart polymer function and programming designs, which may inspire the development of a variety of new shape-memory functions that will meet the specific requirements of different applications.
2) The project will inspire a brand-new direction for SMPs in biomedical applications, which may in turn stimulate a wide range of smart polymer applications in many other areas in the future.
3) The work provides a smart and efficient tool for peripheral nerve regeneration. This novel technology will create opportunities for minimally invasive repair surgery and more smart biomedical devices.

1.5 Methodology

1.5.1 Synthesis and characterization of SMPs

1.5.1.1 Synthesis

From tissue engineering viewpoint, opposite to other biomedical applications where a quick recovery is required, an ideal shape-memory material for smart nerve conduit should possess prolonged and gradual recovery process that is close to that of peripheral nerve regeneration process. This can allow the implanted smart nerve conduit correspondingly to have excellent shape fixity and controllable recovery under physiological conditions such as body fluid or/and temperature. From long recovery viewpoint, instead of heating the SMP to a certain temperature over its T_{trans} to trigger the SME, water-induced SME arising from the drop of T_g due to the plasticizing effect of water is more practical in human body and its shape recovery

process is more natural. Compared with that in thermo-induced recovery, time in water-actuated recovery is relative longer. The reason for this significant phenomenon is probably that the plasticizing effect is a time consuming process. It is easier and quicker to absorb water and reach saturation at the sample surface, while it is more difficult for water to penetrate deep inside into the material to act as a plasticizer. Therefore, we focus on the development of T_g-type SMP for self-shrinkable conduit to achieve a gradual self-recovery in body water (36°C). The glass transition temperature (T_g) of the SMPs mainly depends on their chemical component and structure. In this study, we will mainly use lactide acid and glycolide monomers to design and synthesize SMPs due to the biocompatibility and biodegradability of their copolymers. The polymer network system is synthesized through ring-opening polymerization, and the strategy to adjust T_g stems from the Fox-Flory equation.

1.5.1.2 Characterization

The molecular structure, morphology, miscibility, thermal properties of SMPs will be determined by FTIR, DSC, XRD, GPC, and SEM. In addition, the cyclic tensile test were used to characterize the thermal-induced shape-memory effect, namely investigate the shape recovery, shape fixity and recovery time of the series of synthesized SMPs. Further investigations on the water absorption behavior and plasticizing effect of water on SMPs will be systematically studied, such as the changes in T_gs during different immersion time.

1.5.2 Fabrication and characterization of SNCs

The smart nerve conduit with an inner diameter of 2-3 mm and a thickness of 0.1-0.3

mm will be fabricated. Their required initial lengths, such as 2 or 4 mm, will be obtained by cutting prepared SNCs with a heated penknife. Electrospinning technique will be primarily used, and other methods will also be considered, the electrospun tube can be collected from a shape-suitable collector. The process is carried out until the required thickness and structure of the nanofiber is deposited onto the rotating collector. Then the morphologies of conduits will be observed by SEM. Our study aims to develop a new method for nerve regeneration based on SNCs with SME function, and the thermal-induced and water-induced SME of the SNCs will be investigated by the cyclic tensile test and *in vitro* water recovery test, respectively.

1.5.3 Investigation of biological properties of SNCs

Biocompatibility of conduits: as implanted biomedical devices, it is necessary to ensure the biocompatibility of SNCs even though they are mostly made of FDA approved biomaterials. *In vitro* biocompatibility, such as that determined by cytotoxic and hemolytic properties of SNCs, will be studied. For instance, the viability of attached cells on conduits for various cell seeding time intervals will be obtained from an MTT assay, and the number and morphology of attached cells will be observed by fluorescent microscope technology. The *in vivo* biocompatibility of SNCs will be studied during the evaluation of repair efficacy with rabbit models.

1.5.4 Investigation of nerve repair efficacy of SNCs with rabbit models

1.5.4.1 Rabbit models and implantation of conduits or autografts

In this study, we will mainly study the nerve repair efficacy of SNCs with rabbit models. Thus, New Zealand White rabbits with sciatic nerve injuries will be set up for

SNCs. In addition, we will compare the efficacy of autografts and common conduuits. During the implantation process, conduits or autografts will be performed by end-to-end suturing with 8-0 mono-filament nylon to connect the nerve tube and nerve.

1.5.4.2 Evaluation

4, 8 and 12 weeks after implantation, we will evaluate the repair performance. The middle part of a regenerated nerve will be sampled for paraffin embedding and microtome sectioning. The investigation includes: a) histological staining. The neural part of the group sections will be HE stained to observe the conduit length, thickness, and completeness. b) special microsurgery to stain nerves. Special dyes will be used to micro-stain regenerated nerves to calculate the number of nerves per unit area, and observe neurological recovery. c) the compatibility of SNCs will also be evaluated by histological analysis, and the degradation of SNCs will be also studied.

1.6 Arrangement of the thesis

The thesis comprises 7 chapters described as follows:

Chapter 1 stated the general background of this research, academic and biomedical application progress of shape-memory polymers, the mechanism about the shape-memory effect, statement of problems, objectives and significance and research methodology.

Chapter 2 included literature review about the development of shape-memory

polymer & biomedical application, peripheral nerve regeneration strategy, and electrospinning technology in biomedical application.

Chapter 3 is the experiments part, including the preparation of samples and the characterization techniques used in this study.

Chapter 4-6 are the main parts of the thesis consisting of the following contents: characterization of SMP; performance of SNC made from the synthesized SMP; and the biological assay of the SNC.

Chapter 7 presented the summary of conclusions, and some future work including theoretical study and applied technology was suggested.

References are attached in the end of this thesis.

CHAPTER 2 LITERATURE REVIEW

2.1 Development of shape memory polymers

Shape-memory materials including shape-memory alloy (SMA), shape-memory polymer (SMP) and shape-memory ceramic are stimuli-responsive materials, which are able of changing their shape upon external trigger such as temperature, light or pH value[3,12-14]. Among these shape-memory materials, SMP possesses the advantages of low cost, good processing ability, high elastic deformation, excellent shape recoverability, and potential biocompatibility. Shape-memory behavior is not related to a specific material property of certain polymers, but a combination of the molecular structure and morphology together with the applied processing and programming method. From the molecular structure and morphology standpoint, SMP often consists of net point and switch point. The net points are responsible for the permanent shape, which could be made of either covalent or physical cross-links. The driving force for geometric recovery is the entropic elasticity of the polymer network. Similarly, the switch points determine the shape fixity and recovery upon a certain external stimulus. Until now, the amorphous, crystalline, liquid-crystal phases, supramolecular entities, and light-reversible coupling groups have acted as the switch points in SMPs, as shown in figure 2.1[3,4,15,16].

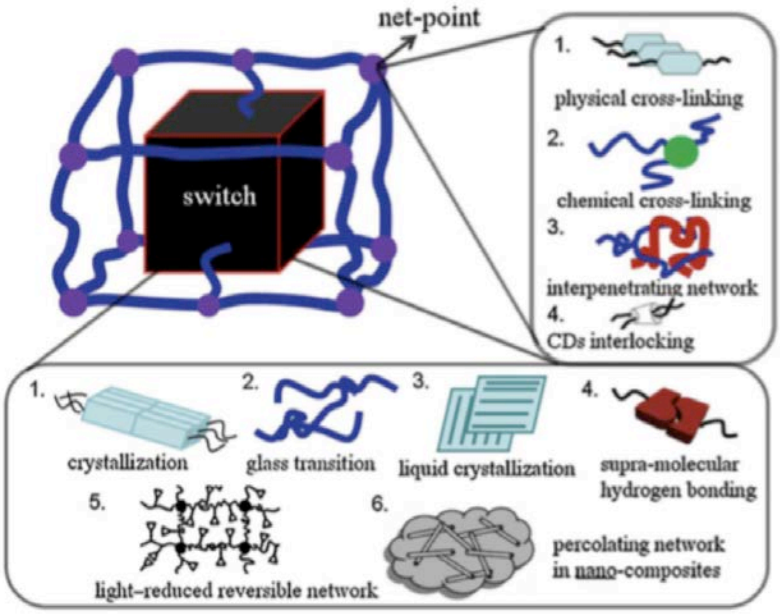

Figure 2.1 The overall architecture of SMPs

From the processing and programming standpoint, several types of evaluating methodology, such as thermal-induced cyclic tensile investigation, strain recovery test, and bending test, were established to meet the academic and practical requirement. The typical thermal-induced shape-memory behavior is shown schematically in figure 2.2. First, the polymer is traditionally processed to possess its original shape. Then, the polymer is deformed and the temporary shape is fixed. This process is called programming, it often consists of heating up the sample, deforming, and cooling the deformed sample. Now the permanent shape is stored in a temporary state. Then heating up the SMP above a transition temperature (T_{trans}) would trigger SME and the recovery of permanent could be observed.

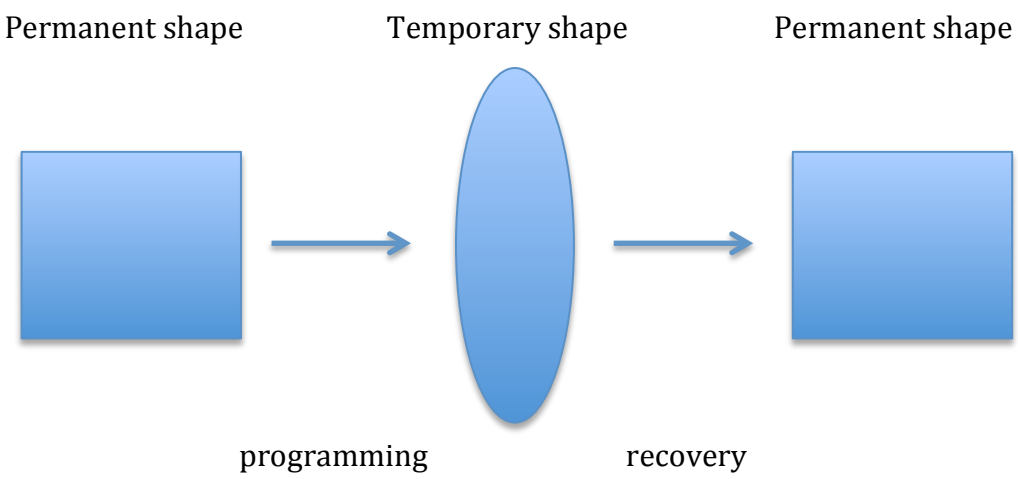

Figure 2.2 Schematic representation of thermal-induced shape-memory behavior

Since 1960s, when covalently cross-linked polyethylene (PE) found its application into heat shrinkable tubing and films, the commercial significance of SMPs began to be recognized. In this case, there exists two distinctive phases in cross-linked PE, called amorphous regions and crystalline regions, respectively. Ionizing radiation can introduce cross-linking structures into amorphous regions, which was believed to form a three dimensional network. Crystalline regions can keep the temporary shape when the temperature is below the T_m of crystalline regions[4]. Heating up the deformed polymer above T_m could release the restraint, then the shape-memory effect was triggered and the original shape will be recovered. Presently, several types of polymer have been reported to possess shape-memory functions for diverse applications[17,18]. According to the differences in temporary shape fixing mechanism and formation of permanent shape, the SMPs can be divided into four types.

2.1.1 Chemically cross-linked T_g-type SMP

The simplest type of SMP is a covalently cross-linked amorphous polymer possessing a sharp T_g range at the temperature of interest[19,20]. This type of SMP obtains attractive properties including excellent shape recoverability due to the nature of chemical cross-linking, tunable work capacity that can be adjusted through the extent of cross-linking, and an absence of disentanglements between molecular chains due to strong covalent cross-linking[21-24]. However, since the original shape is permanently determined, these processed shape memory materials are difficult to reshape again. An example of this type is a covalently cross-linked vinylidene copolymer made of methyl methacrylate and butyl methacrylate whose homopolymers have T_gs at 110°C and 20°C, respectively. The copolymer presents a single and sharp T_g that is tunable between T_gs of the related homopolymers. To meet each particular application requirement, rubbery modulus of the SMP can be adjusted by varying the extent of cross-linking, in this case achieved by copolymerization with a tetraethylene glycol dimethacrylate. Therefore, this synthesized SMP possesses excellent shape fixing and recovery function. Besides the chemically cross-linked SMP with a sharp T_g range, Larock used renewable natural oils with a high degree of unsaturation, styrene and divinylbenzene to synthesize SMP. In his study, broad glass-transition gap was observed and apparently slowed the shape-recovery speed[4]. In addition to the aforementioned examples, other materials have been reported as SMPs based on the same mechanism, such as poly(alkyl methacrylate) copolymers, polystyrene copolymers, filler-modified epoxy networks, and amorphous

polyurethane networks.

2.1.2 Chemically cross-linked T_m-type SMP

Besides the glass transition temperature as a transition temperature, the melting transition of crystalline segments can also be employed to trigger SME[25]. In this type, the temporary shapes are fixed by crystallization instead of by vitrification. Similar to the first T_g type, the permanent shapes are also determined by covalent cross-links and cannot be reshaped after processing, and the stiffness of this material is sensitive to the degree of crystallinity rather than to the extent of cross-linking. This category includes semi-crystalline polymers, liquid-crystal elastomers (LCEs), and hydrogels with phase separated crystalline microdomains[26,27]. Semi-crystalline polymers are prominent shape-memory materials due to their superelastic rheological characteristics, fast shape recovery speed, and flexible modulus at the fixed stage. One classic material of this type is chemically cross-linked *trans*-polyisoprene (TIP), which is a semi-crystalline polymer with a T_m of 67°C and a degree of crystallinity around 40%, possessing a stiffness of about 100 MPa at room temperature. The three dimensional network of TIP was chemically cross-linked by peroxides, that determined the permanent shape and created the super elastic property. However, thermal instability inhibits the end-application of this material due to the existence of abundant unsaturated double bonds. A. Lendlein and co-workers have reported a SMP with biodegradable properties by copolymerizing oligomeric poly(ε-caprolactone) dimethacrylate with *n*-butyl acrylate under UV radiation to yield a multiblock structure[4,28-30]. The polycaprolactone segments could form a crystalline structure

to fix the temporary shape at low temperature, leaving the melting points of the PCL segments to control the shape-recovery temperature. Meanwhile, the amorphous *n*-butyl acrylate together with the PCL dimethacrylate could also form a three dimensional network, and its low glass-transition temperature (T_g = -55°C) determines the permanent shape and trigger the shape recovery. The merit of this material includes the very sharp melt transition, which is due to the uniformity of the crystals introduced by PCL segments. A sharp transition temperature gap would assure excellent shape recovery behavior. Another contribution of this report is the application of a photo-cure method to easily fabricate SMPs with permanent shapes. Recently, other synthetic methods based on radiation cross-linking were also proposed to fabricate biodegradable polycaprolactone networks exhibiting excellent shape-memory properties. Due to the impediment of crystal formation, cross-linking the semi-crystalline material might generate a lesser degree of crystallinity, broader crystal-size distribution, and a broader melting-transition temperature span[31,32]. In order to maintain a sharp transition and to avoid a drop in the transition temperature, efforts are undertaken to specifically cross-link the amorphous segment but not the crystalline fraction. Successful implementation of this method was reported for special curing techniques being performed to only cross-link the rubber matrix, leaving the semi-crystalline phase unaffected.

2.1.3 Physically cross-linked T_g-type SMP

Processing ability has been a key factor for commercial advancement of SMPs, and this class SMP displays rheological characteristics to facile processing with traditional

thermoplastics technology[33-35]. The example for this category is a melt-miscible blend composition of poly(vinyl acetate) (PVAc) and poly(lactic acid) (PLA). In addition, in this SMP class, crystalline or rigid amorphous domains may serve as physical cross-links affording the super-T_g elasticity, mainly in the form of phase-separated block copolymers. When the temperature is above the T_m or T_g (symbolized as T_{high}) of these discrete physical domains, the material will flow and can be processed and reshaped. Another continuous phase, with a lower T_g (symbolized as T_{low}), exists a rubbery state at $T_{low} < T < T_{high}$ and fixes a secondary shape on cooling to $T < T_{low}$. For some block copolymers especially polyurethanes, a sharp glass-transition of the soft domain is useful for shape-memory. Although the room-temperature stiffness of these materials is similar to the first class, their physically cross-linked structure yields the advantage of being processed. For example, norbornene was copolymerized with a polyhedral oligosilsesquioxane (norbornenyl-POSS) hybrid monomer, yielding a micro-phase separated copolymer with fewer repeating units in the backbone. Such a composition also improved the thermal processability, the critical temperatures and the stored energy during deformation, while the T_g of the copolymer broadened to some extent, which slightly retarded the shape-recovery speed. P. T. Mather has worked on two miscible blend systems: poly(vinyl acetate) (PVAc) with poly(lactic acid) (PLA) and PVAc or PMMA with poly(vinyldiene fluoride) (PVFD). Both polymer systems are miscible for all blend ratios. In addition, PVAc and PMMA are totally amorphous, PLA and PVDF are semi-crystalline and have a degree of crystallinity of about 50%,

individually. Therefore, the degree of crystallinity of the blends varies from 0 to 50% according to the blend ratio, with crystals acting as physical cross-links and the extent of crystallinity controlling the rubbery modulus. While the T_g of the amorphous segment works as a transition temperature and can be tailored between the T_g values of the two homopolymers. In addition, polymers with T_g > room temperature and with ultra-high molecular weight, $>10^6$ g mol^{-1}, can also be attributed to this class due to their low mobility above T_g and complete shape fixing by vitrification. Such entanglements form a three-dimensional structure introducing excellent elasticity above T_g. The widely applied SMPs with these characteristics include polynorbornene PN, with $T_g \approx 40°C$, and high molecular weight poly(methyl methacrylate) PMMA, with $T_g \approx 105°C$. However, the disadvantages of these SMPs are: 1) the transition temperature cannot be easily and precisely adjusted; 2) the SMP will creep under stress at high temperature ($>T_g$) due to the limit lifetime of entanglements; and 3) difficulty of processing due to the high viscosity associated with high molecular weight.

2.1.4 Physically cross-linked T_m-type SMP

In addition to the T_g-type, the soft segment of some SMPs could crystallize and, instead of T_g, their T_m values function as shape-memory transition temperatures and the secondary shapes are thus fixed by crystallization of the soft domains. The example for this type is a multiblock polyurethane featuring PEO as a soft segment. Another example is a styrene-*trans*-butadiene-styrene (STBS) triblock copolymer. STBS is a strongly segregated ABA-type triblock copolymer with a minor component

of polystyrene (PS) segments, serving as A-domains at each end of the macromolecular chains, and a major component of semi-crystalline poly(*trans*-butadiene) (TPB) segments, serving as B-domains in the middle of the macromolecular chains. Due to the immiscibility between PS and TPB blocks, PS blocks form discontinuous, amorphous micro-domains having T_g = 93°C, TPB blocks form semi-crystalline, comparatively compliant micro-domains having T_m = 68°C and a T_g far below room temperature, at -90°C. The rigid PS micro-domains remain rigid up to 90°C and thus act as physical cross-links. When heated to 68 < T < 90°C, the material becomes flexible and rubbery due to the melting of the TPB crystals in the matrix, but does not flow due to the rigid PS micro-domains, maintaining a stress-free permanent shape. At this stage, the materials have a storage modulus resembling rubber and dictated by the TPB matrix crystallizes so that a secondary shape can be fixed by those crystals. The energy generated during deformation is then frozen into the material. Then the deformed shape can return to the permanent shape upon melting of TPB. The STBS block copolymer, and other materials in this class, possesses the advantages of having a permanent shape that can be reshaped by thermal processing above 100°C, when both domains flow. The possible disadvantage is that the hard micro-domains may creep under stress when setting the temporary shape near T_g, limiting the level of recoverable strain. As a similar approach, thermoplastic polyurethanes with semi-crystalline segments have also been investigated for shape-memory effects. Conventionally, polyurethanes are multiblock copolymers consisting of hard and soft segments. The hard segments form physical

cross-links by way of polar interaction including hydrogen bonding, or crystallization, with such cross-links being able to withstand moderately high temperatures without being destroyed. Meanwhile, soft segments form the thermally reversible phase and the crystallization of these soft segments governs the secondary shape. Polyurethanes feature the advantages of easily adjusting the room-temperature stiffness and transition temperature by manipulating their compositions, with some being potentially biocompatible.

2.2 Shape-memory polymers for biomedical application

Recently SMPs have attracted substantial attention for biomedical applications. SMPs offer the ability to promote minimally invasive surgery, release therapeutic drug, generate stabilizing force, and provide structural support[8,36-39].

2.2.1 Motivation for introducing SMP to biomedical applications

Polymeric biomaterials are currently applied in controlled drug delivery system, scaffolds, surgical instruments, wound dressing, and extracorporeal devices. The rapid advance in surgical techniques, especially in minimally invasive surgery, proposes many complicate requirements for current biomedical implants[5-7,40]. Typical questions arising include: how to insert a bulky implant into the body through a small incision; or how to adjust an implant to the individual geometric requirement of a patient. Here, shape-memory effect could potentially solve the aforementioned problems. SMPs can change their shape in a predesigned way when exposed to external stimulus. Examples are thermally induced SMPs, of which the SME was triggered by heat. A bulky implant possessing a transition temperature between room

temperature and body temperature could be inserted into the body through a small incision in a compact temporary shape. Once the implant is placed in the body, it is heated to body temperature and recovers to its original application-required shape[41]. Furthermore, the deformed temporary shape can be adjusted to the individual needs of the patient. In addition, the SME also could be combined with other desired functions, such as degradability or drug release. Degradability would be a valuable additional function, as a second surgery for explanation could be avoided. Many groups worldwide, industrial and academic are pursuing medical applications of SMP. For example, to achieve proper closure of an incision, Lendlein et al. demonstrated the concept of biodegradable thermal-induced SMP sutures. An extruded monofilament of oligo(ε-caprolactone)diol-based SMP was elongated under heat and cooled to keep the temporary shape. an abdominal wound was loosely sutured using the SMP fiber, and then heated to body temperature to achieve wound closure (Figure 2.3)[40].

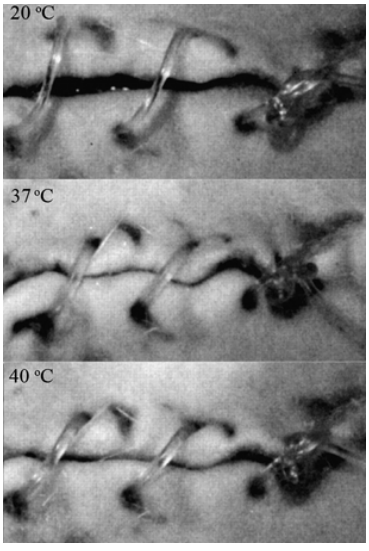

Figure 2.3 Biodegradable SMP suture for wound closure

Drug-loaded SMPs possess great promise for applications in the fields of controlled drug release. Due to the limited numbers of contributions in this field, only a few practical examples of potential applications have been reported. One of these is a ureteral stent that can be anchored in the ureter, as demonstrated in figure 2.4. Such stents might be useful to keep the ureter open, for example in patients with abdominal tumors. In addition, self-anchoring implant rods for a sustained drug release and different SMP reservoir system for fast stimuli-induced drug release have been suggested.

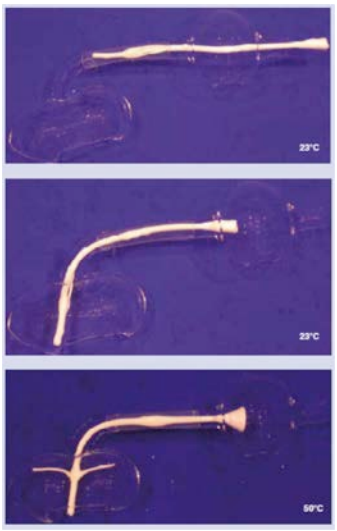

Figure 2.4 Illustration of the principle of a shape-memory polymer ureteral stent from a PCGDMA network

In the long term, there are a number of potential areas for innovation in medical applications of SMP. For examples, the requirements of improved stress recovery, better manufacturability, and remotely modified chemistry are proposed. Since SMPs have superior strain recovery in comparison to SMAs, a reduction in strain recovery could increase stress recovery. The first area of improvement would be to develop a

hybrid SMP-SMA device to actuate the device. For the second area of material improvements, a thermoplastic SMP could be easily molded and machined and then subsequently treat to form a permanent shape. The third development would open up a new application window that SMP-based device could be remotely triggered to change from a biostable to a biodegradable chemical structure. In many cases biomedical devices are only needed for months but are placed permanently. If these devices could be triggered to become biodegradable then the negative side effects of a permanent device could be avoided.

2.2.2 SMP for biomedical applications

With respect to SMPs, each biomedical application requires a specific combination of material characteristics and certain practical functions, which can be fulfilled by the suitable choice of SMP architectures[42-44]. For example, when functions of tissues are replaced by a polymer-based implant or device, biofunctionality is required. For biomedical devices in contact with blood, such as artificial heart valves or scaffolds, the hemocompatibility of device surface is essential. For biomedical implants supporting wound healing or regeneration (e.g., scaffolds as temporary substitute of the extracellular matrix), the hydrolytic biodegradability is the prerequisite.

Physically cross-linked SMPs

An important group of physically cross-linked SMPs are linear block copolymers. As most polymer segments with a sufficient difference in the molecular structure are not mixable with each other, multiblock copolymers, in which T_{trans} relies on T_g or T_m, can be obtained. Typical thermoplastic SMPs can be synthesized by direct coupling of

pre-synthesized polymer blocks with a chain extender. The application of the prepolymer method enabled the production of thermoplastic polyurethane on an industrial scale. In this process, isocyanate-terminated prepolymers are synthesized by reaction of hydroxytelechelic oligo-esters or -ethers with an excess of a low-molecular-weight diisocyanate. Examples of such polymers are polyurethanes (PUs) with a hard segment from methylenediisocyanate (MDI), and butanediol and poly(tetrahydrofuran) (PTMEG) or poly(caprolactone) (PCL) as the soft segment. For example, in a commercially available PU synthesized from 4,4-diisocyanatodicyclohexylmethan (H_{12}MDI), 1,4-butanediol, and PTMEG, T_g is at 74°C. This material is used in artificial hearts, wound dressings and pacemaker leads. Determination of shape-memory properties revealed an R_f of 100% and R_r of 80%. The incorporation of silica-coated magnetic nanoparticles of iron (III) oxide core into Tecoflex® enabled the remote actuation of the thermally induced SME in alternating magnetic fields.

Chemically cross-linked SMPs

Covalently cross-linked SMPs can be obtained by cross-linking of linear or branched polymers, as well as by polymerization of one or several monomers, whereby at least one monomer has to be at least tri-functional. The shape-memory behavior of chemically cross-linked SMP could be controlled by certain general parameters, such as the density of the cross-links, the network chain segment length, or the number of phases. For example, the mechanical property could be controlled by the cross-link density, which is a function of the chain segment length and the functionality of

cross-links. Moreover, the switching segment influences the hydrolytic degradation, as well as the characteristics of the SME, which can extend either over a broader temperature interval (T_g) or a sharp melting temperature (T_m).

For example, covalently cross-linked SMP with $T_{trans} = T_g$ could be obtained as AB copolymer networks from the copolymerization of diethylene glycol dimethacrylate (DEGMA) with *t*-butyl acrylate, the T_g was around 55°C. the rubbery modulus could be adjusted between 1.5 and 11.5 MPa by the variation of the cross-linker content between 0 and 40 wt%. When methacrylate was used in such AB copolymer instead of *t*-butyl acrylate, the T_g could be adjusted between 56 and 92°C, while values of rubbery modulus between 9.3 and 23 MPa were obtained. Moreover, Fe_3O_4 particles could be added to the copolymer, enabling remotely controllable SMP network composites[14]. Another example for SMP with $T_{trans} = T_g$ is star-shaped hydroxytelechelic *co*-oligoesters yielded copolyesterurethane network. In this case, ring-opening polymerization of α-hydroxy acids with hydroxytelechelic initiators introduced the cross-link points into *co*-oligoester segments. 1,1,1-tris(hydroxymethyl) ethane or pentaerythrite were used as initiator, resulting in trifunctional or tetrafunctional netpoints, respectively. The final polymer networks were obtained by addition TMDI to the *co*-oligoesters and subsequent heating. R_f and R_r of all synthesized SMP networks were higher than 90%[2,45].

Similar to covalently cross-linked SMP networks based on acrylates, polymer networks with $T_{trans} = T_m$ can be synthesized based on PCL diol as the component forming a crystallizable switching segment[22,46]. For this purpose, PCL diols have been functionalized with methacrylate end groups that can undergo a polymerization reaction. The cross-linking was performed without the addition of an initiator by photo-polymerization. The molecular weights of the PCL dimethacrylates used varied between 1500 and 10,000 g mol^{-1}. T_{trans} of the materials was adjustable via the molecular weight of the macrodimethacrylates used in the synthesis, and was varied between 30 and 50°C. The photoset materials, named N-PCLDMA, displayed excellent shape-memory properties, with R_r between 92 and 97% and R_f between 86 and 97% after five cycles.

2.3 Peripheral nerve regeneration strategy

The complex physiology of the nervous system presents unique challenges to tissue-engineering research. The nervous system contains two main types of cells: neurons and glial cells. The most fundamental property of neuron is their communication with other cells via synapses. Many types of neuron possess an axon, a protoplasmic protrusion that can extend to distant parts of the body and make thousands of synaptic contacts[47]. The structure of a typical neuron is illustrated in figure 2.5. Glial cells are non-neuronal cells that provide support and nutrition, maintain homeostasis, form myelin and participate in signal transmission in the nervous system. The most important functions of glial cells are to support neurons; to supply nutrients to neurons; to insulate neurons electrically; to destroy pathogens; and

to provide guidance cues directing the axons of neurons to their targets.

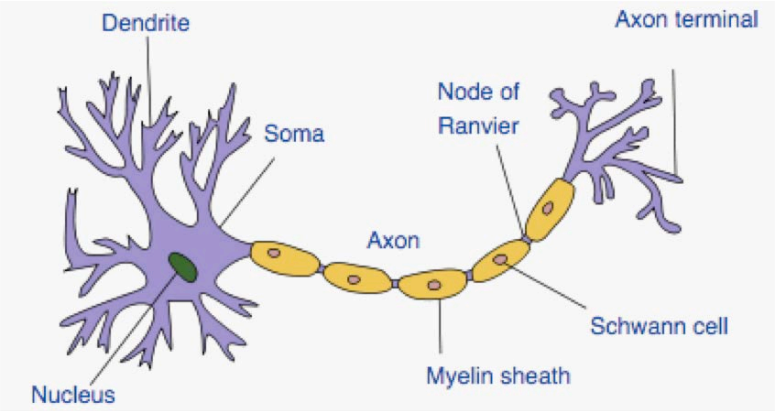

Figure 2.5 Structure of a typical neuron

In addition, the nervous system includes the central nervous system (CNS) and the peripheral nervous system (PNS). The CNS mainly includes two parts: brain and spinal cord. The main function of the CNS is to conduct and integrate signals receiving from all parts of the bodies as well as to provide excitatory stimuli to the PNS. The PNS mainly includes three parts: cranial nerves arising from the brain, ganglia arising from the spinal cord, and sensory systems. The main function of the PNS is to connect the CNS to the limbs and organs, essentially acting as a communication medium between the brain and the extremities. An essential difference between the PNS and CNS is the capacity for injured nerve to regenerate: CNS does not regenerate apparently in their native environment, because glycoproteins existing in the native extracellular environment of the CNS inhibit nerve regeneration. For peripheral nerve injury, treatments typically include direct end-to-end surgical reconnection of the severed nerve ends, the use of artificial nerve conduits, and the use of an autologous or allograft nerve graft.

2.3.1 Direct nerve repair

Among the above-mentioned three repair methods, tension-free suture remains the preferred treatment option for nerve injury. Direct nerve repair is applied in case of nerve injury with minimal gap. The ideal surgical condition for this method is an injury zone with excellent blood supply and soft-tissue coverage, and the proper alignment of nerve ends is also critical to nerve recovery (Figure 2.6)[48]. Besides simple direct end-to-end repair, end-to-side repair may be favorable when the proximal aspect of the injured nerve is not salvageable. The distal stumps of the injured nerve can be sutured to an adjacent nerve with subsequent collateral sprouting. Yu et al. evaluated end-to-side neurorrhaphy in the ulnar nerve as the donor and in the musculocutaneous nerve as the recipient. The development of microsurgical techniques and instruments led some researchers to promote grouped fascicular repair. This approach attempts more accurate approximation of regeneration axons but requires more dissection and potential soft-tissue disruption. In nerves with defined motor and sensory topography, such as median or ulnar nerves in the forearm and the sciatic nerve in the thigh, such repair method is often used.

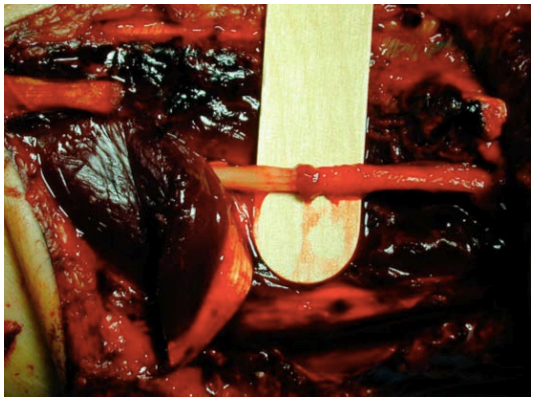

Figure 2.6 A median nerve laceration in forearm repaired by direct end-to-end repair

2.3.2 Use of conduits

Since tensionless repair is a major requirement for the successful nerve regeneration. When direct end-to-end repair cannot be achieved, autologous nerve grafting is the gold standard for nerve defects. However, autologous grafting possesses some drawbacks including requirement for two anastomotic sites, increased operative time, and expensive costs. Research interest has turned toward guidance therapies[49,50]. Potential advantages of nerve conduits include absorbability, lack of donor-site morbidity, and lack of axonal escape. There are three main types of biocompatible conduits that are currently approved by the U.S. Food and Drug Administration (FDA): collagen, polyglycolic acid, and caprolaction. Synthetic materials are attractive because their chemical and physical properties (e.g., degradation rate, porosity, mechanical strength) can be specifically adjusted for a particular application. However, the biocompatibility of synthesized materials introduces a challenge because the body's inflammatory response can vary considerably from one material to another. In addition, some synthetic materials that are tolerated by the body's immune system are unfortunately incompatible with cell adhesion and tissue repair[51]. These materials are often modified to make them more cell-friendly. Research is under way to identify synthetic materials that can be used for nerve repair applications. There are several general properties for an appropriate nerve conduit material: (a) they must be easily fabricated into a conduit with desired dimensions, (b) they must be sterilizable, (c) they must possess sufficient mechanical property, and (d) they must be easy to suture. Since permanent implant would introduce a higher risk for infection, which

could provoke a chronic inflammatory response and have the possibility to compress the regenerated nerve over time. A nerve conduit fabricated from biodegradable synthetic materials is preferred. Additionally, nerve conduits should be pliable, but could maintain their shape and resist collapse during implantation and regeneration course. Researchers have also shown that guidance channels should be semipermeable and should have a smooth inner wall. A number of synthetic materials have been studied for nerve regeneration. Poly(glycolic acid) (PGA), poly(lactic acid) (PLA), and poly(lactic-*co*-glycolic acid) (PLGA), were some of the first explored synthetic polymers because of their biodegradation characteristics, ease of processing, and approval by the FDA. These materials continue to be studied to date. For example, PLGA has been processed into foams (Figure 2.7) and seeded with Schwann cells to improve their regenerative function. In addition to poly(esters), biodegradable poly(urethane), poly(organo phosphazene), methacrylate-based hydrogels, and poly(3-hydroxybutyrate) have shown a capacity for guiding nerve regeneration.

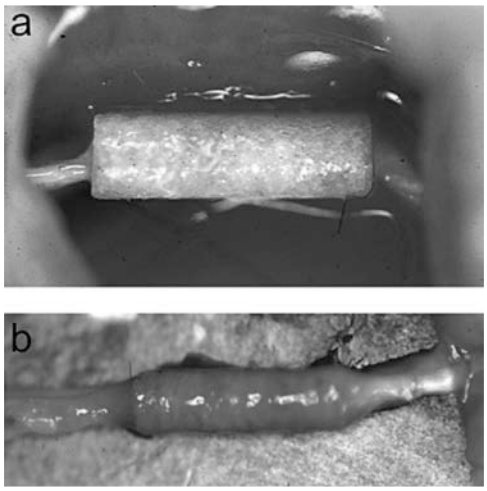

Figure 2.7 Poly(L-lactic acid) foam nerve conduits. Porous biodegradable poly(L-lactic acid) (PLLA) conduits were fabricated using a solvent casting, extrusion, and leaching technique. (a) Nerve guidance channels from 10 mm to 22 mm in length were used

to repair transected rat sciatic nerves, a common model for studying peripheral nerve regeneration. (b) After 4 months, the PLLA conduits remained structurally intact, supported tissue infiltration and vascularization, and resulted in structural and functional regeneration comparable to isografts, the current clinical gold standard

In addition, nondegradable artificial materials have been also studied in nerve regeneration applications, including silicone conduit, which has been applied in clinical settings as well as in research settings, and expanded to poly(tetrafluoroethylene). Silicone has been studied since the 1960s, and much fundamental insight into nerve regeneration has come from this model system. In general, inert silicone tubes can be used to bridge short gaps with some success. However, it is commonly accepted that impermeable, inert guidance channels, such as silicone, do not support regeneration across defects larger than 10 mm without exogenous growth factors. Therefore, research is now focused on developing semipermeable or degradable guidance channels that can actively stimulate improved regeneration over longer and more clinically relevant defect lengths. Poly(ethylene glycol) (PEG) has also been used in nerve regeneration applications. For example, PEG has been applied to fuse the membranes of severed nerve ends of sciatic nerves. These studies have shown that the axon potential conduction can be restored immediately with this method. Unfortunately, this procedure can only be applied for large nerve defects. Additionally, cross-linked PEG hydrogels modified with growth factors to mimic ECM are under active development, particularly for cardiovascular

applications. Recent studies on this field are also looking into their potentiality to aid nerve regeneration. For example, PC12 cells are supposed to extend neuritis on the PEG hydrogel when the cell adhesion motif Arg-Gly-Asp-Ser (RGDS) is covalently incorporated into the materials. Research has also shown that electrical charges play a significant role in stimulating the cellular differentiation. For example, neurite extension is significantly enhanced on piezoelectric materials (materials can generate a surface charge with small deformations), such as poly(vinylidene fluoride) (PVDF), and on electrically conducting polymers, such as poly(pyrrole). Further modification of these materials with biological stimuli (e.g., hyaluronic acid) may provide these aforementioned biomaterials for use as nerve conduits.

2.3.3 Grafting

For larger injury gaps in which aforementioned direct end-to-end repair method would cause tension, autografting remains the standard golden method for nerve regeneration. Recent advances in allografting technique and biomaterials continue to introduce promising prospects for the future of PNR[52].

Use of autograft

Autologous tissue grafts have been used extensively for nerve repair application and possess several advantages. Autologous materials are more likely to be biocompatible than artificial materials, and could provide a support structure to promote cell adhesion and migration. Drawbacks, on the other hand, include potential difficulties with isolation and controlled scale-up. Nerve autografts are typically derived from cutaneous nerves, such as the sural or saphenous nerve, with an available length up to

about 40 cm and a cable diameter of 2-3 cm. In addition to the nerve autografts, other natural tissues, such as autologous muscle and vein grafts, have been also used in the clinic. Therefore, some current research efforts are focused on natural tissue grafts for peripheral nerve repair, including the use of tendon grafts, muscle-vein grafts, inside-out vein grafts, and vein grafts impregnated with autologous Schwann cells. All have exhibited encouraging results in research but still suffer from the key drawback that tissue must be removed from the patient.

Use of allograft

Because of the limitations with using autologous tissue, research attention has turned toward nonautologous tissue and extracellular matrix (ECM)-based materials. Allogenic and xenogeneic tissues (donor tissue from cadavers and animals, respectively) have the merits that supplies can be large and does not require harvest from the patient. However, these allograft tissues may possess some risk of disease transmission and must either be used in conjunction with immunosuppressants or be processed to remove immunogenic components. Many efforts are being made to process intact nonautologous tissue, rendering it less immunogenic for clinical use. These methods focus on removal of the immunogenic cells and the preservation of the ECM components that are essentially conserved between species.

2.4 Electrospinning technology in biomedical application

Electrospinning has gained attention in the last decade due to an increased interest in nanoscale properties and technologies[53-55]. Electrospinning allows for the production of polymer fibers with diameters varying from 1 nm to 10 μm. Potential

applications of electrospinning include tissue engineering scaffolds, filtration membranes, and nanofiber-based sensors. Typical electrospinning setup consists of a syringe pump, a high voltage source, and a collector (Figure 2.8)[54]. During the electrospinning process, the injected polymer solution is held at the needle tip by surface tension. The nozzle serves as an electrode, to which a high electric field of is applied, and the distance to the collector is 10-25 cm in laboratory setup. The applied electrostatic force opposes the surface tension, and eventually overcomes the surface tension, causing the initiation of a jet. As this jet flies, the solvent evaporate and an appropriate collector is used to collect the polymer fiber. Figure 2.9 indicates a typical scanning electron microscopy image of an electrospun polymer mat[56]. Electrospun fibers and mats have provided several advantages such as high surface to volume ratio, high porosity and enhanced mechanical properties. In addition to these, manipulation of the process parameters can be easily done to obtain the desired fiber morphology and mechanical properties. Since electrospun scaffolds could positively promote cell-matrix and cell-cell interactions, electrospun nanofibers are broadly applied in biomedical applications recently, as tissue engineering scaffolds, in wound dressing, drug delivery, and small diameter vascular graft implants[57-59]. For tissue engineering, biodegradable scaffold is generally considered as an indispensable element because they can be used as temporary templates for cell seeding, invasion, proliferation, and differentiation[60-62]. The diameter of electrospun fibers is of similar magnitude as that of fibrils in extracellular matrix (ECM) that mimics the natural tissue environment and has presented effectiveness as a substrate for cell

growth.

Natural polymers are often used for fabricating nanofibrous scaffolds because of their excellent biocompatibility and biofunctional motifs such as collagen, alginate, silk protein, chitosan, and others. In addition to these, their blending into synthetic polymers can enhance the overall cytocompatibility of the scaffold. Meanwhile, a variety of polymeric nanofibers have been considered for use as scaffolds for engineering tissues such as arterial blood vessels, heart, nerves, bones, etc. Among the synthetic polymers, electrospun PLGA fiber mats are considered ideal for tissue engineering scaffolds because their porosity is greater than 90% and the presence of multiple focal adhesion points on different fibers that allow higher cellular attachment. Geng et al. reported this electrospun mat could support growth and proliferation of a wide variety of cell types for example, mouse fibroblasts adhere and spread well on PLGA nanofibers according to fiber alignment. Li et al. reported that silk nanofiber scaffold containing bone morphogenetic factor 2 (BMP-2) had been applied for *in vitro* bone formation from human bone marrow-derived mesenchymal stem cells and suggested that nanofibrous scaffolds of silk fibroin served as ideal candidates for bone regeneration. Since marrow stromal cells (MSC)' ability to differentiate into multiple cell lineages, electrospun PCL scaffolds have been studied to support the attachment, proliferation and differentiation of MSCs into adipogenic, chondrogenic, and osteogenic. The cell biocompatibility of PLGA electrospun scaffolds with MSCs has also been demonstrated.

In addition to scaffolds, electrospinning technology has shown promising future in wound dressing. For wound healing, an ideal dressing should possess certain characteristics such as haemostatic ability, bacterial barrier efficiency, absorption ability of excess wound fluid, appropriate water vapor transmission rate, functional adhesion, and conformability to the contour of the wound area. Electrospun materials seems to meet most of the aforementioned requirements for wound healing purpose because the nanofibrous and microfibrous structures provide the nonwoven textile with desirable properties and there are also studies of cytocompatibility and cell behavior on electrospun nanofibrous membranes. Rho et al. have investigated the wound healing properties of electrospun type I collagen fibers on wounds in mice and they found that the healing effect was better with nanofibrous mats with conventional wound care. Spasova et al. have also demonstrated that fibrous poly(L-lactide) (PLLA) and PLLA/poly(ethylene glycol) mats coated with chitosan could increase the haemostatic activity[63-66].

In sum, electrospinning is a simple and cost-effective method fabricating non-woven fibers with high surface area to volume ratio and tunable porosity. Because of these excellent properties this technology seems to be a promising candidate for tissue engineering applications.

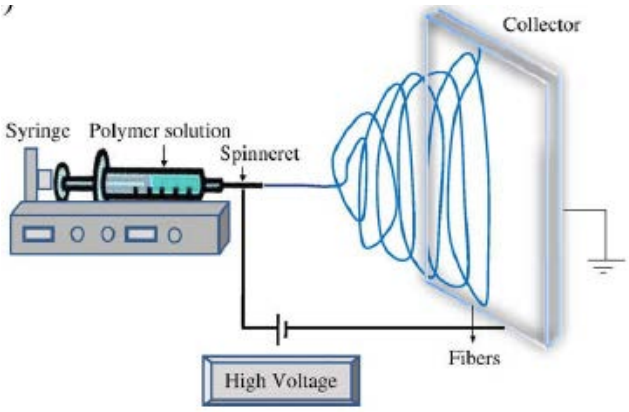

Figure 2.8 A laboratory setup for an electrospinning experiment

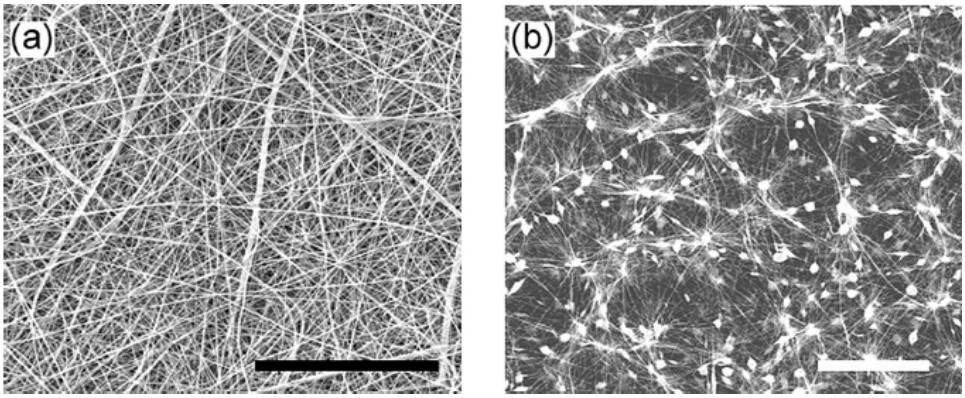

Figure 2.9 (a) A random polymer fiber mesh produced by electrospinning a 9% PCL solution. (b) Electrospun mesh fabricated using a 5% PCL solution

2.5 Biological assay

2.5.1 In vitro models

The selection of *in vitro* models for biocompatible assay and nerve regeneration research can go in three directions: immortalized cell lines (neuronal and glical), primary cultures (neuronal and glial), and organotypic and 3D cultures.

Immortalized neuronal and glial cell lines

A number of immortalized neuronal and glial cell lines have been obtained either from neoplastic nervous tissue or by genetic manipulation of neuronal and glial

precursors. These lines represent stem/precursor cells that can differentiate into neurons under adequate medium conditions. The main advantage of cell lines compared to primary cultures is the availability of a large and unlimited amount of cells without requiring the sacrifice of animals and with limited costs. Yet, primary culture preparation is labour-intensive, the cell population is heterogeneous, often containing contaminating cells, and survives only few weeks in culture. Cell lines are thus particularly adequate for large-scale studies at cellular and molecular level.

The main disadvantage of cell lines is related to the possibility that they can react differently from animal tissue cells to environmental conditions, including treatments and manipulations that are investigated in vitro. In fact, it should always be taken into consideration that the neoplastic origin may have altered the biological properties of cells and therefore the translation of the results obtained from cell line studies must be interpreted with great caution.

Primary neuronal and glial cultures

The relevant biological differences that may occur between cell lines and cells from living tissues provide the justification for the employment of primary cell cultures in nerve regeneration studies, in spite of the above-mentioned short-coming. In fact, effective techniques for obtaining primary cultures from most neuronal and glial cell populations are available today. Regarding nerve cells, the most used for investigating nerve regeneration are motor neurons and primary sensory neurons since most peripheral nerve axons come from these neurons. Regarding glial cells, Schwann cells

are the most used since they are the glial cells of peripheral nerves. In addition, primary cultures of olfactory ensheathing cells also deserve mention because of the versatility of their employment which has raised great expectations for their use for grafting purposes not only in the peripheral but also in the central nervous system.

3D and organotypic cocultures

The usefulness of the *in vitro* study of nerve regeneration can be improved if the culturing conditions mimic the 3D organization of the nerve tissue. This can be created either by 3D cocultures, where the spatial organization of neuronal and glial cells is maintained by synthetic scaffolds, or by organotypic cultures of full tissue. The former approach is very promising though required complex matrices. On the other hand, organotypic cultures, especially obtained from dorsal root ganglia explants, are much easier to be obtained and provide a very good model for peripheral nerve *in vitro* regeneration research. Thus, though still poorly known, in our opinion, their employment should be promoted among peripheral nerve researchers. Finally, recently published studies using this type of *in vitro* model are refining the techniques used in order to increase the culture's potential. Using a genetic algorithm, which had been optimized to promote growth, axons showed improved growth rate. With such mathematical modeling to explore and predict axon regeneration mechanisms, these culturing protocols have become even more intriguing.

2.5.2 *In vivo* models

When moving from an *in vitro* to an *in vivo* experimental model, it is important to choose the animal model which best fits with the study goals, while taking into

consideration the pros and cons of the different options available. While in most biomedical application rats and mice are the two most employed laboratory animal models, in nerve regeneration studies there is a clear prevalence of rat use. A PubMed analysis of a random sample of 1500 research papers on nerve regeneration showed that more than 90% of them adopted the rat animal model. The main reason appears to be the larger physical size of rat nerves, which reduces the complexity of the microsurgical procedures, the possibility to have standardized and comparable functional tests and the fact that rats are more resilient than mice.

Whereas rat and mouse studies in most cases represent the first choice for nerve regeneration studies, several authors believe that the translation to clinical application may benefic from a preclinical study on large animal nerves since, as for many other organs, the regeneration process of nerves in large animals is more similar to humans. In addition, most studies on brachial plexus reconstruction are not possible in small newborn animals, large animal are the only possibility. Various large animal models have been employed for nerve regeneration including rabbits, sheep, pigs, and primates. The use of cats and dogs has been progressively reduced over the last years because of more restrictive laws on the employment of these animals for experimental surgery.

2.5.3 Morphological techniques for nerve research

2.5.3.1 Staining procedures

Hematoxylin and Eosin Staining

Hematoxylin and eosin is the most commonly used stain for light microscopy observation in histology and histopathology. Hematoxylin labels nuclei in blue while eosin is detectable as a pink stain in cell cytoplasm. Normally, the slides are immersed in 0.1% hematoxylin for 10 min, washed in tap water for 15 min, then immersed in 0.1% eosin for 5 min and washed in distilled water. The sections are finally dehydrated in ethanol and mounted in DPX. Although very popular, it must be emphasized that hematoxylin and eosin is not an adequate method for nerve tissue staining because the myelin sheaths are not labeled and they are thus difficult to be detected.

Masson's Trichrome Staining

The quality of the histology of nerve sections stained with Masson's trichrome is higher compared to HE staining because it also highlights the connective tissue. However, unless osmium tetroxide postfixation is carried out, myelin sheaths are not labeled with this method too. For Masson's trichrome staining, the normally procedure is described as follows: six drops of Weigert's iron hematoxylin (solution A) and six drops of Weigert's iron hematoxylin (solution B) are combined together and used to stain slides for 10 min. Without washing, the slides are then drained and incubated with ten drops of alcoholic picric acid solution for 4 min. after washing in distilled water, sections are stained with ten drops of Ponceau acid fuchsin for 4 min

and washed again in distilled water. Further on, ten drops of phosphomolybdic acid solution are added to the section for 10 min. Without washing, the slides are drained and 10 drops of aniline blue are added to the section for 5 min. Finally, after washing in distilled water, dehydrating rapidly in ethanol and clearing in xylol, the slides are mounted in DPX.

Pre-embedding Myelin Sheath Stain with Osmium Tetroxide before Paraffin Embedding

The rationale for this procedure is to introduce osmium tetroxide's immersion prior to the embedding procedure also in case of paraffin embedding. This technique allows a better fixation of the myelin resulting in a better quality of the imaging. In fact, due to its action as a lipid fixative, post-fixation in osmium prevents myelin sheath swelling, which usually occurs during paraffin embedding, and provides the typical dark and sharp myelin stain, which greatly facilitates the identification of nerve fibers.

Toluidine Blue Staining of Semithin Sections from Resion-embedded Blocks

The best quality for nerve analysis in light microscopy is obtainable after resin embedding and toluidine blue staining. With this procedure, most of the myelinated axons can be clearly identified and myelin sheaths are sharply delimited due to lipid staining of osmium tetroxide post-fixation.

Polychrome Staining of Semithin Sections from Resin-embedded Blocks

This method serves the same purpose as the Toluidine blue procedure for staining semithin sections, but provides with red and blue colors. After staining with 1% Toluidine blue in 1% borax on a 80°C hot plate for 30-45 s, sections are incubated

with a 1:1 solution of 0.1% basic fuchsin and in 1% borax on a 80°C hot plate for few seconds.

2.5.3.2 Immunohistochemistry and Confocal Microscopy

Both axon and glia can be detected by immunohistochemistry using specific antibodies. In particular, the most used antibodies as axon markers are those against neurofilament subunits. Normally, anti-NF 200kDa and anti-PAN-NF are both used. anti-PAN-NF reacts with all three NF proteins (68kDa, 150kDa, and 200kDa) and therefore it allows staining almost all myelinated nerve fibers. Figure 2.10 indicates sciatic nerve of monkey, rat, mouse, stained with NF-200 kDa. Another useful axonal marker is anti-peripherin that predominantly labels unmyelinated axons. Double labeling with anti-peripherin and anti-NF 200kDa, which predominantly labels myelinated axons, permits to distinguish between the two types of fibers (figure 2.11A, B). Other axonal marker is anti-PGP 9.5, which is found specifically in the PNS, and anti-GAP43 (growth associated protein 43 that is expressed at high levels during development and axonal regeneration. Finally, a marker selectively specific for motor axons is the anti-ChAT (choline acetyltransferase).

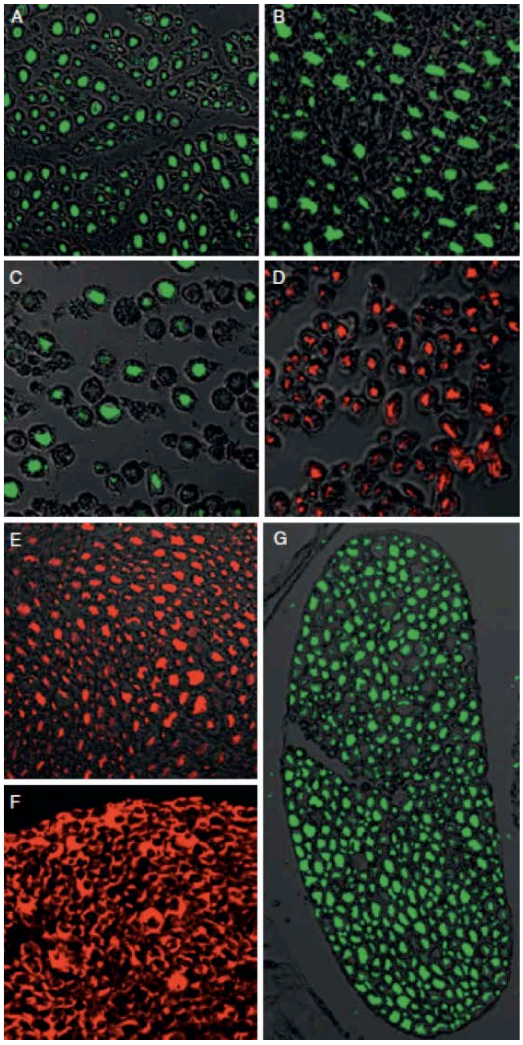

Figure 2.10 Confocal images of different animal species normal nerves. (A-C) Immuno-staining with anti-NF 200kDa of monkey (A), rat (B), and mouse sciatic nerve (C). (D) Immuno-staining with anti-PAN-NF. (E) Immuno-staining with anti-PGP 2.5. (F) immuno-staining with anti-S100 antibody. (G) Immuno-staining with anti-ChAT.

As far as Schwann cell recognition is concerned, they can be detected by immunohistochemistry using specific glial markers, such as GFAP and S100. Anti-GFAP antibody is the commonly used marker for immature and un-myelinating Schwann cells. Anti-S100 antibody labels the cytoplasm and nucleus of Schwann cells and has been shown to be a very good marker of human peripheral nerves (figure

2.10F). Glial markers can be associated with neuronal markers in double immunostaining providing useful information on the relationship between axons and glial cells (figure 2.11C). Besides their use as markers of different axons and glia, immunohistochemical analysis is also a useful tool to investigate cell function and molecular activity, for example the cellular signaling pathways. Particularly interesting for nerve regeneration is the NRG/erbB pathway system (figure 2.11D).

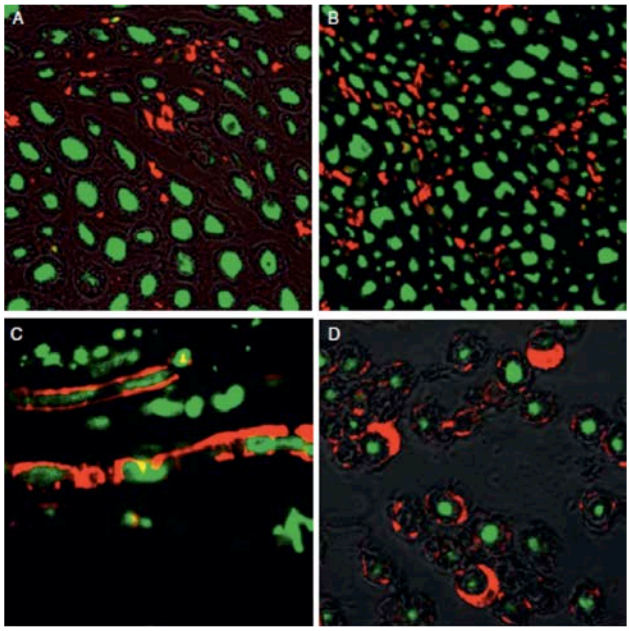

Figure 2.11 Confocal images of monkey normal nerve (A) and rat normal sciatic nerve (B) double labeled with anti-NF 200 kDa and anti-peripherin. (C) Regenerating rat fibers double stained with anti-NF 200 kDa and S100. (D) Mouse median nerve double stained with anti-NF 200 kDa and erbB2.

CHAPTER 3 EXPERIMENTS

3.1 Preparation of SMP

3.1.1 SMP selecting principle

Based on the literature review, it can be found that a wide range of biomaterials has been studied for the fabrication of traditional nerve conduit[1,67]. Of these nondegradable materials, such as silicone rubber have been widely used in general clinical case due to their good inert and mechanical properties[68,69]. However, after regeneration, these materials may become detrimental due to mechanical impingement, foreign body reaction or infection. On the contrary, biodegradable materials potentially avoid these drawbacks and make secondary surgery unnecessary. Different kinds of biodegradable biomaterials have been developed, such as polygylcolic acid (PGA), poly(3-hydroxybutyrate) (PHB), gelatin, collagen, chitosan, and silk[70-73]. However, the properties of these above-mentioned biodegradable materials such as mechanical property, processibility and biocompatibility cannot fully meet the requirements of an ideal SNC. For example, nerve conduits made from collagen had excellent results in nerve regeneration, but it is rather expensive and difficult to handle during suturing, furthermore, it can produce inflammatory reactions and has shown complete bioerosion within 2 months after implantation due to its mechanical weakness.

Poly(L-lactide) is widely studied for scaffold fabrication due to its biodegradability and excellent biocompatibility. Meanwhile, PLLA possesses sufficient mechanical properties for SNC fabrication. In neural tissue engineering, porous PLLA conduits and filaments were evaluated in animal model that presented promising results in peripheral nerve regeneration, and PLLA scaffolds have also presented excellent adhesion and proliferation of neural cells. It is therefore desirable to modify PLLA with simple method to fulfill the critical requirements of SNC[74,75]. An ideal shape-memory material for manufacturing nerve conduits should fulfill following requirements:

1) The SMP should possess excellent shape-recovery and fixity rate at physiological conditions.
2) The implanted smart nerve conduit should have long recovery time that is close to that of peripheral nerve regeneration.
3) The conduit should support nerve cell adhesion and proliferation, and can be gradually absorbed to eliminate the need for a second surgery.

3.1.2 Molecular design for SMP

From tissue growing viewpoint, opposite to other applications where a quick recovery process is required, an ideal SMP for manufacturing SNC should have prolonged and gradual recovery process that is close to that of peripheral nerve regeneration process. Instead of heating the SMP to a certain temperature over its T_{trans} to trigger the SME, water-induced SME arising from the drop of T_g due to the plasticizing effect is more practical and natural when the decreasing T_g reaches the ambient water temperature

because the generated stress is lower. From the viewpoint of prolonged and gradual recovery process, time in water-actuated recovery is longer than that in thermo-induced recovery. The reason for this is probably that the plasticizing effect is a time consuming process. It is easier to absorb water and reach saturation at the sample surface, while it is more difficult for water to penetrate deep inside into the material. Therefore, we focus on the development of T_g-dependent biodegradable SMP as self-shrinkable conduit to achieve a gradual self-shrinkage in body water (36°C).

The most intriguing aspect of our molecular design lies in the selection of hard segment. Huang demonstrated gradual shape recovery function and found that water-induced recovery time is determined by the temperature gap between T_g and the ambient water temperature, the recovery process of a polymer with lower T_g starts and ends earlier. Intuitively, one might deduce that gradual shape-memory effects (SMEs) can be realized by introducing several glass transitions[76-78]. When a polymer type (PLLA or PLGA) is determined after considering many requirements, the work of introducing more than two distinctive T_gs, however, is extremely challenging. In addition, a nerve conduit should support nerve cell adhesion and proliferation and can also be gradually absorbed to eliminate a second surgery. To meet these essential requirements, instead of synthesizing a SMP with gradient T_gs in microscopic view, we hereby describe a feasible approach to fabricate a tri-segment SMP-based device with different T_g in macroscopic view.

A typical SMP consists of two segments: the hard segment for the determination of permanent shape and the switch point for the fixation of temporary shape. As for hard segment, chemically-crosslinked segment presents certain advantages in mechanical behavior while also limiting many aspects of material processing capability. Exclude covalently-crosslinked type, amorphous polymers with ultra-high molecular weight, $>10^6$ g mol^{-1}, have been reported as SMPs due to their lack of flow above T_g and excellent shape fixing by vitrification. In these polymers, entanglements of the molecular chain function as physical cross-links to provide elasticity above T_g. In this study, to meet the requirements of electrospinning technique and biodegradability, the molecular weight of our proposed polymer is decreased to almost 10^5 g mol^{-1} and the entanglements of molecular chain are supposed to still function as net points. Therefore, we change the molecular architecture of PLLA from semicrystalline to amorphous by replacing L-lactide with *rac*-lactide and introduce glycolide to the copolymer network to adjust the glass transition temperature. Our designed polymer is synthesized by copolymerization method and the strategy to adjust T_g is derived from the Fox-Flory equation, which allows controlling T_g of amorphous copolymer from T_gs of the related homopolymers. High molecular weight PLGA can be synthesized through ring-opening polymerization in bulk or in solution. Therefore, in this study an amorphous, PLGA system was designed to exhibit tunable T_g, water-induced shape-memory function and good biocompatibility, as well as advanced electrospinning process capabilities (Figure 3.1).

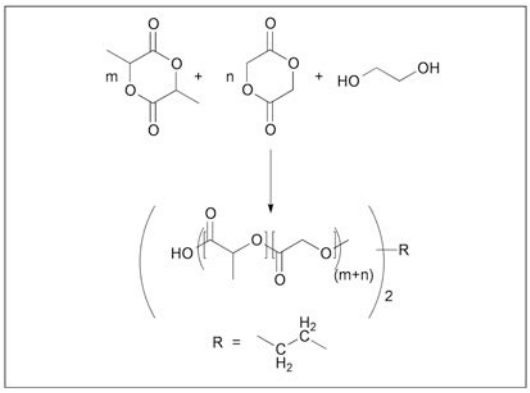

Figure 3.1 Synthesis of poly(*rac*-lactide-*co*-glycolide) copolymer networks

3.1.3 Synthesis routine and sample preparation

3.1.3.1 Raw materials

All raw materials were listed in table 3.1.

Raw materials	Abbreviations	Supplier	Pre-treatment
rac-lactide	LA	Aldrich	Recrystallization
Glycolide	GA	Aldrich	Recrystallization
Ethylene glycol	MEG	Aldrich	No pre-treatment
Dibutyltin oxide	DBTO	Aldrich	No pre-treatment
Dichloromethane	DCM	Aldrich	No pre-treatment
Hexane	--	Aldrich	No pre-treatment
Ethyl acetate	EA	Aldrich	No pre-treatment

Table 3.1 Raw materials for the synthesis of poly(*rac*-lactide-*co*-glycolid) copolymer

3.1.3.2 Copolymer Synthesis

A series of PLGA copolymers were synthesized by ring-open copolymerization with *rac*-lactide:glycolide weight ratio 60:40, 50:50, 40:60, 30:70, and 20:80 respectively. The formula of the PLGA copolymers are shown in table 3.2. The monomers rac-lactide and glycolide and the initiator ethylene glycol were added into a dry glass

tube. Dibutylin oxide (0.2 wt % DBTO) was added into the tube followed by three cycles of vacuum and purging with nitrogen, and then the glass tube was sealed. After reacting at 160°C for three days, the resulting copolymers were dissolved in dichloromethane and then precipitated in hexane. The series of copolymer samples is designated as PLGA-XX, where XX denotes the mass content of *rac*-lactide in copolymer sample.

Sample	LA (mol)	GA (mol)	MEG (mol)	DBTO wt%	M_n
PLGA-60	4.17	3.45	0.01	0.2	100204
PLGA-50	3.47	4.31	0.01	0.2	100416
PLGA-40	2.78	5.17	0.01	0.2	100140
PLGA-30	2.08	6.03	0.01	0.2	100036
PLGA-20	1.39	6.89	0.01	0.2	100076

Table 3.2 Formula of the synthesis of poly(*rac*-lactide-*co*-glycolid) copolymer

3.1.3.3 Film preparation

PLGA films are prepared by transferring the copolymer solution to Teflon molds with 8-15 wt% solid content and allowed them to solidify at room temperature in air ventilation for 24 hours. To remove the residual CH_2Cl_2, the films were held at 60°C under vacuum of 1-2 mmHg for another 24 hours subsequently. The thickness of the films for cyclic thermo-mechanical investigation was about 0.1-0.5 mm.

3.2 Preparation of SNC

3.2.1 Technology selecting principle

Many methods have been considered to fabricate the SNC, since the morphology, permeability, and mechanical properties of SNC are influenced by fabrication methods. In 2004, to enhance the mechanical strength of conduits, Bini and co-workers prepared a braided conduit by using a spindle-braiding machine[79,80]. However, this braiding technology requires the fabricated material could be obtained by melt spinning, which is a challenge for the synthesis of SMP. According to the literature review, electrospinning has been widely developed as one of the most promising technologies to produce nanoscaled fibers that are suitable for several biomedical applications. In particular, the use of electrospun nanofibers to construct biomimetic scaffolds for diversified tissue-engineering purposes has been well reported as they closely mimic the nanofibrillar components (e.g., collagen) of the extracellular matrix (ECM), which naturally surrounds the cells of any biological tissue. Such nanofiber-based scaffolds with high porosity and specific surface area and nanotopography make them ideal candidates for engineering ECM to promote the cells functioning naturally. Hence, electrospinning technology represents an attractive approach to the fabrication of fibrous SNC and is primarily used in this study[81,82].

3.2.2 SNC structure design for PNR

In this study, the fabricated SNCs possess the gradual shape recovery function for nerve regeneration in comparison with the traditional nerve conduit, whose function is merely to bridge the nerve gap. The achievement of the SMEs not only depends on

the materials themselves, but also on the corresponding fabrication process. In the view of SMP, there is a necessity to introduce some mechanisms in the polymer to have prolonged recovery time or multi-shape-memory polymer. One strategy for designing a triple-shape-memory polymer is to incorporate two discrete thermal transitions into the material[83-86]. Typical examples include macroscopic homogeneous polymers consisting of microseparated distinctive segments, polymer composites, and macroscopic polymer bilayers. An alter- native strategy relies on a single broad thermal transition, instead of multiple distinct transitions. Tao Xie reported perfluorosulphonic acid ionomer (PFSA), which has only one broad phase transition, presents dual-, triple-, and at least quadruple-shape-memory effect without any change to the material composition. In addition, W.M. Huang and co-workers proposed immersing the different parts of polyurethane SMP in water in sequence could produce the gradient in the T_g. Intuitively, one might deduce that gradual SMEs can be realized simply by introducing several glass transitions. However, the task of synthesizing a polymer with more than two distinctive T_gs is extremely challenging[87]. Moreover, a nerve conduit should support nerve cell adhesion and proliferation and can also be gradually absorbed to eliminate a second surgery. Facing these challenges, instead of synthesizing a SMP with gradient T_gs in microscopic view, we hereby describe a feasible approach to fabricate an SMP-based device with segment structure with different T_gs in macroscopic view, as shown in figure 3.2. Our fabrication strategy relies on electrospinning technology. In this study, by ejecting a series of polymer solutions with different T_gs in sequence, a multi-segment conduit

with gradual-recovery function can be fabricated on the rotating drum surface. Each segment with an individual T_g connects with one another from head to tail. Therefore, we can manufacture a conduit with gradient T_gs in macroscopic level. In addition, these electrospun nano-size polymeric fibres also provide a more conductive environment for cellular functions by mimicking the size scales of fibres consist of the extracellular matrix of tissues and organs.

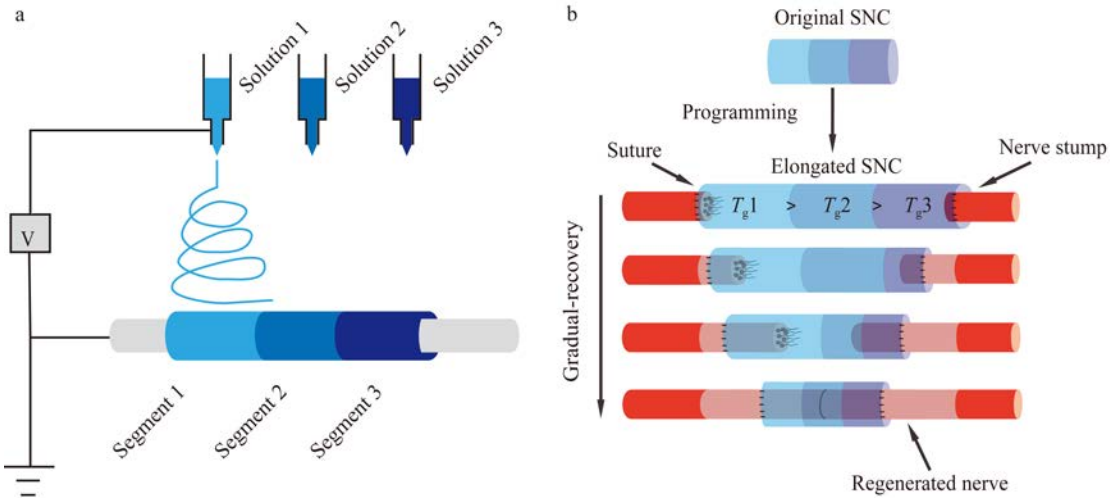

Figure 3.2 (a) Schematic diagram for smart nerve conduit fabrication: Polymer solutions with different T_gs were ejected into the syringe in sequence. (b) SNC with shape-memory function for nerve repair

3.2.3 Fabrication routine of SNC

In this study, electrospinning technology was employed to fabricate a fibrous tri-segment smart nerve conduit. Three types of synthesized copolymers, PLGA-60, PLGA-40, and PLGA-20 were dissolved in dimethylformamide (DMF) and tetrahydrofuran (THF) at DMF:THF = 1:3 (v/v) at the concentration of 25% (w/v), respectively. Then each polymeric solution was injected into the electrospinning apparatus in sequence to fabricate the corresponding component of the SNC. The polymeric solution was pumped at a rate of 1 ml h^{-1} through the spinneret, which was

positively charged to 15.0 kV. The rotating drum was negatively charged to 0.4 kV with a 15 cm distance from the spinneret to rotating drum. The diameter of the rotating drum was 2 mm and the rotating speed of the collecting drum was set at 500 rpm and the duration of the electrospinning process for each component was 6 h. Electrospinning technology is known to stretch amorphous polymer chains.

Since electrospinning would stretch amorphous polymer chains, when the electrospun conduit was subsequently heated to above T_g to trigger SME, the stretched amorphous chains would relax and release molecular-level strain, which subsequently causes dimensional changes. In this study, to remove the molecular-level strain and to prevent the shrinkage, the electrospun conduit was annealed with the collecting drum at 60°C for 5 h to release the molecular-level strain while the collecting drum prevented dimensional change in nerve conduit shape.

3.3 Characterization techniques

3.3.1 Differential scanning calorimetry (DSC)

DSC is a thermo-analytical technique in which the heat flux compensated to the test sample is measured and recorded against temperature and time. In practice, it is to detect difference in heat flux to a pan containing a sample and reference. DSC is used widely for examining polymers to determine their thermal-properties from two aspects:1) Glass transition temperature (T_g); and 2) Melting/re-crystallization temperature (T_m). The glass transition temperature is non-equilibrium property and is a parameter sensitive to heating rate and the method used. Therefore, T_g measured

differs from one technique to another and is over a range of several degrees. T_g is referred to the temperature region at which the amorphous phase of a polymer is transformed from glassy material into a rubber-like status and is accompanied by a "step-wise" increase of the heat flow curve. The glass transition temperature can be defined in different ways. In literature, both the onset temperature and the inflection point temperature is utilized to define T_g (shown in figure 3.3). In this study, T_g is defined as the inflection point.

It is well known that thermal histories of specimens including the scanning rate of instrument, heating procedure of instrument, and sample weights will have a strong influence on the glass transition process. Therefore, in our measurement, all samples weighting ~5 mg were heated to 100°C at a rate of 10°C min^{-1} to remove the thermal history and then cooled to -50°C at a rate of 10°C min^{-1}. After 5 min at this temperature, a second scan was conducted from -50°C to 100°C at 10°C min^{-1}. The data presented are the data obtained in the second scan.

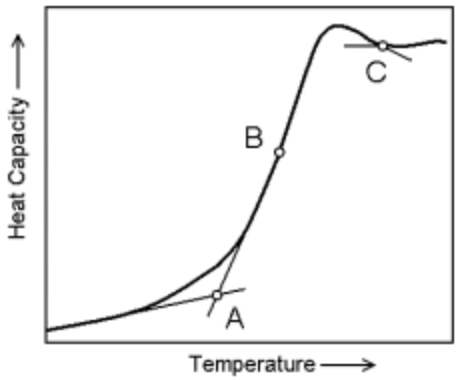

Figure 3.3 A, B the onset temperature and the inflection point, respectively

3.3.2 Fourier transform infrared spectroscopy (FTIR)

Fourier transform infrared (FTIR) is to measure the chemical bonding vibrations between the atoms within a molecule. An infrared spectrum is obtained by ejecting an infrared light beam through a sample and determining which fraction of the incident radiation is absorbed at each wavelength. The energy at peaks in an absorption spectrum corresponds to the frequency of a part of the sample molecule. Therefore, it can be used to identify a polymer, monitor the polymerization stage, and characterize any structural changes under different conditions. In our measurement, Fourier Infrared Spectra equipped with attenuated total reflectance accessories were determined with 0.1-0.5 mm thickness specimen film by using Perkin-Elmer (2000 FT-IR) spectrometer in the region of 700-4000 cm^{-1} at room temperature. Each sample was scanned 30 times at a resolution of 2 cm^{-1} and the scans signals were averaged. The region of O-H stretching at 3000 to 3600 cm^{-1} was used to detect existence of bound water.

3.3.3 Gel permeation chromatography (GPC)

GPC, a type of size-exclusion chromatography (SEC), is a technique that employs porous non-ionic gel beads packed in a column to separate polymers in solution. When a solution containing the polymer of interest is pumped down into the column, the polymers attempt to enter the pores in the packing material. But only sufficiently small polymers can enter the pores more easily and therefore spend more time in these pores, increasing their retention time. Conversely, larger polymers spend little time in the pores and are eluted quickly. Then, retention time is converted to

molecular weight, and all columns have a range of molecular weights that can be separated. In this measurement, a molecular weight and polydispersity index (PDI) of the resulting PLGA copolymers were measured by GPC together with column (PLgel Mixed-C type, Polymer Laboratories Ltd, USA) and refractive index detector. The M_n linearity range of this column is from 200 to 2,000,000. After testing the solubility of PLGA copolymer samples in tetrahydrofuran (THF) at room temperature, the testing temperature is set up to 25°C. The flow rate of mobile phase is 1.0 ml/min. Integral method was used to calculate the number-average molecular weight (M_n) and polydispersity (M_w/M_n) of the resulting polymers accordingly. The standard PS samples were tested with the same eluent and testing condition.

3.3.4 Thermal-induced shape-memory properties investigation

The thermal-induced SME could be quantified by cyclic thermo-mechanical measurements including programming the test sample and recovering its permanent shape in single cycle. Byung Kyu Kim and co-workers have reported the typical protocol about the testing process as follows:

1) the test sample is stretched to the maximum strain ε_m at the high temperature T_{high} above the switching temperature T_{trans} and below the processing temperature T_{perm} which will cause the polymer to melt or decompose;

2) the stretched sample is cooled down below the T_{trans} under a constant strain ε_m to a temperature T_{low}, thus fixing the temporary shape;

3) retracting the crosshead of tensile tester to the original position;

4) increasing the temperature of sample to T_{high} again, the permanent shape is

recovered.

The cyclic tensile test is shown in figure 3.4 and there are several parameters to descript the shape-memory effect quantitatively as below:

$$R_r(N) = \frac{\varepsilon_m - \varepsilon_p(N)}{\varepsilon_m - \varepsilon_p(N-1)}$$

R_r quantifies the ability of the material to memory its permanent shape.

$$R_f = \frac{\varepsilon_u(N)}{\varepsilon_m}$$

R_f describes how exactly the sample could be fixed in the deformed shape.

In this study, cyclic thermo-mechanical tensile tests were performed on Instron 5566 with a thermo-chamber and a deformation rate of 10 mm/min was applied. Tensile tests were conducted for 10 cycles and result for each cycle was recorded. The tests were shown in figure 3.4 and conducted as follows: First, the sample was strained to ε_m=100% at a temperature of T_{high} (60°C) at a tensile rate of 10 mm/min. After that, while keeping ε_m the stretched sample was cooled to T_{low} (ambient temperature) and equilibrated for 10 min, thus the elongated sample was in its temporary shape. Then, retracting the crosshead of tensile tester to the original position that results in the temporary shape characterized by ε_u at σ = 0 MPa. Thereafter, the deformed sample was heated to T_{high} again and the original shape was recovered. The elongation after the recovery process is ε_p. This program was repeated 10 times with the same sample (N = 10).

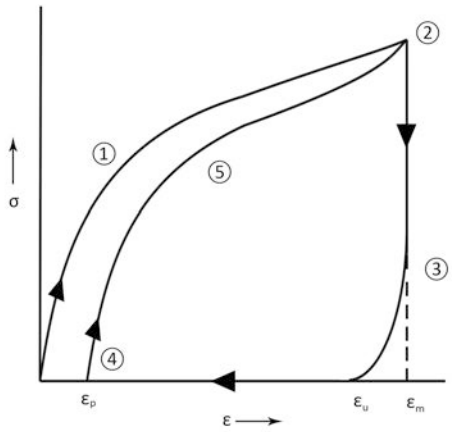

Figure 3.4 Schematic representation of the cyclic thermomechanical investigation

3.3.5 Water-induced shape-memory properties investigation

Bending tests were performed by programming an angle 0° at 60°C followed by cooling below T_g. The samples were then immersed in water (25°C) until a maximum recovery was observed, and the angle of recovery (θ_r) was monitored over time. The bending-derived shape recovery ratio ($R_{r,\theta}$) was calculated according to equation, while the corresponding bending test is illustrated in figure 3.5.

$$R_{r,\theta} = \frac{\theta_r}{180} \times 100\%$$

Bending test was employed to determine the water-induced shape-memory effects. Straight strips of the synthesized copolymers were folded at 60°C and kept the deformed shape during cooling back to 20°C (ambient temperature). After the folded strips were placed in a dry cabinet (Relative Humility 30, 36°C) for three days, no apparent recovery was found. Subsequently, the deformed strips were immersed in water (36°C) and the macroscopic angle change under moisture stimulating was recorded[88].

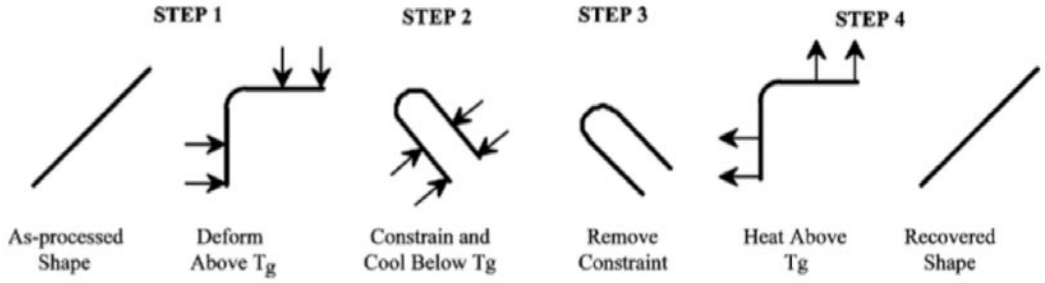

Figure 3.5 Schematic of the bending test for PLGA samples recovered in 36°C water

3.3.6 Water contact angle (WCA)

The contact angle quantifies the wettability of a solid surface via the Young equation, and is conventionally measured through the liquid. The theoretical description of contact angle arises from the consideration of a thermodynamic equilibrium between the three phases: the liquid phase (L), the solid phase (S), and the gas phase (G). The contact angle θ_c is shown in figure 3.6. If the liquid drops are strongly attracted to the solid molecules then the liquid drop will completely spread out on the solid surface, indicating a contact angle of 0°. This is often the case for water on bare metallic or ceramic surfaces. Generally, if the WCA is smaller than 90°, the material is considered hydrophilic, and if the WCA is larger than 90°, the material is considered hydrophobic.

In this study, the WCA of the PLGA samples were measured by Krüss DSA 100 machine according to the sessile drop method. A single, 20 µL drop of distilled water was deposited onto the sample's surface, and the contact angle at room temperature was recorded after 30 s using a camera connected to a computer. The final contact angle values were taken as the average of five measurements.

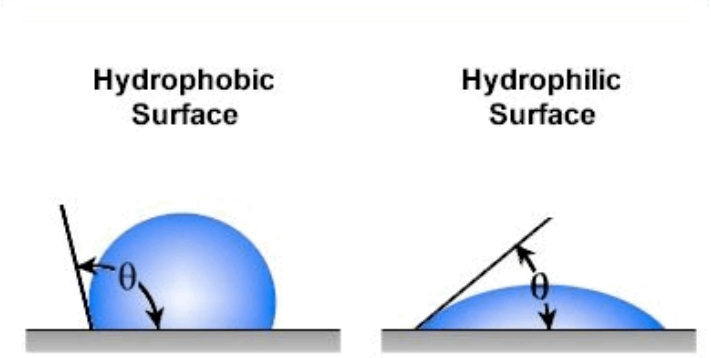

Figure 3.6 Schematic of a liquid drop showing the contact angle θ_c

3.3.7 X-ray diffraction (XRD)

XRD can be employed to obtain structural information about semi-crystalline polymers. When X-ray, an electromagnetic radiation, pass through the crystal or semi-crystalline polymers, diffraction occurs and it obeys the Bragg's law.

$$2d \sin\theta = n\lambda$$

Where d is the spacing between diffracting planes, θ is the incident angle, n can be any integer, and λ is the wavelength of the X-ray. Through XRD measurement, structural information, such as the size of the crystals, the crystallinity of a polymer as well as the distance between the parallel planes in the crystallites can be measured.

In this study, the XRD spectra are recorded in the X-ray Diffractometer (Rigaku Smartlab System) at 45KV and 40mA which was equipped with Goebel mirror and Cu Kα radiation with a wavelength of 1.54 Å. Diffraction patterns were obtained in the range of Bragg's angle 2θ=10°~30°. The scanning speed was 0.02° min^{-1}.

3.3.8 Scanning electron microscope (SEM)

Scanning electron microscope (SEM) is a type of electron microscope that by

scanning samples with a focused beam of electrons to produce images. The electrons interact with atoms in the sample, producing various signals that can be detected and that contain information about the sample's surface topography and composition. In this study, SEM was employed to characterize the inner surfaces of nerve conduits with longitudinally and circumferentially aligned electrospun fibers, respectively. According to the literature review, electrospun scaffold has been applied widely in tissue-engineering direction due to its large surface area and highly interconnected pore spaces. This architecture mimics the organization of the native extracellular matrix and can be selectively tailored to support a wide variety of cell types.

Since the native extracellular matrix, tendons, ligaments, blood vessels and other organs exhibit varying degrees of anisotropy, the fiber alignment and overall scaffold anisotropy also have a key position in defining the electrospun material properties[89]. Anisotropic properties can be expected to represent a source of guidance cues that can be exploited to regulate cell phenotype, cell migration, and the distribution of cells within an engineered tissue. James H. Henderson and co-workers have developed a thermal-actuated SMP and demonstrated that changes in internal architecture and shape can control cell morphological behavior. Based on the results, they anticipated that these SMP scaffolds would facilitate cell preparation, minimally invasive scaffold delivery and mimicry of dynamic biological processes. Although SEM can be employed to demonstrate fiber alignment in electrospun scaffolds, this approach lacks precision and is obviously highly subjective. In their study, 2-D FFT image analysis,

an objective measurement of fiber alignment, was used to determine how specific degrees of anisotropy might contribute to the performance of a scaffold.

The detailed description of the 2D FFT approach for measuring scaffold anisotropy is presented as follow:

1) For analysis, grayscale brightfield microscopic images were captured and converted to an integer power of 2 pixel dimensions (256 × 256, 512 × 512, 1024 × 1024, etc.). If images have been captured in color they must be converted to grayscale for 2D FFT analysis.
2) Processing a brightfield data image by 2D FFT produces a frequency plot, or power spectrum. This plot is composed of grayscale pixels that are distributed into a pattern that can be used to measure the degree of fiber alignment present in an original data image.
3) After obtaining the resulting frequency plot containing a cluster of white pixels that are concentrated in a symmetrical, circular pattern. ImageJ circular marque tool is employed to place a circular projection on the frequency plot.
4) ImageJ oval profile plug-in is used to sum the pixel intensities along the radius for each angle of the circular projection.
5) The summed pixel intensities for each radius are then plotted against the corresponding angle of acquisition to produce a 2D FFT alignment plot.

In this study, all images were stored and analyzed as uncompressed .TIF files to

preserve image integrity; the image compression used in .JPG format will degrade image integrity and should not be used for archival storage. Grayscale 8-bit images were cropped to 2048 × 2048 pixels for analysis. ImageJ software supported by an oval profile plug-in was used to conduct 2D FFT analysis. All alignment data was normalized to a baseline value of 0 and plotted in arbitrary units ranging from 0 to approximately 0.15.

3.4 Biological assays

3.4.1 *In vitro* experiments

Before applying artificial nerve conduit *in vivo*, we first tested the biocompatibility of electrospun poly(rac-lactide-co-glycolide) scaffolds with Schwann cells through adhesion observation and proliferation assay *in vitro*.

3.4.1.1 Cell culture

Schwann cells were used to investigate the effect of PLGA scaffold on cell attachment, viability and morphology. This cell type was selected because Schwann cells are the dominating glial of the peripheral nervous system. Schwann cells form the myelin sheath, and are involved in many principal aspects of peripheral nerve biology, including the production of neurotrophic factors and extracellular matrices, the conduction of nervous impulses along axons, and nerve regeneration. Nerves in the PNS consist of many axons myelinated by Schwann cells. If a nerve is damaged, the Schwann cells will aid in digestion of its axons. Then, the Schwann cells can guide regeneration by forming a type of tunnel that leads toward the target neurons. The stump of the damaged axon is able to sprout, and those sprouts can grow through

the Schwann cell channel at a certain recovery rate. With the help of Schwann cells, the damaged nerve can therefore reconnect with the muscles or organs they previously controlled. In addition, during the regeneration process, Schwann cells can also produce a variety of growth factors, including neurotrophins, and transfer essential molecules across to axons.

In this study, Schwann cells were harvested as follows. The bilateral sciatic nerves of neonatal Sprague-Dawley rats (2 d) were excised out under sterile condition. After enzymatic digestion with collagenase and dispase, the crude cell suspension was plated in Dulbecco modified Eagle medium (DMEM), enriched with 10% fetal bovine serum (FBS) and antibiotic (penicillin-streptomycin solution). After three daily treatments with cytosine arabinoside to eliminate rapidly proliferating fibroblasts, the subcultured Schwann cells were seeded in a 96-well plate at a cell density of 1×10^4/well with fresh DMEM and 10% FBS, after that the DMEM was changed for every 2 d until the bottom of the flask was filled with cells. The cultures were examined by using light microscope on a daily basis for observations of adherence, survival and proliferation.

3.4.1.2 MTT assay

MTT assay is a colorimetric assay for assessing cell metabolic activity. MTT 3-(4,5-dimethylthiazol-2-yl)-2.5-diphenyltetrazolium bromide is a yellow tetrazole, that can be reduced to purple formazan in living cells. NAD(P)H-dependent cellular oxidoreductase enzymes can reflect the number of viable cells and also be capable of

reducing the tetrazolium dye MTT to its purple formazan. Therefore, increasing amounts of cells result in increased purple coloring, and the results can be qualitative determined under a microscope.

In this study, MTT assay was utilized for testing the proliferation of SCs within the extracts of our synthesized copolymers. Briefly, 80 mg of electrospun film prepared from each of aforementioned copolymers (PLGA-60, PLGA-40, PLGA-20) was sterilized in 70% sterilized ethanol, dried and incubated in 5 ml of DMEM for 72 h at 37°C for extraction. Serial dilutions of 0, 0.15625, 0.3125, 0.625, 1.25, 2.5, and 5 mg/ml of the extract were made using growth medium. Cultured Schwann cells were re-suspended in the culture medium and plated into 96-well plate at a density of 1×10^4 cells/well. The plates were incubated for 4 h at 37°C and then the mediums were replaced by the extract dilutions. After 48 h incubation in different mediums, the cell culture was treated with 20 µl/well of 5 mg/ml MTT and then was further incubated for 4 h at 37°C. The supernatant was discarded and the formazan crystals were solubilized by adding 100 µl of DMSO solution. The plates were gently agitated until the formazan precipitate was dissolved, followed by measurement of optical density value by spectrophotometer at 490 nm.

3.4.1.3 Cell morphology observation

Fluorescent immunocytochemistry was employed to characterize the morphology of SCs attached to the conduits. After 6, 24, and 48 h culture of SCs on aforementioned nanofibrous films, the samples were fixed with 4% paraformaldehyde (v/v) in PBS for

30 min at room temperature. The fixed samples were then transferred to PBS containing 0.1% Trition X-100 for 10 min to allow cell permeabilization. Cells were stained with fluorescein isothiocyanate(FITC)-Phalloidin to stain the actin filaments, while 4,6-diamidino-2-phenylindole (DAPI) was used to stain the cell nuclei. Analysis was performed using confocal laser scanning microscopy.

After 6, 24, and 48 h culture, the samples were fixed following the abovementioned process. For the immunofluorescence of S-100, the fixed samples were incubated with 10% goat serum, 3% bovine serum albumin (BSA) and 0.1% Triton-X 100 at room temperature for 1 h to block nonspecific binding. Subsequent incubation with the mouse monoclonal anti-S-100 antibody (1:200 dilution, Sigma) was performed overnight at 4°C. After being washed three times with PBS, the samples were further incubated with FITC-labeled goat anti-mouse lgG (1:250 dilution, Sigma) for 2 h at 37°C. Cells were then stained with DAPI and analyzed with confocal laser scanning microscopy.

3.4.1.4 Statistics

All numerical data presented were expressed as mean ± standard deviation. Significant differences among groups were analyzed by a one-way analysis of variance (ANOVA). Statistically significant value was defined as $p < 0.05$.

3.4.2 *Ex vivo* experiments

To demonstrate our proposed concept of gradual-recovery for nerve regeneration, simulated *in vivo* measurement was conducted to test the macroscopic shape change

of SNC. The annealed SNC was uniaxial stretched to 100% strain at 60°C in Instron 5566 with a thermo-chamber and fixed in that temporary shape by cooling to 20°C (ambient temperature). Then two ends of the pre-elongated nerve conduit were sutured to two tightened elastic bands, of which the modulus approximates that of peripheral nerve. To actuate the nerve conduit, the recovery process was carried out in water at 36°C and macroscopic shape change was measured.

3.4.3 *In vivo* experiments

3.4.3.1 Surgical procedure

Adult New Zealand white rabbits approximately 2 months of age were used to evaluate the nerve regeneration performance of PLGA conduits. The animals were divided into 3 groups each with 6 rabbits. Group A: elongated PLGA nerve conduits; group B: PLGA nerve conduits with original length; group D: autograft nerve group as a positive control. Briefly, the animals were anesthetized with 50 mg/kg body weight pentobarbital sodium. The skin from the clipped lateral thigh was scrubbed in a routine fashion with antiseptic solution. The sciatic nerve was then exposed after the skin incision, and separation of muscles around the nerve tissues using blunt dissection. Subsequently, 6 mm of the nerve was resected to obtain a 15 mm nerve gap. Both the proximal and the distal stumps were sutured with 6-0 nylon to a depth of 1mm into the conduits, leaving a 15-mm gap between the stumps. In a similar microsurfical technique, nerve autografts were used to repair defects in the rabbit sciatic nerve. Nerve autografts were placed in a reverse fashion to prevent axonal branching during proliferation through side branches from the donor nerve. Muscle

and skin were closed using 4-0 nylon monofilament suture stitches. Each rabbit received one implant, which was removed at various time intervals: namely, 4, 8, and 12 weeks, respectively. At each time interval, histomorphology evaluation was performed to evaluate the efficiency of nerve conduits for nerve regeneration.

3.4.3.2 Histological evaluation

Hematoxylin and eosin (HE) stain is one of the principal stains in histology. The staining method involves application of hematoxylin and eosin. Hematoxylin is a violet stain that is positive. It binds to basophilic substances (such DNA/RNA in the nucleus, which are acidic and negatively charged) and stains them violet. Eosin is a pink stain that is negative. It binds to acidophilic substances (such proteins in the cytoplasm, which are basic and positively charged) and stains them pink. Moreover, the stained proteins include cytoplasmic filaments in muscle cells, intracellular membranes, and extracellular fibers. Masson's trichrome is a three-color staining protocol utilized in histology, which is suited for distinguishing cells from surrounding connective tissue. This method stains keratin and muscle fibers red, collagen and bone blue, cytoplasm pink, and cell nuclei black. It is widely employed to study muscular dystrophy, cardiac infarct or kidney pathologies.

In this study, at week 4, 8, and 12, the regenerated nerves were fixed in 4% paraformaldehyde for 48 h and then embedded in paraffin wax and cut into 5 um thick longitudinal sections that were then stained with hematoxylin/eosin (HE) and Masson's trichrome staining, respectively to detect structures. Moreover, 12 weeks

post-implantation, for histological evaluation, excised important organs from the heart, liver, spleen, and kidney were also frozen and embedded in paraffin wax, were sectioned into 8 um slices, were stained by hematoxylin/eosin (HE) stain method, and were observed by microscopy to determine effects of PLGA conduits on important organs.

CHAPTER 4 CHARATERIZATION OF SMP and SMP-BASED SNC

4.1 Characterization of SMP

A wide range of materials has been developed for conventional nerve conduit. Of these materials, poly(L-lactide) has had a longstanding history in scaffold fabrication because it is biodegradable and generally exhibit excellent biocompatibility. Also, PLLA possess sufficient mechanical properties for nerve conduit fabrication. In neural tissue engineering, porous PLLA conduits and PLLA filaments were evaluated in rat sciatic nerve model that yielded promising results in peripheral nerve regeneration. Moreover, textured PLLA scaffolds made up of nanofibers have presented excellent adhesion and proliferation of neural cells. It is therefore desirable to modify PLLA using simple method to fulfill the additional requirements of smart nerve conduit.

4.1.1 GPC measurement

Amorphous linear poly(*rac*-lactide-*co*-glycolide) copolymers were synthesized. Their comonomer content was varied from 20 wt% to 60 wt% for comonomer glycolide. The characteristics of synthesized copolymer networks determined by GPC and DSC are presented in table 4.1. M_n of the oligomers was controlled by the molar ratio of monomers to initiator. M_n was between 100,000 and 120,000 g/mol, determined by GPC. M_n of approximate 100,000 g/mol was chosen to ensure that the material in the

M_n range where T_g is independent from the M_n of the linear copolymers. Furthermore, this relatively high M_n leads to a high chain segment length in the network providing enough entanglements.

Macromer	M_n [g mol^{-1}][a)]	T_g [°C][b)]	T_g [°C][c)]
LA(60):GA(40)	1.1×10^5	49.10	37.58
LA(50):GA(50)	1.2×10^5	46.37	36.89
LA(40):GA(60)	1.2×10^5	45.31	36.18
LA(30):GA(70)	1.3×10^5	42.38	35.25
LA(20):GA(80)	1.5×10^5	41.74	31.20

[a)] Determined by GPC; [b)] Determined by DSC in the 2nd heating run before water immersion; [c)] Determined by DSC in the 2nd heating run after water immersion.

Table 4.1 Characteristics of synthesized poly(*rac*-lactide-*co*-glycolide) networks. The table shows the molecular weight and glass transition temperatures of the corresponding networks before and after water immersing

4.1.2 DSC measurement

In the DSC measurement, all synthesized polymer networks exhibit only one T_g in DSC, and were tunable over the range of 41-49°C by varying glycolide monomer constitutes, as shown in figure 4.1. Moreover, T_gs of networks are generally higher than those of the corresponding co-oligomers. This is attributed to the limited mobility of free chain ends upon incorporation into the polymer network. In addition, thermal properties are shown to be much dependent on the monomer composition. T_g of poly(*rac*-lactide-*co*-glycolide) copolymer increased from 37.13 to 55.36°C with the content of *rac*-lactide increasing from 10 to 90 wt %. The obtained dependence of T_g from the comonomer content is shown in figure 4.2. The observed T_gs of copolymers were approximately fitting to the Fox-Flory equation, thus indicating a randomized distributing of the comonomers within the polymer chains and all prepared copolymer

networks were amorphous. The adjustable nature of T_g is critical to the use of SMPs in biomedical applications, allowing shape-memory properties of the polymer to be optimized for a given application by adjusting the amounts of monomer and not introducing any new monomers or additives into the system. In this study, for our intended tri-segment nerve conduit application, three different T_gs with approximate interval are desired, in which the gradual shape-recovery can occur in a wide range. We select networks prepared from PLGA-60/40, PLGA-40/60, and PLGA-20/80 for the further shape-memory effect experiments, as these copolymers have the most widely and average T_g distribution.

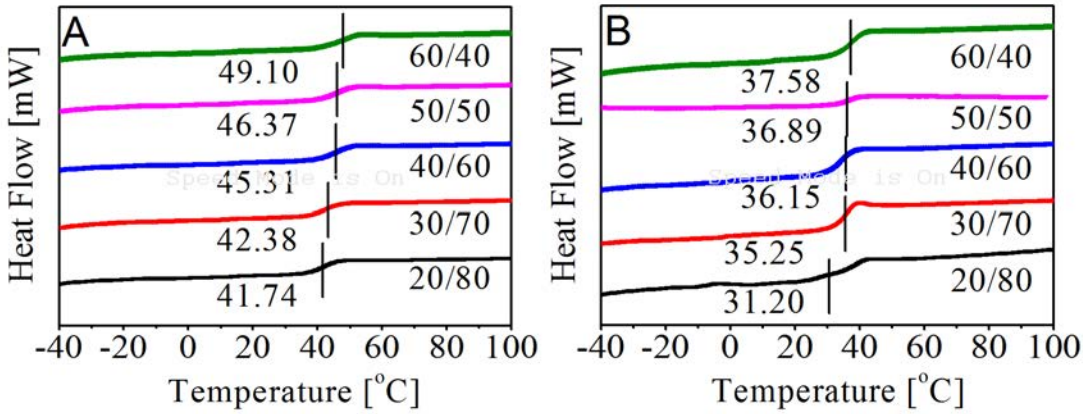

Figure 4.1 DSC results of synthesized PLGA copolymers

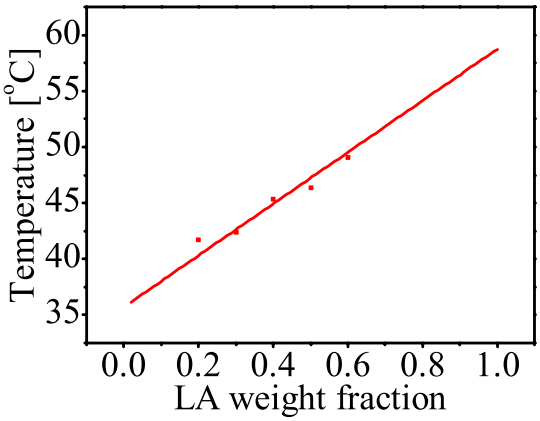

Figure 4.2 Dependence of T_g of copolymer on comonomer (lactide) content in wt%.

The curve was calculated from the Fox-Flory equation

4.1.3 XRD measurement

Figure 4.3 is the XRD measurement results of the synthesized PLGA copolymers. In the XRD results, no diffraction peaks attributed to crystalline segments are observed proving that the synthesized copolymer system is a T_g-type polymer.

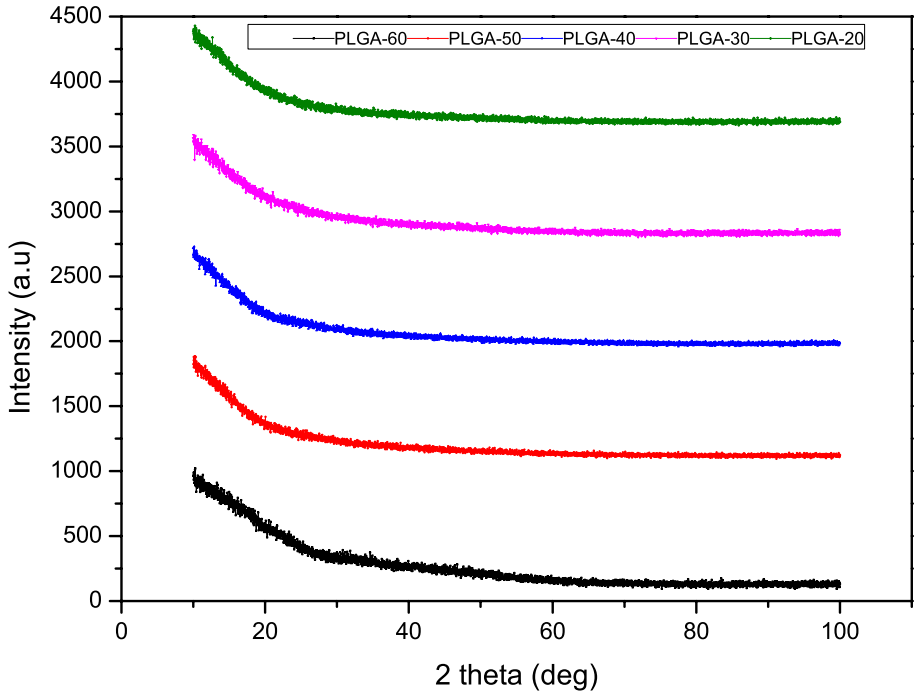

Figure 4.3 XRD measurement results of PLGA copolymers

4.1.4 Thermal-induced SME

To test the hypothesis that the entanglements of molecular chain with molecular weight of 10^5 g mol^{-1}, can act as "net points", the shape-memory functionality of the synthesized copolymers with the molecular weight of approximately 1.0×10^5 g mol^{-1} was quantified in cyclic thermo-mechanical experiments between 20°C and 60°C, the data was shown in table 4.2. Figure 4.4(A_1-A_3) presents the thermo-mechanical experiments of PLGA-60, PLGA-40, and PLGA-20, the shape-memory properties of a network can be described by two important quantities, i.e. the strain fixity ratio R_f

and the strain recovery ratio R_r. R_f is a measure for shape stability of the SMP during deformation at the lower temperature while R_r value is representative of shape recoverability at the higher temperature. For all the networks, R_fs were near 99% under stress-free conditions, even after ten thermo-mechanical cycles. These good shape-fixities are the results of vitrification at the temperature of 20°C and could prevent uncontrolled implant deployment during implantation.

Figure 4.4(B_1-B_3) illustrates the shape recovery ratio R_r corresponding to the number of testing cycles N. It indicates that R_r decreases from about 90% to 50% during the first 5 testing cycles and then becomes relatively stable after the 6^{th} cycle, remaining at approximately 50%. The significant drop of R_r in the early stages of testing cycle (N-1 to N-5) is mostly caused by internal molecular rearrangement and chain disentanglements. Subsequent stress-strain curves are much closer to each other as less disentanglement occurs and the materials become mechanically conditioned, as shown in figure 4.5. This indicates that these copolymers can recover from deformation and return to their original shape, although the R_r decreases with the increase of test time. This verifies the hypothesis that the entanglements of molecular chain with high molecular weight, i.e 10^5 g mol^{-1}, can function as physical cross-links. It is important to note that the decrease in R_r with increasing testing cycle indicates our proposed physically cross-linked SMP possesses a loose net-points structure that may creep during the programming process, however, from a biomedical materials development standpoint, the decreasing R_r data provide initial evidence of the

entanglements of molecular chains. Moreover, in practical application, the device is only amenable to one-time activation, and the decreasing R_r would not introduce negative effects.

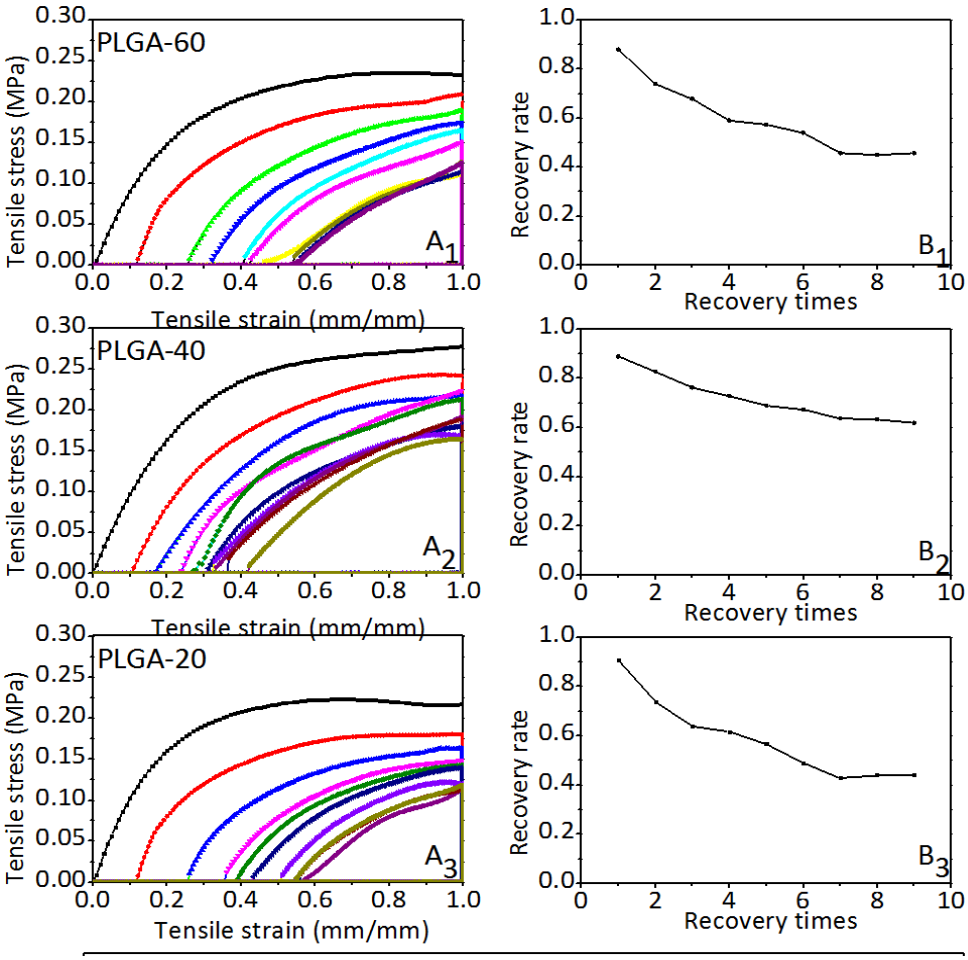

Figure 4.4 Materials characterization data demonstrating the shape-memory effects of the synthesized copolymer networks PLGA-60, PLGA-40, and PLGA-20. (A_1-A_3) Ten-cycle thermal-induced shape-memory characterization results for the three types of synthesized copolymers respectively; (B_1-B_3) Cycle times-R_r functions of the corresponding copolymers

	PLGA-60		PLGA-40		PLGA-20	
	R_r	R_f	R_r	R_f	R_r	R_f

1st cycle	0.87	0.97	0.89	0.98	0.90	0.98
2nd cycle	0.74	0.98	0.83	0.98	0.74	0.97
3rd cycle	0.68	0.97	0.76	0.98	0.64	0.97
4th cycle	0.59	0.97	0.73	0.98	0.62	0.97
5th cycle	0.57	0.97	0.69	0.98	0.57	0.97
6th cycle	0.54	0.97	0.67	0.98	0.49	0.97
7th cycle	0.46	0.97	0.64	0.98	0.43	0.97
8th cycle	0.45	0.97	0.63	0.98	0.44	0.97
9th cycle	0.46	0.97	0.63	0.98	0.43	0.97

Table 4.2 Shape memory test results of synthesized copolymer networks

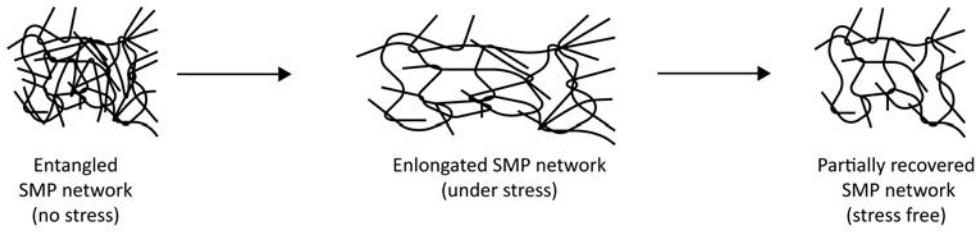

Figure 4.5 Schematic representation of the entanglement changing during the thermo-mechanical process

4.1.5 Water-induced SME

For our intended tri-block nerve conduit application, three different T_gs with approximate interval are desired, in which the gradual shape-recovery can occur in a wide range. We select networks prepared from PLGA-60, PLGA-40, and PLGA-20 for the further shape-memory effect experiment, as these have the most widely and average T_g distribution. To investigate the body-water-induced shape-memory effect,

test of the recovery angle versus time was conducted at the temperature of 36°C in water. Figure 4.6 illustrates macroscopic body-Liquid-induced shape recovery process indicating that the SMP with higher T_g recovers slower, while the lower T_g SMP generally recover faster.

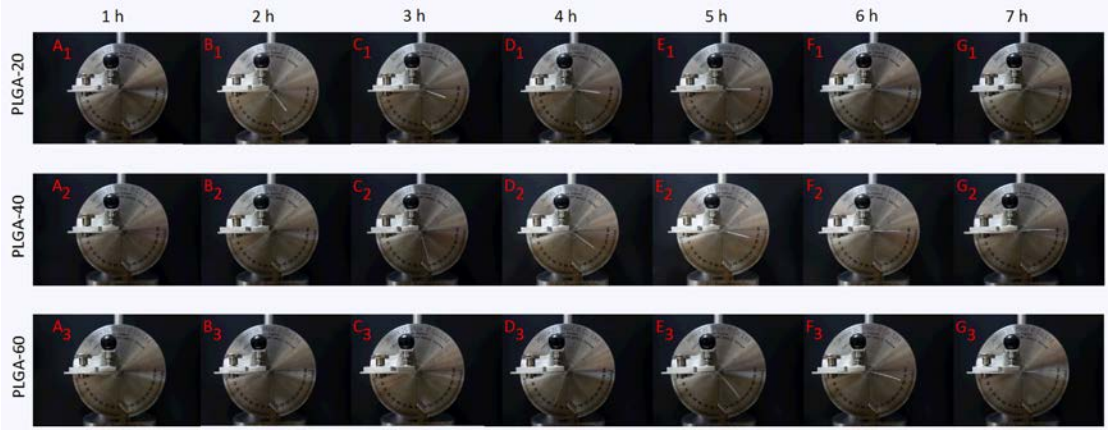

Figure 4.6 A series of photographs showing body-water-induced SEM of the films prepared from PLGA copolymers with different T_gs, the folded strips were put in water bath at 36°C after 1h, 2h, 3h, 4h, 5h, 6h, and 7h, respectively

Figure 4.7 shows the relationship between recovery ratio and recovery time. The whole recovery curve presents an "S" shape and can be divided into three phases: early-immersing stage, accelerating stage, and saturation stage. The comparison of early-immersing time of SMPs with different T_gs shows SMP with lower T_g has an obviously shorter immersing time. Therefore, the gradual recovery application of these synthesized copolymers can be realized by overlapping these recovery time intervals. Figure 4.1 indicates the DSC results before and after the immersion in water. T_gs of synthesized copolymers decrease from 49.10, 46.37, 45.31, 42.38, and 41.74 to 37.58, 36.89, 36.18, 35.25, and 31.20°C respectively.

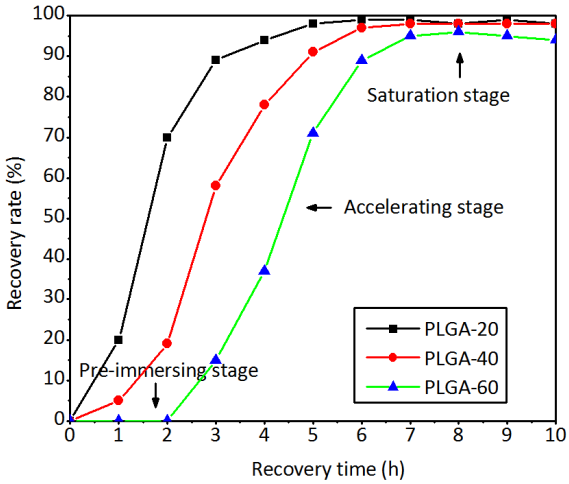

Figure 4.7 Time-recovery rate curve of bending test for three different PLGA copolymers

4.1.6 Water-induced SME analysis

It is generally acknowledged that SMP can be triggered by water. W.M. Huang and co-workers identified the possible mechanism behind the interaction of water with SMP[90-94]. In their research, the SMP used is polyurethane, which is a multi-block copolymer consisting of both hard and soft segments. Polyurethane SMPs have a wider range of shape recovery temperature (30-70°C), high recoverable strain, and excellent biocompatibility. Their results indicated that: 1) water absorbed in the SMP can be split into two parts, namely, free water and bound water. Their quantities in the SMP can be determined by the cyclic DSC test. It is found that the free water can be totally removed at around 120°C through evaporation; 2) free water absorbed in the SMP has negligible effects on the T_g, while bound water significantly reduces the T_g in an almost linear manner; 3) water absorbed in the polyurethane SMP weakens the hydrogen bonding between N-H and C=O groups, which could cause a significant decrease in the T_g[95]. In the conclusion, they also mentioned with the function of

water as a plasticizer the T_g is reduced.

In this study, FTIR is employed as an effective measurement to investigate the interaction of water with the PLGA copolymers and identify other possible factors. The samples used for FTIR test were thin PLGA films with a thickness of 1.0 mm. FTIR spectra were collected by averaging 30 scans at a resolution of 2 cm^{-1} in a reflection mode from a FTIR spectrometer (Perkin-Elmer 2000 FT-IR). To remove the influence of free water, the two types of samples (with/without water immersing) used for FTIR test were heated to about 120°C. The full FTIR spectrums of the poly(*rac*-lactide-*co*-glycolide) copolymers before and after immersion in water are presented in figure 4.8. After immersing in water, it is obvious that the shape of the bound water spectrum in the 3000 to 3600 cm^{-1} region is contributed by O-H stretching and is quite different from that of copolymers without immersion. Utilizing the data obtained from previous tests, namely DSC test, it reveals that bounded water has direct effects on reducing glass transition temperature as a plasticizer.

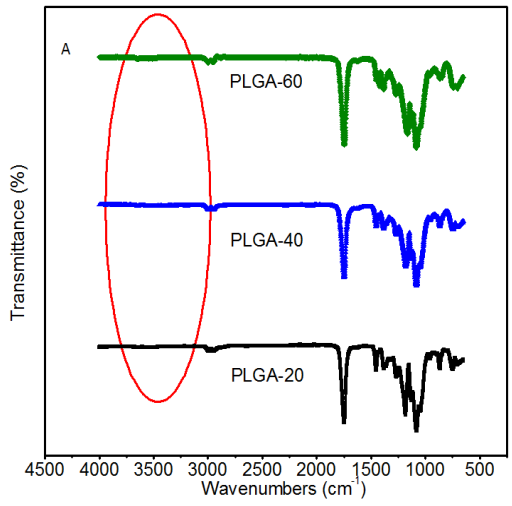

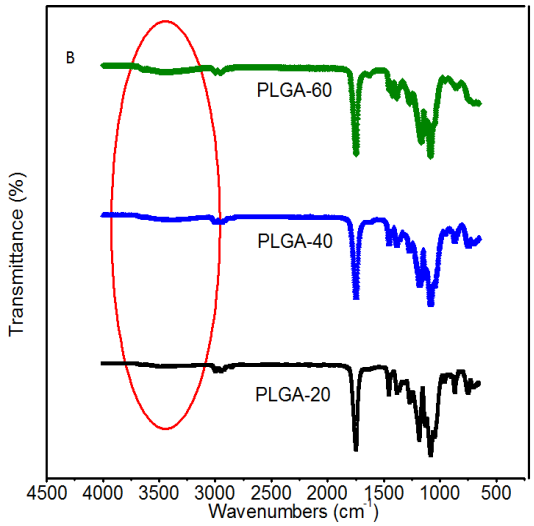

Figure 4.8 (A) FTIR spectra of synthesized copolymers without immersion. (B) FTIR spectra of synthesized copolymers with immersion

4.2 Characterization of SNC

4.2.1 WCA measurement

The hydrophobicity of the surface of PLGA copolymers' film was investigated by water contact angle measurements (WCA). Water contact angle of the films greater than 90˚ were indicated hydrophobic. Water contact angle results listed in figure 4.9 shown that the surface morphology and the copolymer composition of different films significantly impacted the final PLGA hydrophobic performance. With the increase of the glycolide weight fraction, PLGA water contact angle was reduced from 74˚ to 46˚ for the solution films, and 128˚ to 117˚ for the electrospun films. The lower surface tension lactide chain had the higher desperation in the surface, which demonstrated the better hydrophobic performance with higher water contact angle. Moreover, after electrospinning, the electrospun films obtained a porous structure that would increase the water contact angle.

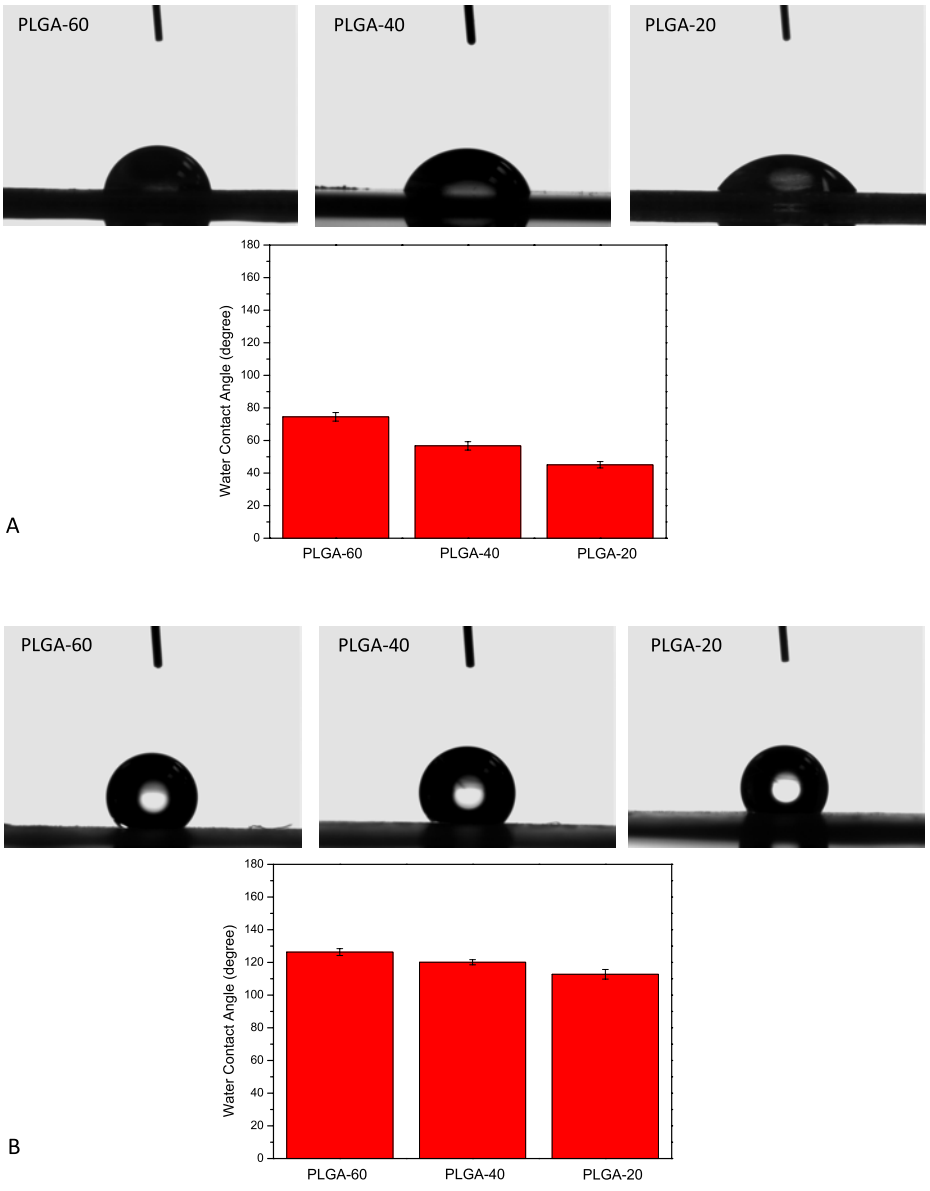

Figure 4.9 (A) WCA results of the copolymer solution films. (B) WCA results of the copolymer electrospun films

4.2.2 Thermal-induced SME

To confirm the hypothesis that the entanglements of molecular chain with molecular weight of 10^5 g mol^{-1}, can act as "net points", the cyclic thermo-mechanical experiments between 20°C and 60°C were also conducted on the electrospun films, the data was shown in table 4.3[96]. Figure 4.10 present the thermo-mechanical results of PLGA-60, PLGA-40, and PLGA-20. For all the electrospun networks, R_fs

were near 99% under stress-free conditions, even after three thermo-mechanical cycles. These good shape-fixities are the results of vitrification at the temperature of 20°C and could prevent uncontrolled implant deployment during implantation. The decrease of the R_r confirms the existence of molecular chain entanglements and further indicates that the entanglements are physically cross-linked and will creep during the programming process[97].

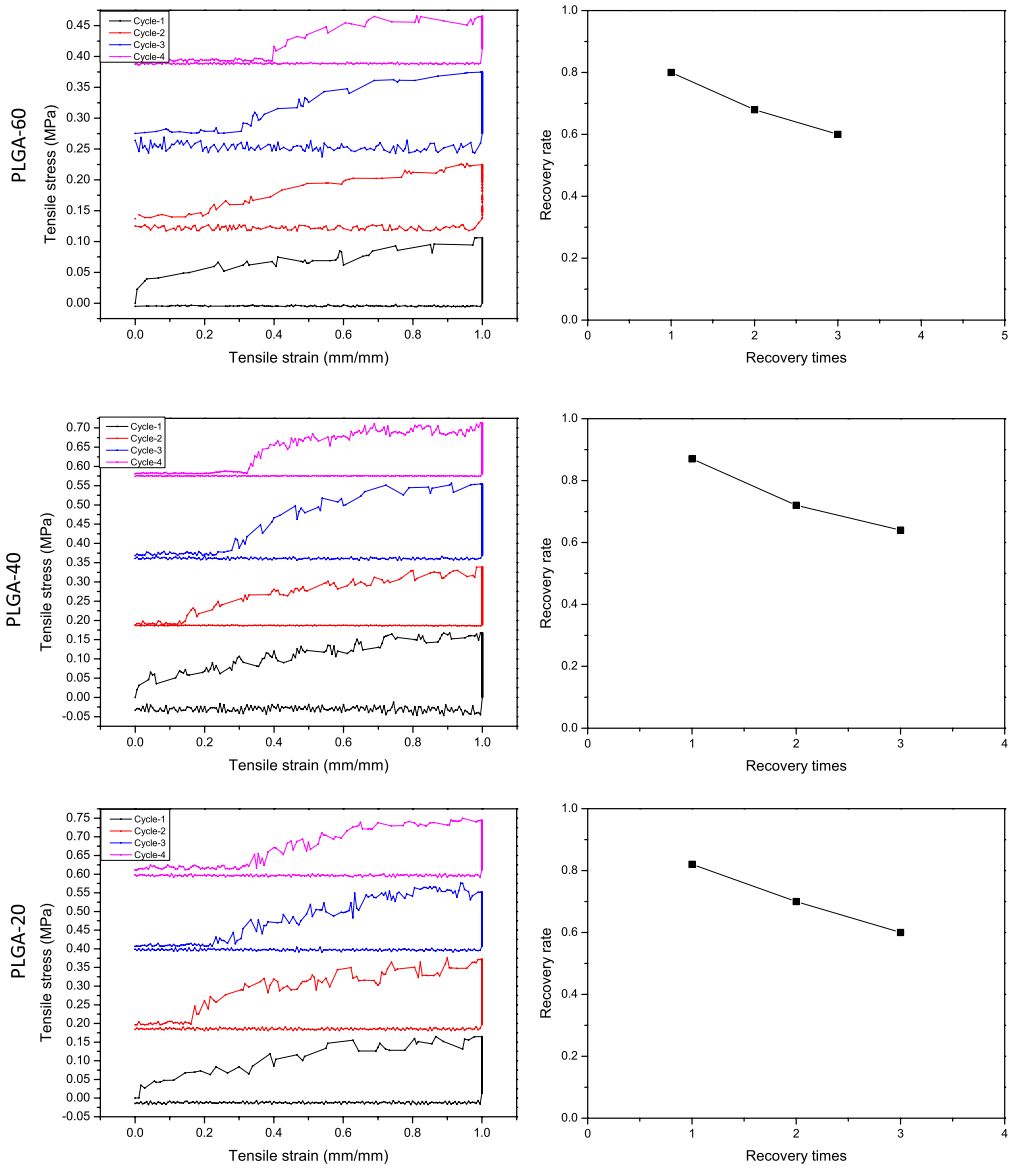

Figure 4.10 Materials characterization data demonstrating the shape-memory effects of the electrospun films PLGA-60, PLGA-40, and PLGA-20. (A_1-A_3) Three-cycle

thermal-induced shape-memory characterization results for the three types of electrospun samples respectively; (B_1-B_3) Cycle times-R_r functions of the corresponding samples

	PLGA-60		PLGA-40		PLGA-20	
	R_r	R_f	R_r	R_f	R_r	R_f
1st cycle	80%	98.2%	87%	99%	82%	98.9%
2nd cycle	68%	98.1%	72%	98.5%	70%	98.4%
3rd cycle	60%	97.8%	64%	98%	60%	98.4%

Table 4. 3 Shape memory test results of electrospun copolymer films

4.2.3 Mechanical properties

Mechanical performance is also one of the essential requirements for a biomedical material to be utilized for a structure-supportive scaffold. An ideal nerve conduit should be easy to handle and suture, and have sufficient mechanical strength to resist in vivo physiological loads after implanting[98]. In figure 4.11, strain-to-failure data were obtained by conducting experiments at room and body temperature. The elastic modulus results of the nerve conduit at room/body temperature were 11 and 5 Mpa, respectively. The further animal experiments confirmed that the mechanical properties ensure that the scaffold can resist muscular contraction and maintain its shape unchanged for a considerable period of time after implanting.

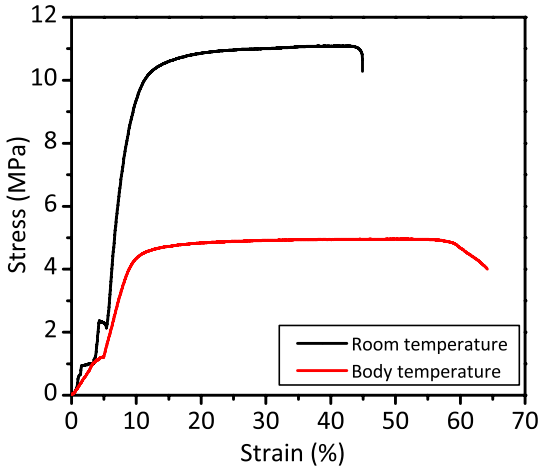

Figure 4.11 Typical of stress-strain curves of the electrospun fibrous PLGA nerve conduit tested at room temperature and body temperature

4.2.4 Macroscopic water-induced SME of SNC

The smart nerve conduit prototype reported in this study is designed to facilitate nerve regeneration. Figure 4.12(A) illustrates the macroscopic image of the fabricated tri-segment smart nerve conduit of 0.3 mm thickness and 2 mm inner diameter in its permanent deployed state. Figure 4.12(B) shows its temporary elongated state after uniaxial stretching above its T_gs and cooling to 20°C. At this temperature, SNC is in the glassy state and presents a good shape-fixity ratio. Therefore it can be implanted efficiently without premature deployment during surgical suturing. A set of experiments to test the feasibility of this concept was performed, as shown in figure 4.12(C-L). Two ends of the elongated nerve conduit were sutured to two tightened elastic bands and then immersed in water at 36°C to mimic *in vivo* condition. With the immersing time elapsing, the deformed conduit gradually recovers to its permanent shape. R_r was calculated from the macroscopic length change, as shown in figure 4.12(M). The curve shows the relationship between recovery rate and recovery time.

The tri-segment SNC starts to recover upon immersion in water (36°C). After being immersed for 7 h, R_r reaches almost 90% and becomes stable indicating the deformed conduit has recovered to its permanent shape. Due to the chain disentanglement during the programming process and the constraint at the two ends by elastic bands during recovery, the R_r cannot reach 100%. Moreover, compared with the moisture-induced analysis data presented in figure 4.6, the recovery curve doesn't represent an apparent "S" shape but becomes smooth, this finding verify our tri-segment SNC design of gradual-recovery function can be generated by the macroscopic combination of polymer segments with different T_g[99].

The relatively slow recovery rate (recovery to a stable architecture with hours at 36°C) presents both immediate applications and future modification for the current SNC or other biomedical device with similar shape-memory functionality. For example, slow and programmable recovery rate, as demonstrated here, could fulfill specific tissue engineering requirement. In addition, the slow recovery rate would provide an opportunity to investigate the long-term influence of dynamic changes in matrix structures on cell behaviors such as cell differentiation and lineage specification. It is worth noting explicitly that prior investigations have demonstrated that externally applied mechanical actuation and shape-changing functionality possess the ability to enable new lines of inquiry. In the present study, the slow and programmable recovery rate was achieved by modifying the chemical composition of the poly(*rac*-lactide-*co*-glycolide) to adjust glass transition temperature and by

introducing electrospinning technology to fabricate a tri-segment nerve conduit. Besides the gradual-recovery function, the nanofibrous structure of the conduit makes it feasible to suture it to the proximal and distal end of the nerve stumps. Furthermore, the fabricated conduit has a porous structure, thus making it permeable to entry of nutrients into the conduit lumen to promote the nerve regeneration. *In vivo* experiments in animal model should be conducted to ensure the conduit has the required bio-mechanical properties to perform adequately under practical conditions.

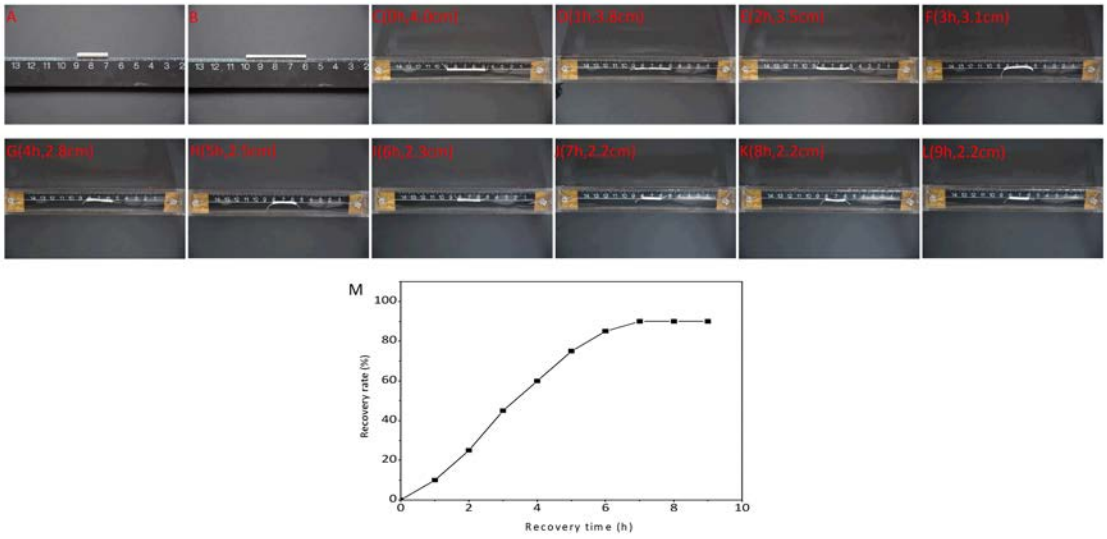

Figure 4.12 Macroscopic demonstration of SME for the tri-segment smart nerve conduit. (A) Permanent shape of the smart nerve conduit. (B) Temporary shape of the device at 20°C. (C-L) shape-memory process of the SNC, in transition from the elongated shape to the permanent shape gradually under simulated *in vitro* condition. (M) Recovery rate-recovery time curve of tri-segment SNC

4.2.5 SEM measurement

When the tri-segment nerve conduit was fabricated by electrospinning technology, the surface morphology of each segment was observed via SEM, as shown in figure 4.13. The diameters of the electrospun PLGA-60, PLGA-40, and PLGA-20 nanofibers were estimated to be 2.27±0.31, 2.25±0.25, and 2.33±0.19 μm, respectively. The diameter

of electrospun fibers is of similar magnitude as that of fibrils in extracellular matrix (ECM) that mimics the natural tissue environment and has presented effectiveness as a substrate for cell growth. In addition, the physical form of the electrospun nerve conduit such as porosity can greatly influences its biocompatibility with tissue in vivo.10 Usually, biologic nerve grafts made from autograft/allograft are revascularized within the first 4-5 days after implantation by longitudinal ingrowth of vessels from the distal and proximal nerve stump and sprouting of collateral capillaries. This process requires diffusion of nutrients, growth factors and other biologically active agents into the area of nerve regeneration. Therefore, porous conduit can allow the influx of external nerve regeneration factors and the outward diffusion of waste products. In addition, porous nerve tube may also facilitate the formation of a supportive fibrin by allowing inward diffusion of local or systemic healing factors[100].

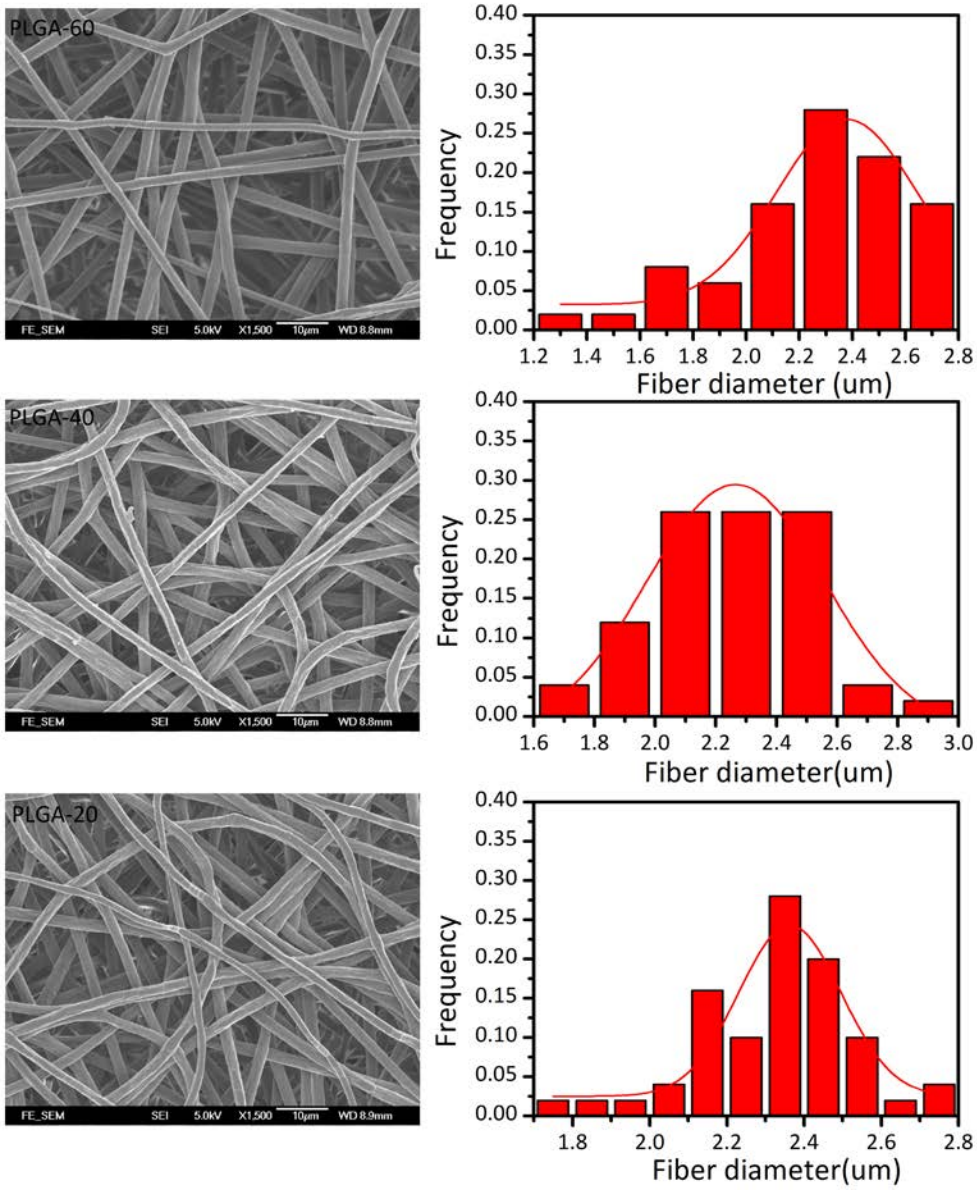

Figure 4.13 SEM micrographs and diameter distribution histograms of electrospun nerve conduit fibers. (a). PLGA-60 segment, (b). PLGA-40 segment, and (c). PLGA-20 segment

Field-Scanning electron microscopy revealed changes in the microscopic architecture of nerve conduit following pre-thermal treatment and water-induced triggering (Figure 4.14). After thermosetting, the conduit showed a randomly orientated

architecture, shown in figure 4.14(A_1-A_3). After programmed stretching, the strain-aligned conduit exhibited prevailing fiber alignment, shown in figure 4.14(B_1-B_3). After immersion in water, the conduit recovered back to a modestly random-orientated architecture (Figure 4.14C_1-C_3). The fiber alignment change following shape recovery process is determined by the peak shape and height in the FFT plots (Figure 4.14D-F)[101]. The microscopic shape-memory effect in fiber alignment is correspondence with the macroscopic shape change. Here we have demonstrated and characterized a water-responsive SMP scaffold capable of changing internal architecture. The architectural change involved, in which fiber alignment can be triggered to decrease on requirement, may find use in a number of *in vitro* and *in vivo* applications. Shape-memory induced microscopic changes in fiber alignment have been reported to control cell morphological behavior, such as the actin filaments and nuclei, prior to triggering changes in scaffold architecture, actin filaments and nuclei preferentially aligned in the direction of the scaffold fiber alignment. After the transition, actin filaments and nuclei became randomly oriented, indicating that changes in architecture of the scaffold could control cell behavior. Moreover, in the field of tissue engineering, differentiation down specific lineages, such as the chondrogenic lineage, appears to be favored when stem cells are cultured on aligned, rather than random, nanofibers; the SMP scaffolds could be utilized to triggered on command differentiation of specific lineages that are supported by random fiber alignment.

The electrospinning technology employed here has found widespread application in tissue engineering due to the presence of biomimetic fibrous structures. However, a common challenge to electrospun scaffold is that cell penetration and distribution is often superficial and non-uniform, respectively. Previously developed techniques, such as the combination of chemotactic ECM components and the incorporation of water-soluble fibers to increase pose size, could be employed to facilitate penetration in electrospun scaffolds. In the present study, although whether shape-memory actuation can affect cell penetration and behavior is not addressed, the microscopic shape control of scaffold architecture demonstrated raises the possibility that the fabricated SNC could be designed to facilitate cell culture.

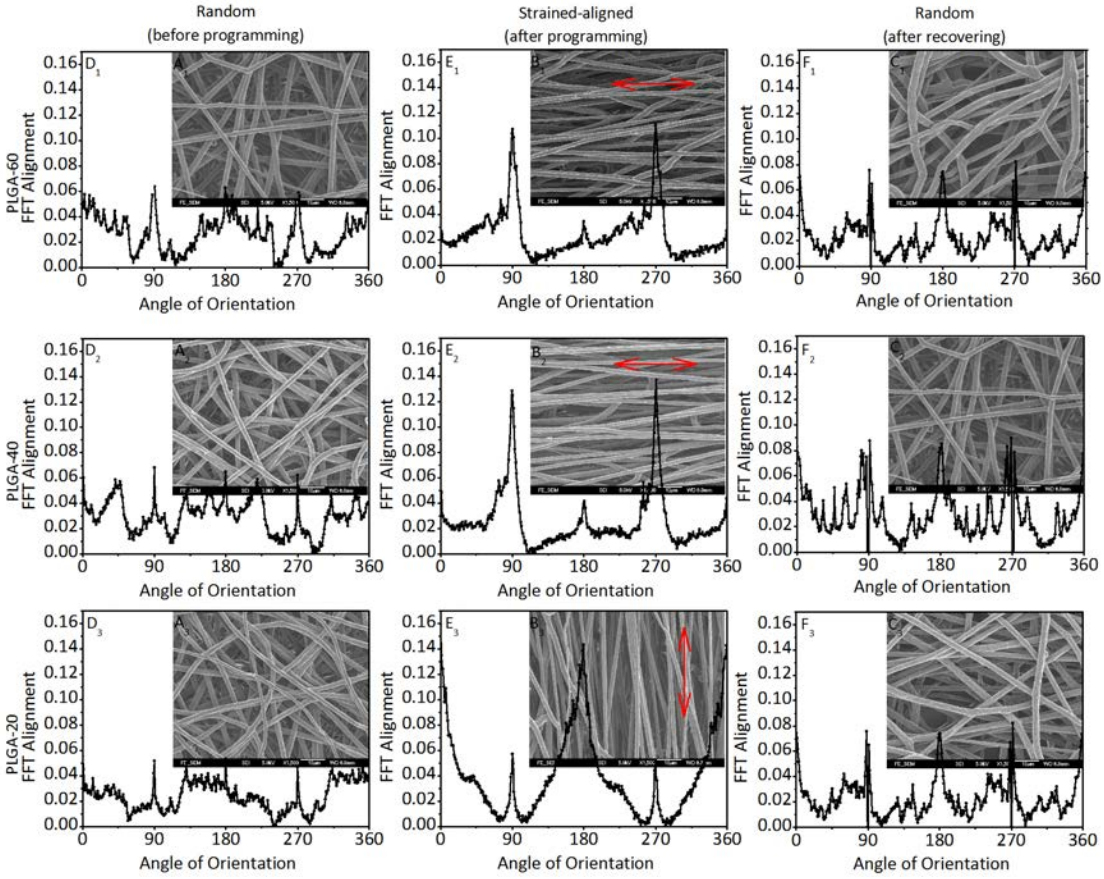

Figure 4.14 SEM micrographs of electrospun fibers of PLGA with different LA:GA weight ratios. (A_1-A_3) A randomly oriented fiber architecture following thermosetting.

(B_1-B_3) A strain-aligned fiber architecture following programmed uniaxial stretching. (C_1-C_3) The fibers recovered to a randomly oriented architecture following shape memory triggering via immersing in water. Double arrows represent the fiber direction. 2-D FFT image analysis of fiber alignment. (D_1-D_3) A lack of distinct peaks in FFT plots represent the fibers after thermosetting have no apparent fiber alignment. (E_1-E_3) Distinct peaks at 90°, 180°, and 270° in the FFT plots indicate that fibers align along a principle direction, corresponding to the direction of applied strain. (F_1-F_3) The decrease of FFT peak represents the fibers recover back to a modest randomly oriented architecture

4.3 Summary

In this chapter, we first time introduced a smart nerve conduit fabricated by electrospinning technology that may achieve desirable peripheral nerve regeneration by prolonged automatic gradual lengthening. For this purpose, this study introduced a poly(*rac*-lactide-*co*-glycolide) copolymer network with a unique blend of material properties including tailorable glass transition, tunable body-water responsive shape recovery behavior and suitability for electrospinning process. Cyclic thermo-mechanical measurements indicate that entanglements of molecular chains formed from high molecular weight ($>10^5$ g mol^{-1}) can function as hard segments. Results demonstrated the sequential and gradual-recovery triggered by body-water (36°C) of these copolymers with different T_gs. Based on this material, a prototype of tri-segment smart nerve conduit was fabricated by electrospinning technology and showed prolonged gradual recovery function under simulated *in vivo* condition.

CHAPTER 5 *IN VITRO* AND *IN VIVO* MEASUREMENT OF SNC

5.1 *In vitro* measurement

To demonstrate the ability of the three types of synthesized poly(rac-lactide-co-glycolide) networks to support the adhesion and proliferation of Schwann cells, cell culturing studies were conducted[102-104].

5.1.1 MTT assay

The MTT assay results are shown in figure 5.1. Optical density (OD) value is consistent with activation of the cells. After 48 h incubation in different mediums, the viability of Schwann cells was assessed. The viability of Schwann cells cultured in the synthesized copolymers extract showed no significant difference in their cell viability as compared to that in normal condition medium, that suggests that silk fibroin extract fluid has no effects on the survival of Schwann cells cultured in it.

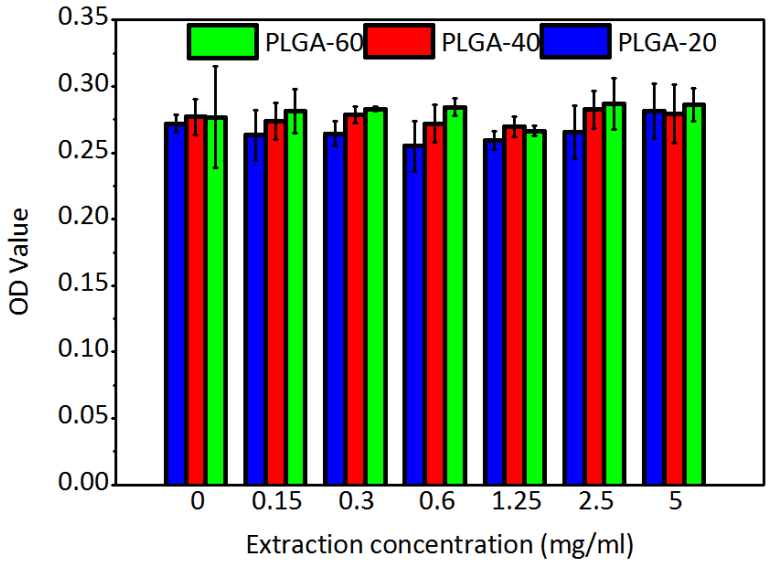

Figure 5.1 MTT assay results: proliferation of Schwann cells cultured in different concentrations of extracts for 48 h

5.1.2 Cell morphology measurement

To demonstrate the ability of degradable PLGA copolymers to support the adhesion and proliferation of Schwann cells and the production of extracellular matrix, cell culture studies were performed. Cell morphology on the different types of material surfaces was utilized to determine the cytocompatibility of the synthesized copolymers. In figure 5.2, the attachment of Schwann cells on the surfaces of PLGA-60, PLGA-40, and PLGA-20 electrospun films is quantified after culturing for 6 h, 24 h, and 48 h culturing based on the fluorescent microscope images showing DAPI staining. In each case the number of viable Schwann cells increased in time, indicating that all the surfaces allow the growth and proliferation of Schwann cells.

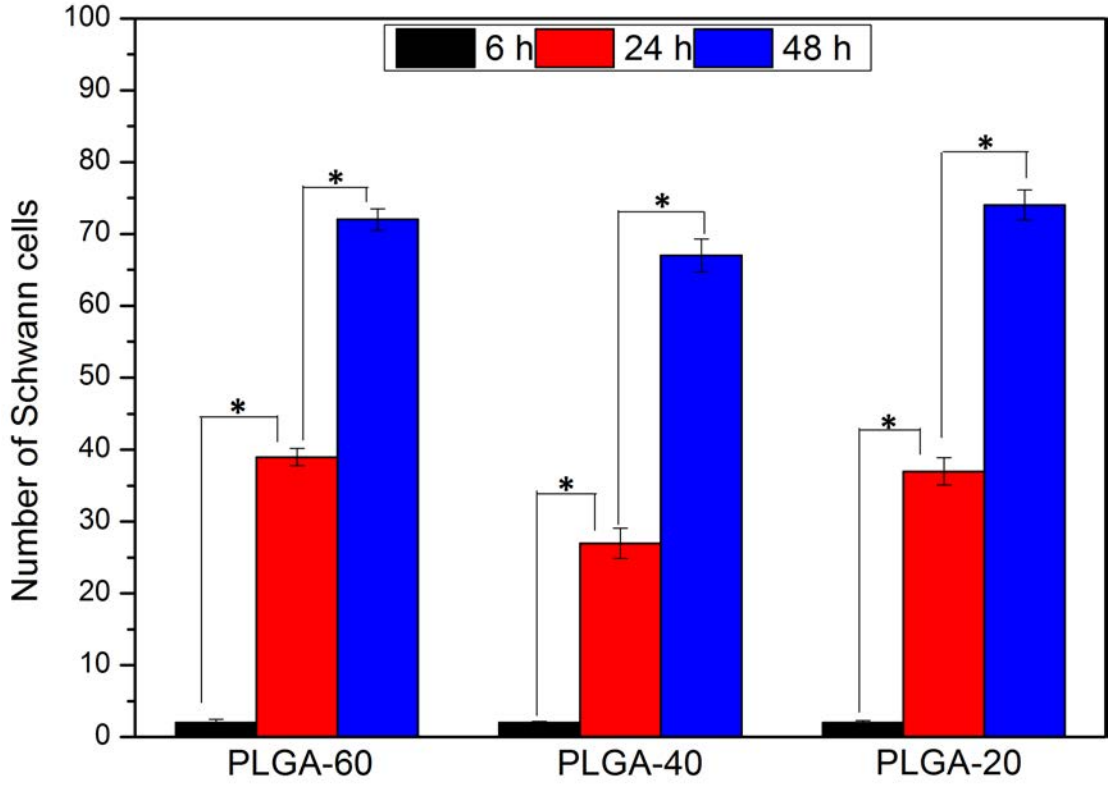

Figure 5.2 The number of Schwann cells attached to the surface of PLGA-60, PLGA-40, and PLGA-20 electrospun films after 6 h, 24 h, and 48 h culturing

Figure 5.3 shows the morphology of Schwann cells cultured on the three types of PLGA nanofirous films, and revealed that Schwann cells flattened and extended in a sequential fashion as cultured for 6, 24, and 48 h. The whole process of adhesion and spreading consists of cell attachment, filopodial growth, cytoplasmic webbing, and flattening of the cell mass that are performed in a sequence. Similarly, the amount of Schwann cells cultured in the extract fluid had increased significantly with time. All the experimental results showed that the synthesized copolymers extract fluid did not influence expressions of S-100 cell marker associated with Schwann cells, providing further evidence for little cytotoxicity of the synthesized shape-memory copolymers

on Schwann cells. Collectively, these data indicate that the synthesized poly(rac-lactide-co-glycolide) copolymers have good biocompatibility with Schwann cells and are also beneficial to the survival without exerting any significant cytotoxic effects on their phenotype or functions, thus providing an experimental foundation for the development of the designed shape-memory poly(rac-lactide-co-glycolide) copolymer as a candidate material for nerve regeneration application.

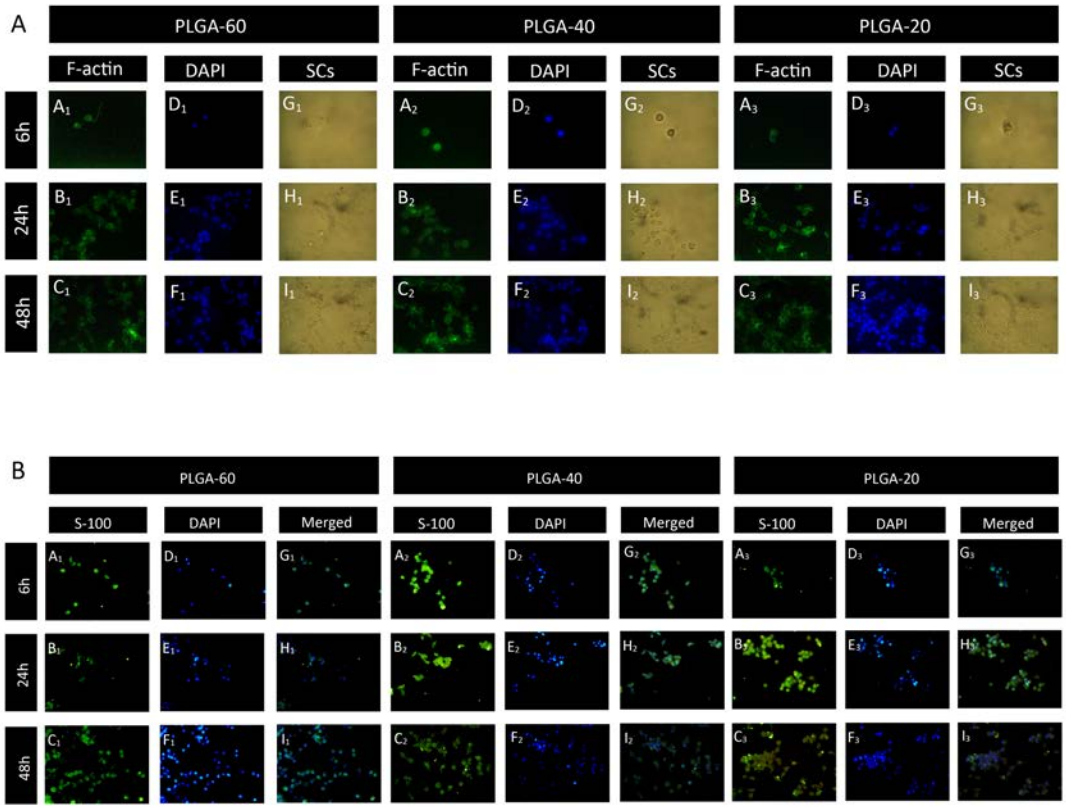

Figure 5.3 (A) Fluorescent microscope images and optical microscopic examination of Schwann cells cultured on three types of synthesized copolymers for 6, 24 and 48 h. Image sets A-C and D-F represent F-actin (green) and nucleus (blue) were stained by FITC-Phalloidin and DAPI, respectively. Image sets G-I represent the morphology of Schwann cells. (B) Fluorescent microscope images of Schwann cells cultured in three types of synthesized copolymer extraction fluids for 6, 24, and 48 h. Image sets A-C, D-F and G-I represent immunostained for S-100, nuleus, and their overlay, respectively

5.2 *In vivo* measurement

As our previous work shown, the electrospun nerve conduits have good biocompatibility with Schwann cells and are also beneficial to the survival without exerting any significant cytotoxic effects on their phenotype or functions. In this study, adult New Zealand white rabbits approximately 2 months of age were used to evaluate the in vivo biocompatibility and the nerve regeneration performance. Briefly, the animals were divided into 3 groups each with 6 rabbits. Group A: elongated nerve conduits; group B: nerve conduits with original length; group C: autograft nerve group as a positive control. Then, the sciatic nerves of animal models were resected to obtain a 15 mm nerve gap under a standard surgical procedure. Subsequently, both the proximal and the distal stumps were sutured with the elongated/original conduits, leaving a 15 mm gap between the stumps. In a similar microsurfical technique, nerve autografts were used to repair defects in the rabbit sciatic nerve. Nerve autografts were placed in a reverse fashion to prevent axonal branching during proliferation through side branches from the donor nerve. Therefore, each rabbit received one implant and histomorphology evaluation was performed to evaluate the in vivo performance.

5.2.1 Surgical procedure

The feasibility of our approach to regenerate the resected peripheral nerve with our designed smart nerve conduit was evaluated in a rabbit model. In figure 5.4 a smart nerve conduit prepared from electrospinning is shown in its permanent state and in its temporary elongated state after deformation above 60°C and cooling at room

temperature. At this low temperature the device is in the glassy state and rigid and has a good shape-fixity ratio. It can therefore be implanted to bridge the resected nerve, while premature deployment during surgical insertion will not occur.

Figure 5.4 illustrate the surgical procedure of implanting the nerve conduit. The sciatic nerve was then exposed after the skin incision, and separation of muscles around the nerve tissues using blunt dissection. Subsequently, 6 mm of the nerve was resected to obtain a 15 mm nerve gap. Then the pre-elongated and original SNCs with a length of 20 mm can be implanted into rabbits with a 15 mm nerve injury. The required lengths of SNCs could be obtained by cutting prepared or programmed SNCs with a heated penknife. 12 weeks after implantation, autografts, original SNC, and pre-elongated SNC were sampled to evaluate the repair performance, as shown in figure 5.5.

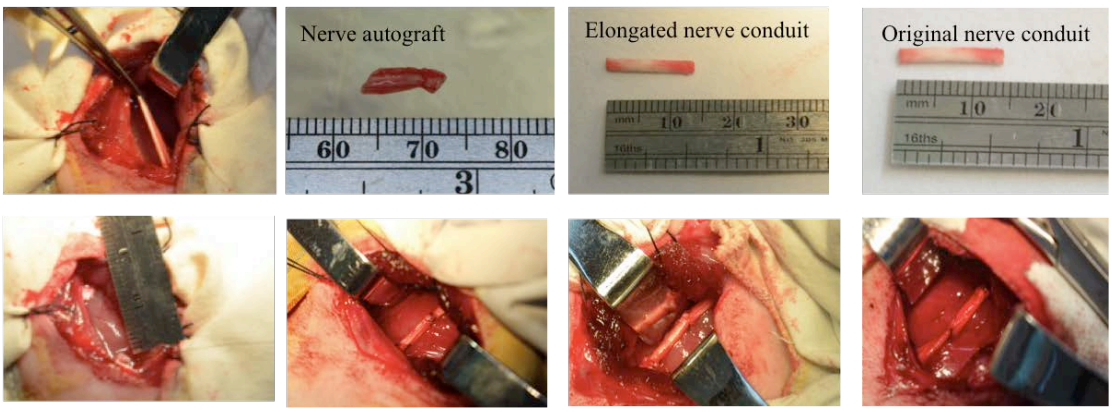

Figure 5.4 The gross view of surgical procedure

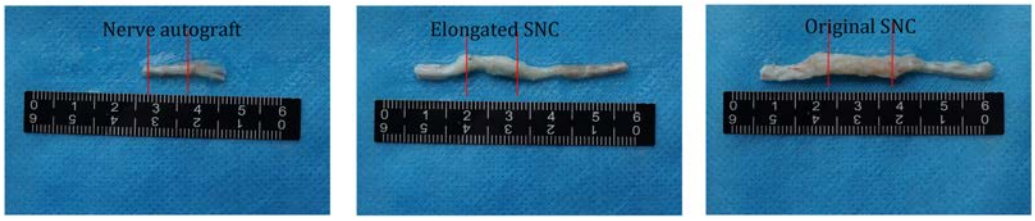

Figure 5.5 Examples of regenerated sciatic nerves from autgraft, elongated SNC, and original SNC, implanted for 12 weeks.

5.2.2 Histological assessment

Hematoxylin and eosin (HE) stain is one of the principal stains in histology. Hematoxylin binds to basophilic substances (such DNA/RNA in the nucleus, which are acidic and negatively charged) and stains them violet. Eosin binds to acidophilic substances (such proteins in the cytoplasm, which are basic and positively charged) and stains them pink. Moreover, the stained proteins could include cytoplasmic filaments in muscle cells, intracellular membranes, and extracellular fibers. Masson's trichrome is suited for distinguishing cells from surrounding connective tissue, which stains keratin and muscle fibers red, collagen and bone blue, cytoplasm pink, and cell nuclei black. It is widely employed to study muscular dystrophy, cardiac infarct or kidney pathologies.

To study the *in vivo* biocompatibility, we evaluated the toxicity of nerve conduit based on the implantation time of poly(*rac*-lactide-*co*-glycolide)-based conduit. Since the degradation of polymeric biomaterials may affect the tissue in several ways, the implanted polymeric biomaterials will gradually release various chemical products of

degradation, including common additives, impurities, monomers, and oligomers. These chemical components would introduce types of toxic reactions in the tissues by slowly migrating from the interior to the surface and the surrounding tissue, causing inflammation or pathologic changes in the tissues of interest. Briefly, 12 weeks post-implantation, excised important organs from heart, liver, spleen, and kidney were frozen and embedded in paraffin wax, were sectioned into 8 um slices, were stained by hematoxylin/eosin (HE) stain method, and were observed by microscopy to fully evaluate the impact of the chronic exposure of conduit in the animal model. As shown in figure 5.6, the implantation of the fabricated nerve conduit did not cause any pathologic damage to rabbit heart, liver, spleen, or kidney, indicating good in vivo biocompatibility.

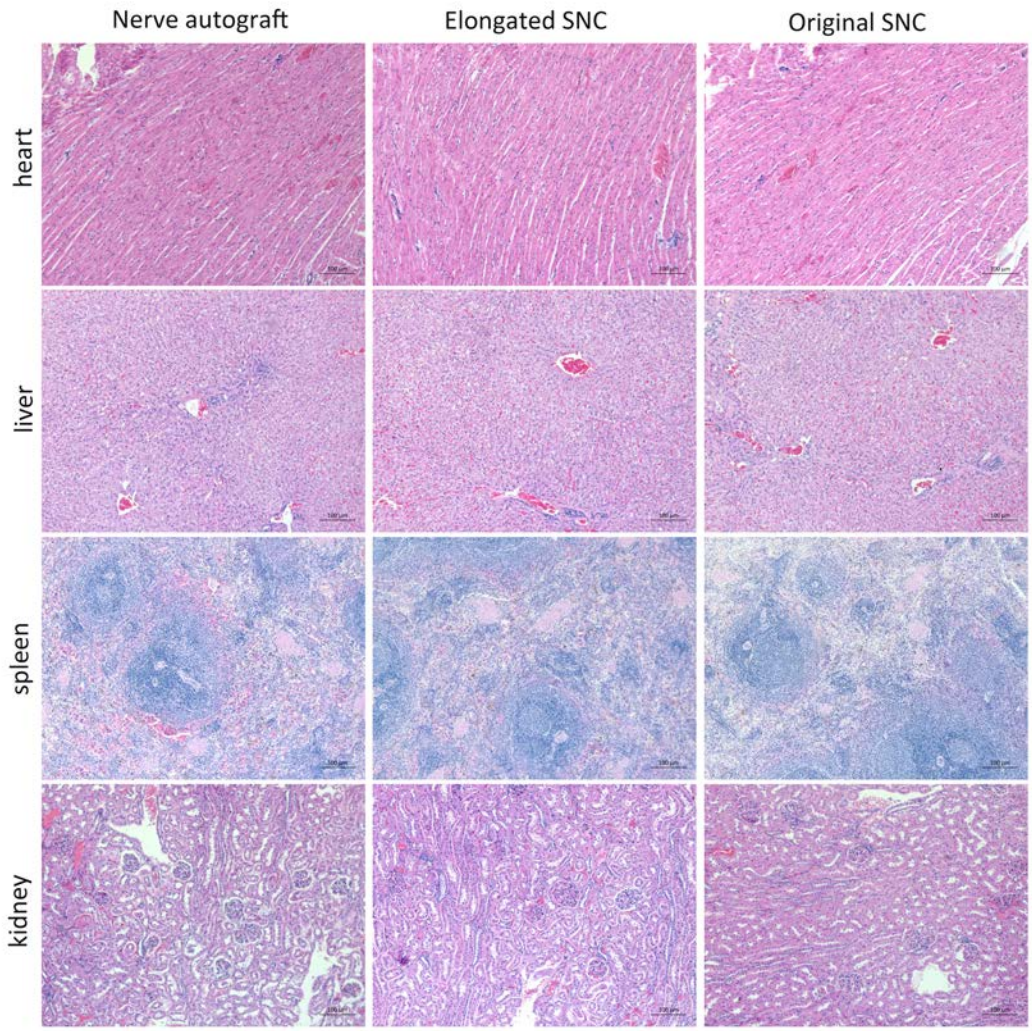

Figure 5.6 HE staining of important organs of heart, liver, spleen, and kidney

Figure 5.7 shows tissue response to specimen implant in the animal model after 4 weeks, 8 weeks, and 12 weeks, respectively. Following implantation for 4 weeks, the tissue reaction to the specimen was very uneven and was characterized mainly by an inflammatory response. 8 weeks after implantation, H&E staining pictures showed the number of inflammatory cells decreased sharply. At 12 weeks, the nerve conduit was almost free of inflammatory cells.

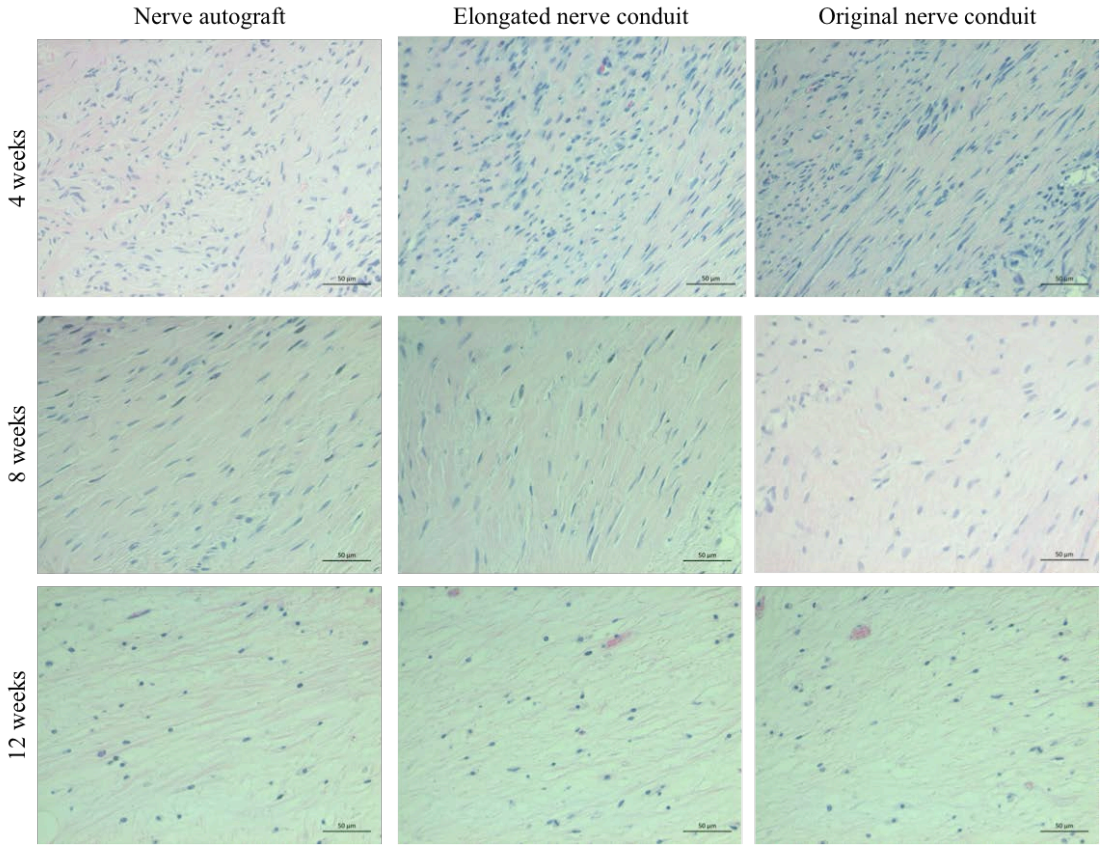

Figure 5.7 Histological observation of different nerve conduits implanted in the animal, in comparison to the control group, for 4 weeks, 8 weeks, and 12 weeks

To study the efficiency of nerve conduits for nerve regeneration, at week 4, 8, and 12, the regenerated nerves were cut into 5 um thick longitudinal sections that were then stained with hematoxylin/eosin (HE) and Masson's staining, respectively to detect structures. As shown in figure 5.8 and figure 5.9, the appearance of the polymeric implants and surrounding tissue varied throughout the course of implantation. On week 4, the appearance and dimensions of nerve conduit without programming was largely unchanged. In contrast, the length of elongated nerve conduit had decreased by 40%. The length decrease can be attributed to the water-triggered shape-memory function, which was demonstrated in our previous study. The tissues showed no gross

inflammation or fibrosis. On week 8, the appearance and dimensions of the non-programmed conduit was still similar to the original implants. But the average length of the elongated conduit was slightly smaller. At week 8, no remarkable inflammation was observed in the tissue surrounding the original and elongated implants; however, minimal fibrosis was observed in the tissue surrounding these two conduits. On week 12, no dimensional data were obtained from both original and elongated conduit. Again, no gross inflammation was observed in the tissue surrounding these two types of conduits but mild fibrosis and scarring was observed in the tissue surround these implants.

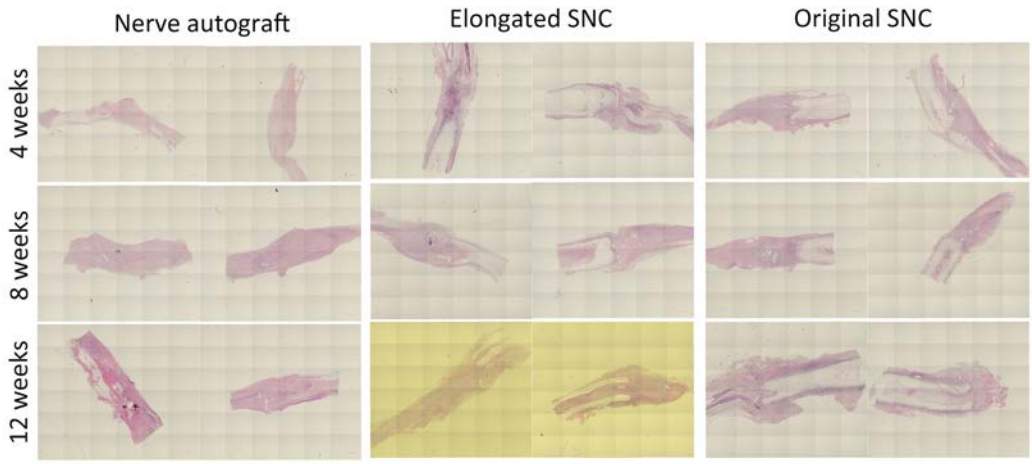

Figure 5.8 (a) Longitudinal section of regenerated nerves taken from types of nerve conduits implanted in rabbit for 4 weeks, stained with hematoxylin/eosin (HE). A: elongated conduit, B: conduit with original length, C: autograft nerve. (b) Implanted for 8 weeks. (c) Implanted for 12 weeks

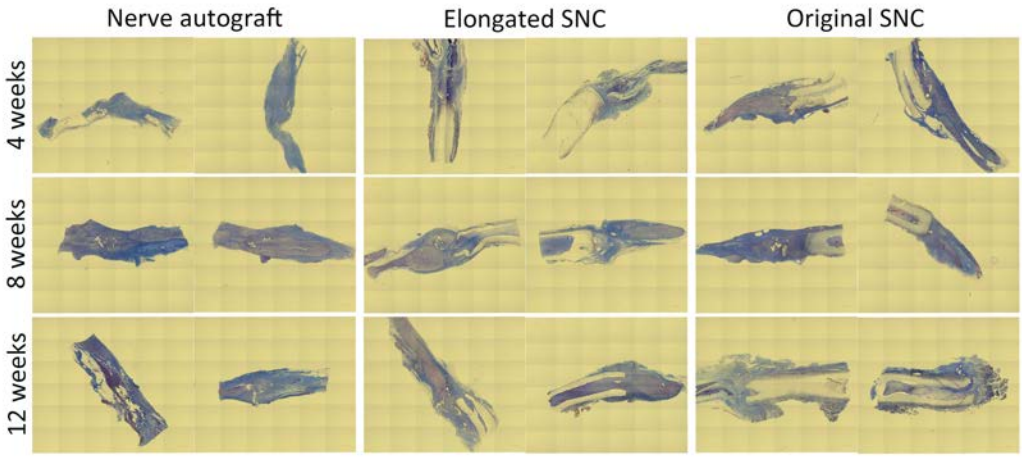

Figure 5.9 (a) Longitudinal section of regenerated nerves taken from types of nerve conduits implanted in rabbit for 4 weeks, stained with Masson. A: elongated conduit, B: conduit with original length, C: autograft nerve. (b) Implanted for 8 weeks. (c) Implanted for 12 weeks

HE staining images of the nerve longitudinal sections from experimental groups reveal the absence of an acute immune response in close proximity to the fibers, indicating the noninflammatory nature of the fabricated PLGA fibers. These results noticeably support efficacy of the fabricated tri-segment conduit to be biocompatible *in vivo* model. In addition, during the nerve regeneration process, the structure of nerve conduit was stable maintained. This is an important factor for axon growth. Although the results of *in vivo* biocompatibility and shape-memory effect are encouraging, the nerve regeneration results are less than those noted with control autografts. We believe the fabricated nerve conduit can serve as a viable scaffold for axonal guidance. Modifications of the biological environment with support cells and nerve induction factors may enhance nerve regeneration[105].

5.3 Summary

In this chapter, Schwann cells cultured on networks and in extraction polymeric fluids with *rac*-LA to GA weight ratios of 60:40, 40:60, and 20:80 showed good *in vitro* biocompatibility. Meanwhile, the implantation of the fabricated nerve conduit did not cause any pathologic damage to rabbit heart, liver, spleen, or kidney, indicating good *in vivo* biocompatibility. Therefore, the fabricated conduit prototype offers excellent biocompatibility, porous structure and consistency in design requirements, but the nerve regeneration efficiency didn't meet our expectations. No remarkable regenerated peripheral nerve was observed. Although equivalent nerve regeneration to autografts was not achieved, this study provides promising results for further investigation.

CHAPTER 6 CONCLUSIONS AND SUGGESTED FUTURE WORK

According to the above chapters about studies of study of smart conduits made of shape-memory polymers for peripheral nerve regeneration, some conclusions were drawn as follows. Such investigations enable ones to have the overall understanding about the shape-memory polymer for biomedical application, so as to open the way to design smart nerve conduit with specific properties. In the second part of this chapter, some meaningful subject matters about smart nerve conduit were suggested on the basis of the previous literatures and results obtained in this project.

6.1 Conclusions

6.1.1 Physically cross-linked amorphous SMP

A series of high molecular weight poly(*rac*-lactide-*co*-glycolide) copolymers were synthesized through ring-opening polymerization. In these synthesized copolymers, entanglements of the molecular chain function as physical cross-links, which form points that provide elasticity above T_g. The strategy to adjust T_g is derived from the Fox-Flory equation.

The DSC test and the XRD measurement show there is no any crystalline segment existing in the synthesized copolymers, thus the poly(*rac*-lactide-*co*-glycolide) is a T_g-type copolymer. The glass transition temperatures obtained from the DSC

measurement demonstrate actuation temperatures (T_gs) are tunable by varying glycolide monomer constitutes and are approximately fitting to the Fox-Flory equation.

The GPC test shows the molecular weights of synthesized copolymers were in the range of 1.1-1.5×10^5 g mol^{-1}, close to the designed value of 1.2×10^5 g mol^{-1}. The cyclic thermo-mechanical measurements indicate that for all the networks R_fs are near 99% and R_rs decrease from about 90% to 50% during the first 5 testing cycles and then becomes stable after 6^{th} cycle. These results verify the hypothesis that the entanglements of molecular chain with molecular weight of 10^5 g mol^{-1} can serve as net points.

The water-induced shape-memory effect test and the FTIR measurement show that water has a significant influence on T_g. SMP with higher T_g recovers slower, while the lower T_g SMP generally recover faster. After immersing in water, it is obvious that the shape of the bound water spectrum in the 3000 to 3600 cm^{-1} is quite different from that of copolymers without immersion. Utilizing the data obtained from previous tests, namely DSC test, it reveals that bounded water has direct effects on reducing glass transition temperature as a plasticizer.

6.1.2 Nerve conduits with shape-memory effect

A tri-segment smart nerve conduit was fabricated by the method of electrospinning. The WCA measurement shows compared with film the electrospun conduits obtain

porous structure that would increase the water contact angle.

The thermo-induced shape-memory effect tests further verify the hypothesis that the entanglements are physically cross-linked and will creep during the programming process. And the mechanical properties during the SME tests show the scaffold can resist muscular contraction and maintain its shape unchanged for a considerable period of time after implanting.

The water-induced shape-memory effect tests verify our tri-segment SNC design of gradual-recovery function can be generated by the macroscopic combination of polymer segments with different T_g. The relatively slow recovery rate (recovery to a stable architecture with hours at 36°C) presents both immediate applications and future modification for the current SNC or other biomedical device with similar shape-memory functionality. For example, slow and programmable recovery rate, as demonstrated here, could fulfill specific tissue engineering requirement.

The SEM measurement shows the diameters of the electrospun PLGA-60, PLGA-40, and PLGA-20 nanofibers were estimated to be 2.27±0.31, 2.25±0.25, and 2.33±0.19 μm, respectively. The diameter of electrospun fibers is of similar magnitude as that of fibrils in extracellular matrix (ECM) that mimics the natural tissue environment and has presented effectiveness as a substrate for cell growth.

6.1.3 Biological assay of fabricated SNC

In vitro measurement shows the SNC fabricated from three types of synthesized poly(*rac*-lactide-*co*-glycolide) networks possess the ability of supporting the adhesion and proliferation of Schwann cells. The MTT assay shows the viability of Schwann cells cultured in the synthesized copolymers extract have no significant difference in their cell viability as compared to that in normal condition medium. Cell morphology measurement shows Schwann cells cultured on the three types of PLGA nanofibrous films flatten and extend in a sequential fashion demonstrating the synthesized shape-memory polymers introduce little cytotoxicity on Schwann cells.

HE staining measurement shows the implantation of the fabricated nerve conduit did not cause any pathologic damage to rabbit heart, liver, spleen, or kidney. HE staining images of the nerve longitudinal sections from experimental groups reveal the absence of an acute immune response in close proximity to the fibers, indicating the noninflammatory nature of the fabricated PLGA fibers. *In vivo* shape-memory effect test shows the elongated SNC could recovery to its original shape to some extend, but the nerve regeneration results are less than those noted with control autografts, which do not fit our expectable aim.

6.2 Suggested future work

More material selections for SNC

In this study, poly(*rac*-lactide-*co*-glycolide) has been presented for biomedical

application. However, another biocompatible monomers could also be introduced. For example, the trimethylene carbonate (TMC) monomer with outstanding tensile strength and flexibility has been studied for applications as heart constructs, cartilage implants, and sustained drug release carriers. Therefore, such kinds of monomers may be an excellent candidate to fabricated SNC with more efficient function.

Modification of SNC

To further mimic the natural regenerative microenvironment, various support cells and/or growth factors could be introduced into our fabricated SNC to improve the regeneration effect. For example, Schwann cells are the main myelin-forming cells in the peripheral nervous system and play a prominent role in neuron regeneration. Meanwhile, nerve growth factor (NGF) is a neuropeptide primarily involved in the maintenance, proliferation, and survival of certain target neurons. Therefore, the aforementioned cells and growth factors could be potential candidate to be filled in our designed SNC.

References

[1] A. Lendlein, Shape-Memory Effect, Angew. Chem. Int. Ed. 41 (2002) 2034–2057.

[2] H. Meng, Jinlian Hu, A Brief Review of Stimulus-active Polymers Responsive to Thermal, Light, Magnetic, Electric, and Water/Solvent Stimuli, Journal of Intelligent Material Systems and Structures. 21 (2010) 859–885.

[3] J. Hu, Y. Zhu, H. Huang, J. Lu, Recent advances in shape–memory polymers: Structure, mechanism, functionality, modeling and applications, Progress in Polymer Science. 37 (2012) 1720–1763.

[4] P.T. Mather, Review of progress in shape-memory polymers, J. Mater. Chem. 17 (2007) 1543.

[5] L. Xue, S. Dai, Z. Li, Biodegradable shape-memory block co-polymers for fast self-expandable stents, Biomaterials. 31 (2010) 8132–8140.

[6] S.S. Venkatraman, L.P. Tan, J.F.D. Joso, Y.C.F. Boey, X. Wang, Biodegradable stents with elastic memory, Biomaterials. 27 (2006) 1573–1578.

[7] A. Lendlein, Biodegradable, amorphous copolyester-urethane networks having shape-memory properties, Angew. Chem. Int. Ed. Engl. 44 (2005) 1188–1192.

[8] J. Karger-Kocsis, Biodegradable polyester-based shape memory polymers: Concepts of (supra)molecular architecturing, Expresspolymlett. 8 (2014) 397–412.

[9] K. Hearon, M.A. Wierzbicki, L.D. Nash, T.L. Landsman, C. Laramy, A.T. Lonnecker, et al., A Processable Shape Memory Polymer System for Biomedical Applications, Adv. Healthcare Mater. 4 (2015) 1386–1398.

[10] C.E. Schmidt, J.B. Leach, N EURALT ISSUEE NGINEERING: Strategies for Repair and Regeneration, Annu. Rev. Biomed. Eng. 5 (2003) 293–347.

[11] Saijilafu, Y. Nishiura, Y. Yamada, Y. Hara, H. Ichimura, Y. Yoshii, et al., Repair of peripheral nerve defect with direct gradual lengthening of the proximal nerve stump in rats, J. Orthop. Res. 24 (2006) 2246–2253.

[12] Byung Kyu Kim, Polyurethanes having shape memory effects, Polymer. 26 (1996) 5781–5793.

[13] T. Xie, Recent advances in polymer shape memory, Polymer. 52 (2011) 4985–5000.

[14] D. Ratna, J. Karger-Kocsis, Recent advances in shape memory polymers and composites: a review, J Mater Sci. 43 (2007) 254–269.

[15] S. Juodkazis, N. Mukai, R. Wakaki, A. Yamaguchi, S. Matsuo, H. Misawa, Reversible phase transitions in polymer gels induced by radiation forces, Nature. 408 (2000) 178–181.

[16] K. Gall, Shape memory polymer nanocomposites, Acta Materialia. 50 (2002) 5115–5126.

[17] T. Xie, Self-Peeling Reversible Dry Adhesive System, Chem. Mater. 20 (2008) 2866–2868.

[18] T. Xie, Self-healable graphene polymer composites, J. Mater. Chem. 20 (2010) 3508–3514.

[19] B.K. Kim, SHAPE MEMORY BEHAVIOR OF AMORPHOUS POLYURETHANES, J. of Macromolecular Sc., Part B. 40 (2001) 1179–1191.

[20] T. Xie, Facile tailoring of thermal transition temperatures of epoxy shape memory polymers, Polymer. 50 (2009) 1852–1856.

[21] T. Xie, Shape memory epoxy: Composition, structure, properties and shape memory performances, J. Mater. Chem. 20 (2010) 3431–3441.

[22] HAN MO JEONG, Shape memory polyurethane containing amorphous reversible phase, Journal of Materials Science 35 (2000) 1579–1583.

[23] L. Xue, S. Dai, Z. Li, Synthesis and Characterization of Three-Arm Poly(ε-caprolactone)-Based Poly(ester−urethanes) with Shape-Memory Effect at Body Temperature, Macromolecules. 42 (2009) 964–972.

[24] J. Xu, W. Shi, W. Pang, Synthesis and shape memory effects of Si–O–Si cross-linked hybrid polyurethanes, Polymer. 47 (2006) 457–465.

[25] F.L. Ji, J.L. Hu, T.C. Li, Y.W. Wong, Morphology and shape memory effect of segmented polyurethanes. Part I: With crystalline reversible phase, Polymer. 48 (2007) 5133–5145.

[26] A. Lendlein, V.P. Shastri, Stimuli-Sensitive Polymers, Adv. Mater. 22 (2010) 3344–3347.

[27] T. Xie, Semi-crystalline two-way shape memory elastomer, Polymer. 52 (2011) 5320–5325.

[28] A. Lendlein, A.M. Schmidt, R. Langer, AB-polymer networks based on oligo(ε-caprolactone) segments showing shape-memory properties, PNAS. 98 (2001) 842–847.

[29] A. Lendlein, Shape-memory polymer networks from oligo(ε-caprolactone)dimethacrylates, J. Polym. Sci, Part A: Polym. Chem. 43 (2005) 1369–1381.

[30] A. Lendlein, Shape-Memory Polymer Networks from Oligo[(ε-hydroxycaproate)- co-glycolate]dimethacrylates and Butyl Acrylate with Adjustable Hydrolytic Degradation Rate, Biomacromolecules. 8 (2007) 1018–1027.

[31] Q. Zhao, M. Behl, A. Lendlein, Shape-memory polymers with multiple transitions: complex actively moving polymers, Soft Matter. 9 (2013) 1744–1755.

[32] H. Zhang, H. Wang, W. Zhong, Q. Du, A novel type of shape memory polymer blend and the shape memory mechanism, Polymer. 50 (2009) 1596–1601.

[33] E.D. Rodriguez, X. Luo, P.T. Mather, Linear/network poly(ε-caprolactone) blends exhibiting shape memory assisted self-healing (SMASH), ACS Appl Mater Interfaces. 3 (2011) 152–161.

[34] X.L. Lu, W. Cai, Z. Gao, W.J. Tang, Shape memory effects of poly(L-lactide) and its copolymer with poly(ε-caprolactone), Polym. Bull. 58 (2006) 381–391.

[35] A. Lendlein, Controlling the Switching Temperature of Biodegradable, Amorphous, Shape-Memory Poly(rac-lactide)urethane Networks by

Incorporation of Different Comonomers, Biomacromolecules. 10 (2009) 975–982.

[36] A. Lendlein, Drug-releasing shape-memory polymers–the role of morphology, processing effects, and matrix degradation, Expert Opin. Drug Deliv. 10 (2013) 1193–1205.

[37] A. Lendlein, From Advanced Biomedical Coatings to Multi-Functionalized Biomaterials, Journal of Macromolecular Science, Part C: Polymer Reviews. 46 (2006) 347–375.

[38] R. Langer, D.A. Tirrell, Designing materials for biology and medicine, Nature. 428 (2004) 487–492.

[39] S.H. Ajili, N.G. Ebrahimi, M. Soleimani, Polyurethane/polycaprolactane blend with shape memory effect as a proposed material for cardiovascular implants, Acta Biomaterialia. 5 (2009) 1519–1530.

[40] A. Lendlein, Biodegradable, Elastic Shape-Memory Polymers for Potential Biomedical Applications, Science. 296 (2002) 1673–1676.

[41] A. Lendlein, Shape-memory polymers as a technology platform for biomedical applications, Expert Rev Med Devices. 7 (2010) 357–379.

[42] A. Lendlein, Temperature-Memory Effect of Copolyesterurethanes and their Application Potential in Minimally Invasive Medical Technologies, Advanced Functional Materials. 22 (2012) 3057–3065.

[43] H.M. Wache, D.J. Tartakowska, A. Hentrich, M.H. Wagner, Development of a polymer stent with shape memory effect as a drug delivery system, Journal of Materials Science: Materials in Medicine. 14 (2003) 109–112.

[44] T. Lammers, V. Subr, K. Ulbrich, W.E. Hennink, G. Storm, F. Kiessling, Polymeric nanomedicines for image-guided drug delivery and tumor-targeted combination therapy, Nano Today. 5 (2010) 197–212.

[45] A. Lendlein, Shape-Memory Effect in Polymers, Macromol. Chem. Phys. 214 (2013) 1175–1177.

[46] B.S. Lee, B.C. Chun, Y.C. Chung, K.I. Sul, J.W. Cho, Structure and Thermomechanical Properties of Polyurethane Block Copolymers with Shape Memory Effect, Macromolecules. 34 (2001) 6431–6437.

[47] P. Sangsanoh, S. Waleetorncheepsawat, O. Suwantong, P. Wutticharoenmongkol, O. Weeranantanapan, B. Chuenjitbuntaworn, et al., In Vitro Biocompatibility of Schwann Cells on Surfaces of Biocompatible Polymeric Electrospun Fibrous and Solution-Cast Film Scaffolds, Biomacromolecules. 8 (2007) 1587–1594.

[48] J.W. Griffin, M.V. Hogan, A.B. Chhabra, D.N. Deal, Peripheral Nerve Repair and Reconstruction, J Bone Joint Surg Am. 95 (2013) 2144–2151.

[49] T. B. Bini, Shujun Gao, Xiaoyun Xu, Shu Wang, S. Ramakrishna, Kam. W. Leong, Peripheral nerve regeneration by microbraided poly(L-lactide-*co*-glycolide) biodegradable polymer fibers, J Biomed Mater Res. 68 (2004) 286–295.

[50] H. Xu, Y. Yan, S. Li, Biomaterials, Biomaterials. 32 (2011) 4506–4516.

[51] S. Wang, M.J. Yaszemski, A.M. Knight, J.A. Gruetzmacher, A.J. Windebank, L. Lu, Photo-crosslinked poly(e-caprolactone fumarate) networks for guided peripheral nerve regeneration: Material propertiesand preliminary biological evaluations, Acta Biomaterialia. 5 (2009) 1531–1542.

[52] X. Gu, F. Ding, Y. Yang, J. Liu, Construction of tissue engineered nerve grafts and their application in peripheral nerve regeneration, Progress in Neurobiology. 93 (2011) 204–230.

[53] D. Li, Y. Xia, Electrospinning of Nanofibers: Reinventing the Wheel? Adv. Mater. Weinheim. 16 (2004) 1151–1170.

[54] A. Greiner, J.H. Wendorff, Electrospinning: A Fascinating Method for the Preparation of Ultrathin Fibers, Angew. Chem. Int. Ed. 46 (2007) 5670–5703.

[55] Z.-M. Huang, Y.Z. Zhang, M. Kotaki, S. Ramakrishna, A review on polymer nanofibers by electrospinning and their applications in nanocomposites, Composites Science and Technology. 63 (2003) 2223–2253.

[56] Darrell H Reneker, Iksoo Chun, Nanometre diameter fibres of polymer, produced by electrospinning, Nanotechnology. 7 (1996) 216–223.

[57] T.J. Sill, H.A. von Recum, Electrospinning: Applications in drug delivery and tissue engineering, Biomaterials. 29 (2008) 1989–2006.

[58] M. Bao, X. Lou, Q. Zhou, W. Dong, H. Yuan, Y. Zhang, Electrospun Biomimetic Fibrous Scaffold from Shape Memory Polymer of PDLLA-

co-TMC for Bone Tissue Engineering, ACS Appl Mater Interfaces. 6 (2014) 2611–2621.

[59] Quynh P. Pham, Upma Sharma, Antonios G. Mikos, Electrospinning of Polymeric Nanofibers for Tissue Engineering Applications: A Review, Tissue Engineering. 12 (2006) 1197–1211.

[60] T. Freier, R. Montenegro, H. Shan Koh, M.S. Shoichet, Chitin-based tubes for tissue engineering in the nervous system, Biomaterials. 26 (2005) 4624–4632.

[61] Y. Feng, J. Lu, M. Behl, A. Lendlein, Progress in Depsipeptide-Based Biomaterials, Macromol. Biosci. 10 (2010) 1008–1021.

[62] F. Zheng, S. Wang, S. Wen, M. Shen, M. Zhu, X. Shi, Characterization and antibacterial activity of amoxicillin-loaded electrospun nano-hydroxyapatite/poly(lactic-co-glycolic acid) composite nanofibers, Biomaterials. 34 (2013) 1402–1412.

[63] S.Y. Chew, R. Mi, A. Hoke, K.W. Leong, Aligned Protein–Polymer Composite Fibers Enhance Nerve Regeneration: A Potential Tissue-Engineering Platform, Adv. Funct. Mater. 17 (2007) 1288–1296.

[64] M. Cheng, J. Deng, F. Yang, Y. Gong, N. Zhao, X. Zhang, Study on physical properties and nerve cell affinity of composite films from chitosan and gelatin solutions, Biomaterials. 24 (2003) 2871–2880.

[65] H. Cao, T. Liu, S.Y. Chew, The application of nanofibrous scaffolds in neural tissue engineering, Advanced Drug Delivery Reviews. 61 (2009) 1055–1064.

[66] T.B. Bini, S. Gao, T.C. Tan, S. Wang, A. Lim, L.B. Hai, et al., Electrospun poly(L-lactide-co-glycolide) biodegradable polymer nanofibre tubes for peripheral nerve regeneration, Nanotechnology. 15 (2004) 1459–1464.

[67] X. Zheng, S. Zhou, X. Li, J. Weng, Shape memory properties of poly(d,l-lactide)/hydroxyapatite composites, Biomaterials. 27 (2006) 4288–4295.

[68] D. Yucel, G.T. Kose, V. Hasirci, Polyester based nerve guidance conduit design, Biomaterials. (2009) 1–8.

[69] M. Yoonessi, Y. Shi, D.A. Scheiman, M. Lebron-Colon, D.M. Tigelaar, R.A. Weiss, et al., Graphene polyimide nanocomposites; thermal, mechanical, and high-temperature shape memory effects, ACS Nano. 6 (2012) 7644–7655.

[70] H. Yoshimoto, Y.M. Shin, H. Terai, J.P. Vacanti, A biodegradable nanofiber scaffold by electrospinning and its potential for bone tissue engineering, Biomaterials. 24 (2003) 2077–2082.

[71] F. Yang, R. Murugan, S. Wang, S. Ramakrishna, Electrospinning of nano/micro scale poly(l-lactic acid) aligned fibers and their potential in neural tissue engineering, Biomaterials. 26 (2005) 2603–2610.

[72] C.M. Yakacki, K. Gall, Shape-Memory Polymers for Biomedical Applications, Advances in Polymer Science. 226 (2010) 147–175.

[73] Y. Xu, Z. Zhang, X. Chen, R. Li, D. Li, S. Feng, A Silk Fibroin/Collagen Nerve Scaffold Seeded with a Co-Culture of Schwann Cells and Adipose-Derived Stem Cells for Sciatic Nerve Regeneration, PLoS ONE. 11 (2016).

[74] N.-Y. Choi, A. Lendlein, Degradable shape-memory polymer networks from oligo[(l-lactide)-ran-glycolide]dimethacrylates, Soft Matter. 3 (2007) 901–909.

[75] E. Ghobadi, M. Heuchel, K. Kratz, Atomistic Simulation of the Shape-Memory Effect in Dry and Water Swollen Poly[(rac-lactide)-co-glycolide] and Copolyester Urethanes Thereof, Macromolecular Chemistry and Physics 215 (2014) 65–75.

[76] T. Xie, Tunable polymer multi-shape memory effect, Nature. 464 (2010) 267–270.

[77] T. Xie, Significant Impact of Thermo-Mechanical Conditions on Polymer Triple-Shape Memory Effect, Macromolecules. 44 (2011) 175–180.

[78] T. Xie, A general approach towards thermoplastic multishape-memory polymers via sequence structure design, Adv. Mater. 25 (2013) 743–748.

[79] G.C.W. de Ruiter, M.J.A. Malessy, M.J. Yaszemski, A.J. Windebank, R.J. Spinner, Designing ideal conduits for peripheral nerve repair, Neurosurgical Focus. 26 (2009).

[80] S.H. Oh, J.H. Lee, Fabrication and characterization of hydrophilized porous PLGA nerve guide conduits by a modified immersion precipitation method, J. Biomed. Mater. Res. 80A (2007) 530–538.

[81] E. Schnell, K. Klinkhammer, S. Balzer, G. Brook, D. Klee, P. Dalton, et al., Guidance of glial cell migration and axonal growth on electrospun nanofibers of poly-ε-caprolactone and a collagen/poly-ε-caprolactone blend, Biomaterials. 28 (2007) 3012–3025.

[82] C. SUNDBACK, J. SHYU, Y. WANG, W. FAQUIN, R. Langer, J. VACANTI, et al., Biocompatibility analysis of poly(glycerol sebacate) as a nerve guide material, Biomaterials. 26 (2005) 5454–5464.

[83] A. Lendlein, Triple-shape polymers, J. Mater. Chem. 20 (2010) 3335–3345.

[84] A.H. Torbati, H.B. Nejad, M. Ponce, J.P. Sutton, P.T. Mather, Properties of triple shape memory composites prepared via polymerization-induced phase separation, Soft Matter. doi:10.1039/C3SM52599F.

[85] G. Liu, X. Ding, Y. Cao, Z. Zheng, Novel Shape-Memory Polymer with Two Transition Temperatures, Macromolecular Rapid Communications. 26 (2005) 649–652.

[86] A. Lendlein, Polymeric triple-shape materials, Proceedings of the National Academy of Sciences. 103 (2006) 18043–18047.

[87] A.R. Nectow, K.G. Marra, D.L. Kaplan, Biomaterials for the Development of Peripheral Nerve Guidance Conduits, Tissue Engineering Part B: Reviews. 18 (2012) 40–50.

[88] K. Paakinaho, T.I. Hukka, T. Kastinen, M. Kellomäki, Demonstrating the mechanism and efficacy of water-induced shape memory and the influence of water on the thermal properties of oriented poly(d,l-lactide), J. Appl. Polym. Sci. (2013) doi:10.1002/app.39513.

[89] L.-F. Tseng, P.T. Mather, J.H. Henderson, Shape-memory-actuated change in scaffold fiber alignment directs stem cell morphology, Acta Biomaterialia. 9 (2013) 8790–8801.

[90] W.M. Huang, Thermomechanical Behavior of a Polyurethane Shape Memory Polymer Foam, Journal of Intelligent Material Systems and Structures. 17 (2006) 753–760.

[91] W.M. Huang, Effects of moisture on the thermomechanical properties of a polyurethane shape memory polymer, Polymer. 47 (2006) 1348–1356.

[92] W.M. Huang, Thermo-moisture responsive polyurethane shape-memory polymer and composites: a review, J. Mater. Chem. 20 (2010) 3367.

[93] W.M. Huang, Thermo-moisture responsive polyurethane shape memory polymer for biomedical devices, The Open Medical Devices Journal. 2 (2010) 11–19.

[94] A. Lendlein, Influence of the addition of water to amorphous switching domains on the simulated shape-memory properties of poly(l-lactide), Polymer. 54 (2013) 4204–4211.

[95] Y. Zhu, J. Hu, H. Luo, R.J. Young, L. Deng, S. Zhang, et al., Rapidly switchable water -sensitive shape- memory cellulose/elastomer nano-composites, Soft Matter. 8 (2012) 2509–2517.

[96] H. Zhuo, J. Hu, S. Chen, Electrospun polyurethane nanofibres having shape memory effect, Materials Letters. 62 (2008) 2074–2076.

[97] F. Ji, Y. Zhu, J. Hu, Y. Liu, L.-Y. Yeung, G. Ye, Smart polymer fibers with shape memory effect, Smart Mater. Struct. 15 (2006) 1547–1554.

[98] E.T. Walbeehm, A. Afoke, T. de Wit, F. Holman, S.E.R. Hovius, R.A. Brown, Mechanical functioning of peripheral nerves: linkage with the "mushrooming" effect, Cell and Tissue Research. 316 (2004) 115–121.

[99] K. Gall, Unconstrained recovery characterization of shape-memory polymer networks for cardiovascular applications, Biomaterials. 28 (2007) 2255–2263.

[100] W. Wang, S. Itoh, A. Matsuda, S. Ichinose, K. Shinomiya, Y. Hata, et al., Influences of mechanical properties and permeability on chitosan nano/microfiber mesh tubes as a scaffold for nerve regeneration, J. Biomed. Mater. Res. 84A (2007) 557–566.

[101] C.E. Ayres, B.S. Jha, H. Meredith, J.R. Bowman, G.L. Bowlin, S.C. Henderson, et al., Measuring fiber alignment in electrospun scaffolds: a user's guide to the 2D fast Fourier transform approach, (2008) 1–20.

[102] S. Panseri, C. Cunha, J. Lowery, U. Del Carro, F. Taraballi, S. Amadio, et al., Electrospun micro- and nanofiber tubes for functional nervous regeneration in sciatic nerve transections, BMC Biotechnol. 8 (2008) 39.

[103] J.S. Belkas, C.A. Munro, M.S. Shoichet, M. Johnston, R. Midha, Long-term in vivo biomechanical properties and biocompatibility of poly(2-hydroxyethyl methacrylate-co-methyl methacrylate) nerve conduits, Biomaterials. 26 (2005) 1741–1749.

[104] G.C. de Ruiter, I.A. Onyeneho, E.T. Liang, M.J. Moore, A.M. Knight, M.J.A. Malessy, et al., Methods forin vitro characterization of multichannel nerve tubes, J. Biomed. Mater. Res. 84A (2008) 643–651.

[105] H.S. Koh, T. Yong, C.K. Chan, S. Ramakrishna, Enhancement of neurite outgrowth using nano-structured scaffolds coupled with laminin, Biomaterials. 29 (2008) 3574–3582.